A STUDY OF ELECTRICAL DOUBLE LAYER AT AN ALUMINUM SURFACE IN AN AUTOMOTIVE COOLING SYSTEM

by

SAURABH DEOBHANKAR

Presented to the Faculty of the Graduate School of

The University of Texas at Arlington in Partial Fulfillment

of the Requirements

for the Degree of

MASTER OF SCIENCE IN MECHANICAL ENGINEERING

THE UNIVERSITY OF TEXAS AT ARLINGTON

May 2016

Acknowledgements

I would like to thank Dr. Bo Yang for his supervision and guidance which formed the backbone of this thesis. His lucid explanation of the most critical topics helped me in understanding the concepts which are applied in this thesis.

I am grateful to Dr. Donghyun Shin and Dr. Ashfaq Adnan for their presence as the committee members.

April 22, 2016

Abstract

A STUDY OF ELECTRICAL DOUBLE LAYER AT AN ALUMINUM SURFACE IN AN AUTOMOTIVE COOLING SYSTEM

SAURABH DEOBHANKAR, MS

The University of Texas at Arlington, 2016

Supervising Professor: Bo Yang

Electrolytic corrosion is identified as a major problem which adversely affects the performance of a cooling system and hence compromises the performance of automobile with it. Electrolysis corrosion is a chemical reaction process that occurs between a metal surface and electrolyte. Mostly, the radiator tubes and tanks are made of aluminum with a high heat transfer rate. The coolant flows under pressure through the aluminum tubes, which gives rise to erosion-corrosion. The present thesis sheds light on the corrosion mechanism of Al 3003 alloy radiator tubes in contact with 50/50 ethylene glycol water coolant. The main objective is to understand the formation of electrical double layer that is necessary in order to understand the charge transfer phenomenon when the metal electrode comes in contact with the electrolyte and corrodes. It includes a mathematical explanation for the governing equations of the dynamic transport of the electrolytic and corroding species.

In order to gain a perspective of the dominant ions responsible for corrosion, the double layer simulation is performed by considering the concentrations of water and ethylene glycol in the

ratio 50:50 by weight %. Parametric study of changes in chemical composition is carried out by taking flux of Al ions, voltage and temperature as the parameters. The simulation results show that at low voltages (0.1V-0.5V), Cl^- ions are dominant corroding species at the metal surface. In contrast, as the voltage increases gradually, Cl^- ions concentration decreases. Meanwhile, the OH^- ion concentration increases, which becomes eventually the dominant counter ion species at the metal surface. This observation implies that at low voltage the dominant Cl^- ions are responsible for the pitting in aluminum surface. The resultant OH^- ions help in formation of aluminum hydroxide which precipitates at the borders of the pit. At low temperature of 333 K and voltage of 0.8 V, it is observed that OH^- ion concentration is more than that at 373 K and 0.8 V. It suggests a higher corrosion rate at higher temperature.

Table Of Contents

List of illustrations

List of Tables

Chapter 1

INTRODUCTION

Aluminum alloys have been widely used in automotive cooling systems due to their low density and high heat transfer capacity. Aluminum also has excellent formability. Aluminum has a corrosion resistance over a wide range of different environments due to the naturally occurring protective oxide film covering. This passive oxide film is formed as soon as Aluminum comes in contact with atmosphere and it blocks the ion exchange thus providing protection to the bare metal against corrosion. However, in environments that contain aggressive anions such as chloride, Cl^-, the passive film becomes unstable and degrades locally causing film breakdown and pitting corrosion [1]. It has generally been accepted that among all anions, chloride ions have the highest power of penetration into natural oxide film, because they are small and very mobile. Chlorides belong to the anions that activate corrosion of aluminum in water, while sulphates, nitrates and phosphates hardly activate it or do not activate it at all. Chlorides substitute oxygen atoms in the alumina network. This leads to a decrease in the film's resistivity, which facilitates the release of aluminum atoms that diffuse into the electrolyte, in this case, coolant [1]. The aggression of a medium with respect to metals in general and aluminum in particular depends to a large extent on its chloride and sulphates concentration. Taking into account the penetration power of the passive Aluminum oxide film by anions, in particular chlorides, the density and depth of pitting generally increases with increasing chloride concentration. The action of chlorides is independent of the action of the associated cation (or cations, if several are present) [2].

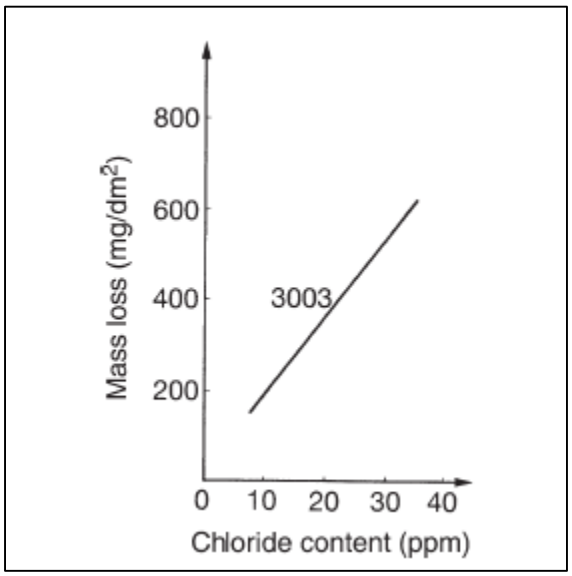

Figure 1.1: mass loss due to Chloride concentration [2]

1.1. Sites of corrosion

Main sites for pitting can be characterized as the local spots under greater pressure/stress; which in this case would be the joint connecting the tube-tank interface. At the tube-tank interface, there is a sudden change in geometry and hence change in the pressure of fluid flow which causes cavitation leading to pitting.

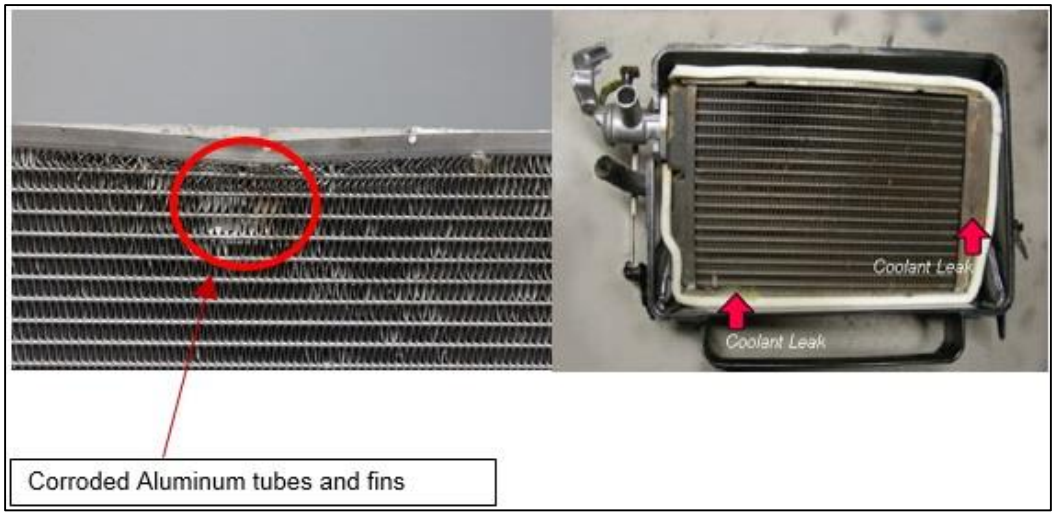

Figure 1.2: Sites of corrosion in radiator [3]

The pitting process is catalyzed by stresses involved due to thermal expansion and contraction of tubes and header plates, changes in pressure within the tube. Fatigue due to vibrations in engine and road travel can also stimulate the pitting process.

1.2. Erosion-corrosion phenomenon

With the increase of fluid flow velocity and Cl^- ion concentration, the total E–C rate increases. Upon fluid flow, passivity of Al alloy that develops in static solution cannot be maintained, and an activation mechanism dominates the corrosion process of Al alloy. The effect of fluid impact angle on Al alloy E–C depends on the competitive effect of normal stress and shear stress. Under normal impact, the surface film would be broken and damaged, but still remain on the electrode surface to provide somewhat protection. With the decrease of impact angle, shear stress becomes dominant, and it would thinner and even completely remove the film. [2] In this case, the coolant runs parallel to tube containing it and hence it would hit the passivating Al oxide layer at 0 deg.

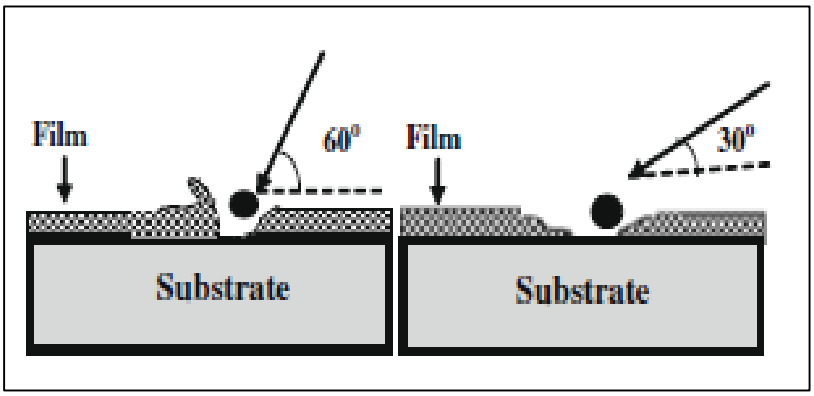

Figure 1.3: Effect of fluid impact angle on resistivity of oxide film [2]

The coolant used is ethylene glycol water mixture because of its considerably high heat transfer characteristics. It has high boiling and low freezing point. Although ethylene glycol has considerably good physical properties, it is susceptible to thermo-oxidative degradation reactions

at higher temperatures. Ethylene glycol decomposes to carboxylic acids like formic, glycolic and oxalic acid. These acids decrease the pH of the coolant and cause depletion of inhibitors in the coolant which accelerates the corrosion process [4]. Electrolytic corrosion process also stimulates if the engine does not have a proper ground connection. Voltage emerging from charging and ignition system causes the current to flow through the coolant which speeds up the corrosion process.

1.3. Pitting initiation and Propagation

Corrosion pitting mechanism starts with pit initiation occurring due to the presence of local defects at the metal surface such as flaws in the oxide or segregates of alloy elements, and the presence of aggressive anions such as chlorides in the environment. The chlorides are believed to locally disrupt the oxide, preferably at pre-existing weak spots, resulting in micro fissures of several nm in diameter. [5]

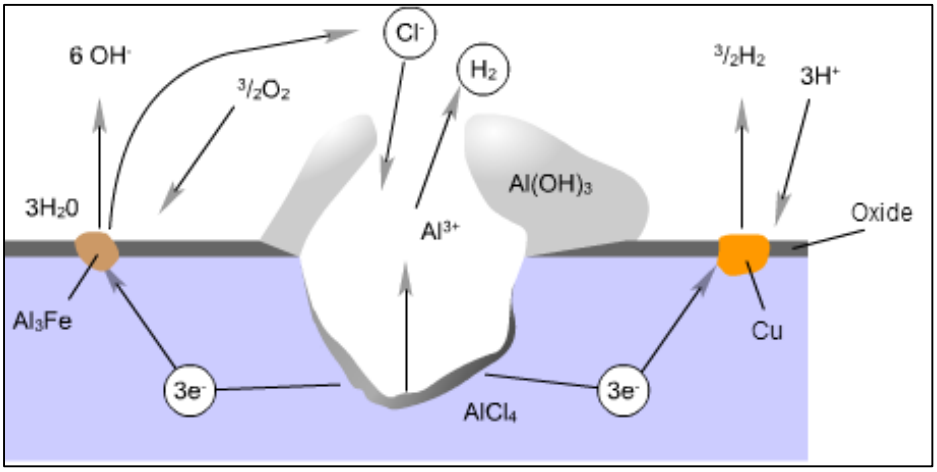

Figure 1.4: Pitting mechanism in Aluminum [5]

Amongst the many initiated pits only a few pits propagate. The overall reaction equation can be described as follows:

$2Al + 3H_2O + {}^3/_2 \cdot O_2 \rightarrow 2Al(OH)_3$ [5]

In the initiated pit, aluminum is dissolved as $Al \rightarrow Al^{3+} + 3e^-$ (anodic reaction), and the Al^{3+} cations react with Cl^- anions to form a complex intermediate species $AlCl^{4-}$. Hydrolysis of this species results in acidification of the bottom of the pit to a pH < 7 (due to formation of H^+). This highly aggressive environment results in auto propagation of the pit. Al^{3+} cations concentrated at the bottom of the pit diffuse out of the pit, where they encounter a more alkaline environment due to the cathodic process of hydrogen gas evolution: $6H^+ + 6e^- \rightarrow 3H_2$, or water reduction: $O_2 + 4H^+ + 4e^- \rightarrow 4OH^-$ (cathodic reaction). As a result, aluminum hydroxide is formed and precipitates at the borders of the pit. This deposit of white corrosion product grows to eventually block off the entrance to the pit for further ionic exchange processes unless acted upon by other factors. [5]

1.4. System Composition

The present thesis orients around the corrosion mechanism of 3003 Al alloy in presence of 50/50 ethylene glycol-water coolant.

The radiator tubes, fins, and tanks are made of EN AW 3003 Al alloy [6], with the following constituent elements according to wt. %:

Cu	Fe	Mn	Si	Zn	Al
0.12	0.48	1.1	0.15	0.01	98.14

Table 1.1: Aluminum alloy EN AW 3003 composition [6]

The conducting coolant is 50/50 ethanol-water solution formed from de-ionized water with Ethylene glycol = 50%, Water = 50%, Chloride concentration = 100ppm. The pH of this solution

is 6.47 at ambient temperature. Electrical conductivity is 105.3$\mu s/cm$. The mass flow rate of coolant is 2.05kg/s. Density of coolant = 101.29 kg/m^3 [7].

The corrosion mechanism gives a general idea about the failure of cooling system due to material disintegration. This thesis sheds lights on dynamic transport and ion exchange of the corroding species and describes its action locally. The motion and action of dominating ions responsible for corrosion is simulated through the study of electrical double layer structure. Study of electrical double layer structure which forms when a metal is plunged into an electrolyte helps in achieving the concentration or density of dominating ions acting over the metal surface.

1.5. Thesis objective

The main objective of this thesis is the simulation of Electric Double Layer structure which is formed on the Aluminum metal surface in presence of ethylene glycol water coolant as the electrolyte. Through this simulation the activity of ions in the double layer is studied. Change in concentration, density and velocity of the ions is observed using potential and temperature as the parameters. It helps in analyzing the effects on corrosion mechanism.

Chapter 2

ELECTRICAL DOUBLE LAYER THEORY

Electrical double layer is a specific interfacial region formed on the surface of the metal when it is immersed in an electrolyte solution. The double layer model helps in the study of the ionic environment in the vicinity of a charged surface. In the double layer, the ions and the water molecules in the electrolyte, align themselves according to the electric field generated by applying potential to the metal surface. The double layer refers to two parallel layers of charge surrounding the metal. The first layer comprises of surface charge, in this case Al^{3+} cations, which are adsorbed over the aluminum surface due to oxidation reaction of Aluminum. This compact charge layer is the **Helmholtz layer** [8]. The second layer is composed of ions or polarized molecules attracted to the surface due to Coulomb forces, electrically screening the first layer, in this case the Cl^- ions. This second layer is loosely associated with the object. It is made of free ions that move in the fluid under the influence of electric attraction and thermal motion rather than being firmly anchored. It is thus called the **Gouy-Chapman** "diffuse layer" [8] [9]. The Gouy-Chapman model treats ions as point charge. The Stern model comprises of Helmholtz layer along with the diffusing Gouy-Chapman layer. Stern model considers ions' finite size instead of treating it as point charges. It also takes into consideration the dielectric permittivity of ions/particles involved in the double layer [8] [9].

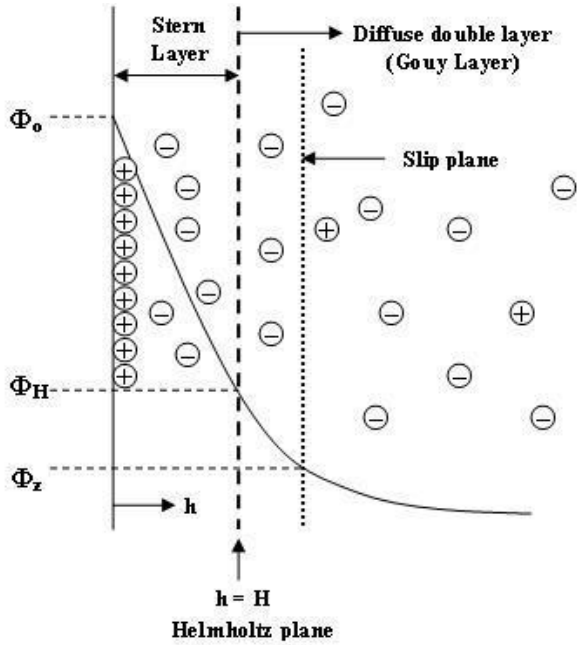

Figure 2.1: Electrical double layer structure [10]

2.1. Chemical Potential

When an electrolyte is brought in contact with a metal surface, a double layer is formed consisting of cations and anions. The electrolyte consists of mobile ions and solvent molecules which are polarized according to the electric field set up in the double layer. The chemical potential which describes the mobility of each particle in the electrolyte is given by:

$$\mu_i = k_B T \ln(n_i) + z_i e\phi - \int_0^{\boldsymbol{\tau}_i} \nabla\phi \cdot d\boldsymbol{\tau}_i + \gamma_i p, \quad (1)$$

Where k_B is the Boltzmann constant, T is the temperature, ϕ is the electrostatic potential, p is the (rate-independent) hydrostatic pressure, e is the unit charge, andn_i, z_i, γ_i and $\boldsymbol{\tau}_i$ are the number concentration, the valance number, the chemical expansion volume, and the induced dipole moment of the i^{th} component, respectively. i represents all the constituent particles in the electrolytic solution. The four terms represent the effects of configurational entropy, charge, dipole moment and mechanical pressure, respectively.

With increasing voltage, ion mobility increases. In order to take into consideration nonlinear polarization effect at high voltage, caused by the random motion of ions and polarizable solvent molecules, the Langevin equation is adopted to describe the polarization phenomenon, given by:

$$\boldsymbol{\tau}_i = -\epsilon_0 \chi_i \nabla\phi, \text{ with } \chi_i \equiv \frac{3}{\bar{\tau}_{0i}E}\left(\coth(\bar{\tau}_{0i}E) - \frac{1}{\bar{\tau}_{0i}E}\right)\chi_{0i} \text{ and} \bar{\tau}_{0i} = \frac{\tau_{0i}}{k_B T}, \tag{2}$$

Where ϵ_0 is the permittivity of vacuum, χ_{0i} and τ_{0i} are the linear polarization susceptibility per particle and the (permanent) dipole moment per particle of the i^{th} component, and$E = |\nabla\phi|$. The Langevin equation is applied to orientation polarization of permanent dipoles only. Here, it is applied to describe all possible polarization mechanisms including electronic as well as orientation type so that a concise form can be presented relating the total polarization strength to measurable linear susceptibilityχ_{0i}. Substituting Eq. (2) in the third term on the right-hand side of Eq. (1) and integrating, the following equation is obtained:

$$-\int_0^{\boldsymbol{\tau}_i} \nabla\phi \cdot d\boldsymbol{\tau}_i = k_B T \left(\ln\left(\frac{\sinh\bar{\tau}_{0i}E}{\bar{\tau}_{0i}E}\right) - \bar{\tau}_{0i}E\coth(\bar{\tau}_{0i}E) + 1\right). \tag{3}$$

In Eq. (1), the first two terms of thermal and electrostatic charge forces are considered to describe the motion of the ions in the electrolyte. The electrostatic polarization effect is introduced by the dipole moment term according to the Dipolar-Poisson-Boltzmann equation. On a mean-field level, internal charge distribution of all particles is taken into consideration. By looking at the DPB equation around a fixed point-like ion, a closed-form formula for the dielectric constant is obtained. We express the dielectric constant using the "hydration length" that characterizes the hydration shell of dipoles around ions, and thus the strength of the dielectric decrement [22]. Thus Langevin equation is introduced to capture the active transport of

dipoles towards the charged metal surface. This is important in corrosion mechanism caused not only by ions but also by polarizable solvent molecules like water as well.

2.2. Dynamic Transport and Other Field Governing Equations

The diffusion of ions/solvent molecules in the electrolyte is given by Fick's law. It relates diffusive flux to the concentration. Flux is basically the driving force for diffusion which is represented as the gradient of chemical potential for a particular particle in the electrolyte. According to Fick's first law, the flux of the i^{th} species may be expressed as $\boldsymbol{j}_i = -M_i n_i \nabla \mu_i$, in which M_i is the mobility of the i^{th} species that can be a complex function of concentrations of all components. By substituting Eq. (1) in the flux equation and effecting Einstein's relation $D_i = M_i k_B T$, the flux of the i^{th} species is obtained as

$$\boldsymbol{j}_i = -D_i \nabla n_i + n_i \left[M_i \left(-z_i e \nabla \phi + \frac{\epsilon_0 \zeta_i}{2} \nabla (\nabla \phi \cdot \nabla \phi) - \gamma_i \nabla p \right) + \boldsymbol{u} \right], \tag{4}$$

Where $\boldsymbol{u}$ is the velocity, and electric field-dependent constant ζ_i is given by

$$\zeta_i = 3 \left(\frac{1}{(\bar{\tau}_{0i} E)^2} - \coth^2(\bar{\tau}_{0i} E) + 1 \right) \chi_{0i}. \tag{5}$$

The above constant $\zeta_i \cong \chi_{0i}$ if $\bar{\tau}_{0i} E \ll 1$. According to the law of mass conservation, the equation of dynamic transport is given by

$$\frac{\partial n_i}{\partial t} = -\nabla \cdot \boldsymbol{j}_i + R_i, \tag{6}$$

Where t is the time, and R_i is the production rate of the i^{th} component from chemical reaction.

The diffusion flux is a result of mechanical force as well as electrostatic force. In order to complete the formulation, two additional field governing equations are required for the electrostatic potential and the pressure, respectively. The electrostatic potential field is captured by the Gauss' law which is stated by Poisson's equation:

$$\nabla \cdot \epsilon_0 (1 + \textstyle\sum_i \chi_i n_i) \nabla \phi + \sum_i z_i e n_i = 0, \tag{7}$$

The second term expresses the total charge density representing the separation of counterions and coions, and the electric field-dependent susceptibility χ_i is given in Eq. (2). It is assumed that the polarization effect is additive from all constituents.

The electrolyte is assumed to be a compressible Newtonian fluid. Thus, the equilibrium equation according to Newton's law is given by

$$-\nabla p + \nabla \cdot \eta \left(\nabla \boldsymbol{u} + \nabla^T \boldsymbol{u} - \frac{2}{3}\mathbf{I}\nabla \cdot \boldsymbol{u}\right) - \sum_i z_i e n_i \nabla\phi + \frac{1}{2}\epsilon_0 \sum_i \zeta_i n_i \nabla(\nabla\phi \cdot \nabla\phi) = 0, \qquad (8)$$

Where the hydrostatic pressure p is due to "elastic" deformation, given by an equation of state, the second term is due to viscous flow, the third term is the electrostatic charge force density, and the fourth term is the electrostatic polarization force density due to induced dipoles. The electrostatic charge force density is expressed as a divergence of Maxwell stress. Fundamentally, the electrostatic force density is the result of forces acting on the constituent particles of the electrolyte that are charged or have electric dipole moment. This force density is derived through the Korteweg-Helmholtz theory, which corresponds to the thermodynamic force for mass transport in Eq. (4). It is worth noting that the above third term of polarization force density reduces to the Kelvin force density $\left(\equiv \frac{1}{2}\epsilon_0 \sum_i \chi_i n_i \nabla(\nabla\phi \cdot \nabla\phi)\right)$ when $\bar{\tau}_{0i}E \ll 1$. However, the Kelvin force density, obtained by multiplying the induced dipole moment with electric field gradient, is inapplicable in the nonlinear case of Langevin dipoles. The microscopic forces that individual induced dipoles (in average) experience do not always add up linearly as the macroscopic electrical force. [21] [22]

Lastly, rate-independent hydrostatic pressure p is expressed in an EOS as $p = p(N, V, T)$, where $N(\equiv \sum n_i)$ is the total number of particles per unit volume, and $V(\equiv \sum \nu_i = \sum n_i \gamma_i)$ is the

packing density. The well-known Carnahan-Starling EOS for repulsion [21] [22] plus van der Waals attraction term [22] is adopted, which is given by

$$\frac{p}{Nk_BT} = \frac{1+V+V^2-V^3}{(1-V)^3} - \frac{a}{k_BT}, \tag{9}$$

with $a = \sum n_i a_{ij} n_j$, where a_{ij} describes the attractive interaction effect between species *i* and *j*. Note that we generalize it for multicomponent mixtures, with $a_{ij} = \sqrt{a_{ii}a_{jj}}$, similar to how the literature has treated the Lennard-Jones potential for mixtures [23]. Constant a_{ii} for a single component can be found from the pressure and temperature at the critical liquid-vapor point [24].

2.3. Finite Volume Method for One-dimensional Planar Problems

A finite volume method is adopted to numerically solve the above set of governing equations (Eqs. (6) to (9)) along with appropriate initial-boundary conditions for fields n_i, ϕ, $\boldsymbol{u}$ and *p* in one-dimensional planar problems of an EDL. By the virtue of a finite volume method, the first step is to present the problem of a divergence equation governing a field over a domain with surface integrals of flux according to the divergence theorem. This is applied to each one of the cells (i.e., finite volumes) used to discretize the whole domain. The flux at cell boundaries is then approximately evaluated from nodal values of a field defined within the cells. When the flux, though approximate, is applied identically to adjacent cells sharing the surface where it is defined, the law of conservation of the field quantity is always satisfied. Since the present multi-physics problem is highly nonlinear, an iterative scheme is indispensable.

Let us discretize a one-dimensional finite domain into *M* cells, numbered in order from 1 to *M*, as shown in Fig. 2. Each cell is assigned with a node at the middle point. Potential ϕ, concentration n_i and velocity $\boldsymbol{u}$ are the basic quantities, and are defined on the nodes. There are *M* nodal degrees of freedom for either one of ϕ, n_i or $\boldsymbol{u}$. Thus, one needs to gather *M* algebraic

equations to solve for each one of them. This is attained by applying Eqs. (6) -(8) to each cell. Based on the nodal values, the fields of ϕ, n_i and $\boldsymbol{u}$ near a knot m are approximated as

$$\phi(x;x^m) = \sum_q N_q^m(x)\phi_q, \tag{10a}$$

$$n_i(x;x^m) = \sum_q N_q^m(x)n_{iq}, \tag{10b}$$

$$\boldsymbol{u}(x;x^m) = \sum_q N_q^m(x)\boldsymbol{u}_q, \tag{10c}$$

where superscript m indicates the m^{th} knot, subscript q indicates the q^{th} node selected to approximate the field around knot m, and $N_q^m(x)\left(=\prod_{p\neq q}\left(\frac{x-x_p}{x_q-x_p}\right)\right)$ is the Lagrange interpolation function in terms of selected nodal coordinates around knot m. In later numerical examples, two nodes from the left side and two nodes from the right side, if available, are chosen to approximate a field about a knot. For knots near the ends (i.e., domain boundary), lower-rank interpolation is used, since there may be less than two nodes available on the end side. Derivatives and integrals of these fields around a knot can be conveniently obtained from Eq. (10). For the sake of brevity, their explicit expressions are not presented here.

By applying the divergence theorem, the governing equation of electrostatics (Eq. (7)) over the m^{th} cell between knots m-1 and m is turned into

$$\epsilon^{m,l}\left(\phi_{,x}\right)^{m,l+1} - \epsilon^{m-1,l}\left(\phi_{,x}\right)^{m-1,l+1} + \sum_i z_i e n_{im}^{,l}\,(\Delta x)_m = 0, \tag{11}$$

where $\epsilon^{m,l} \equiv \epsilon_0\left(1+\sum_i \chi_i^{m,l} n_i^{m,l}\right)$, valid for $\epsilon^{m-1,l}$ as well, $(\Delta x)_m$ is the cell size, superscript l after comma indicates the l^{th} iterative step, and subscript comma indicates partial differentiation with respect to the indices that follow. Again, superscript m (or m-1) in the first two terms indicates that ϵ and $\phi_{,x}$ are evaluated at knot m (or m-1) based on nearby nodal values by Eq. (10) and its derivatives. For example, $\left(\phi_{,x}\right)^{m,l+1} = \sum_q N_{q,x}^m(x=x^m)\phi_q^{,l+1}$. By assuming that all

quantities at the l^{th} iterative step are known, Eq. (11) offers an algebraic equation of unknown nodal values of potential at the $(l+1)^{\text{th}}$ iterative step.

Similarly, the governing equations of mass transport (Eqs. (4) and (6)) within the m^{th} cell between knots m-1 and m are turned into

$$\frac{(\Delta x)_m}{\Delta t}\left(n_{im}^{l+1} - n_{im}^{0}\right) + \left(j_i^m - j_i^{m-1}\right) - (\Delta x)_m R_{im} = 0, \tag{12a}$$

$$j_i^* = -D_i^{*,l}\left(n_{i,x}\right)^{*,l+1} + (A^{*,l} + u^{*,l})n_i^{*,l+1}, \text{ with } *= m, m-1, \tag{12b}$$

$$A \equiv M_i\left(-z_i e\phi_{,x} + \epsilon_0\zeta_i\phi_{,x}\phi_{,xx} - \gamma_i p_{,x}\right), \tag{12c}$$

where n_{im}^0 is the nodal concentration at the previous time step, and Δt is the time step. Though more complicated, Eq. (12) works the same as Eq. (11) to offer an algebraic equation of unknown nodal values of n_i at the $(l+1)^{\text{th}}$ iterative step given all quantities at the previous iterative step. Above p is computed from Eq. (9). The time rate-of-change term in Eq. (6) is treated above as a source term with time-marching step Δt. Meanwhile, all other terms/quantities involved in Eq. (4) of j_i are evaluated at the current time step; thus, an implicit finite difference scheme is used to treat the temporal dynamics of the problem.

Furthermore, the equilibrium equation of force balance (Eq. (8)) over the m^{th} cell between knots m-1 and m are turned into

$$-\left(p^{m,l} - p^{m-1,l}\right) + \frac{4}{3}\left(\eta^{m,l}\left(u_{,x}\right)^{m,l+1} - \eta^{m-1,l}\left(u_{,x}\right)^{m-1,l+1}\right) + (\Delta x)_m f_m = 0, \tag{13a}$$

$$f = -\sum_i z_i e n_i \nabla\phi + \frac{1}{2}\epsilon_0 \sum_i \zeta_i n_i \nabla(\nabla\phi \cdot \nabla\phi). \tag{13b}$$

This set of algebraic equations is solved for velocity field u at each iteration step.

Equations (11) - (13) are only applicable to interior cells. For boundary cells, the quantities evaluated at the knot at the boundary end should be replaced by a prescribed boundary

condition. If a flux boundary condition is prescribed, the replacement is straightforward. If a potential/concentration boundary condition is prescribed, it is converted into a flux boundary condition with a penalty coefficient. For instance, for diffusion at the far end (i.e., knot *M*), it is written: $j_i^M = k^M(n_i^M - \bar{n}_i^M)$, where k^M is the penalty coefficient, a numerical parameter, $\bar{n}_i^M$ is the prescribed value of concentration, and n_i^M is the concentration at knot *M* and expressed in terms of two nodal values next to the end by Eq. (10). If k^M is set sufficiently large, $n_i^M = \bar{n}_i^M$ is approximately obtained, with controlled, negligible numerical error.

The solution procedure is briefly described as follows. Given appropriate initial and boundary conditions, the problem is solved incrementally in time and iteratively over each time step. Marching in time poses little issue in this case of a parabolic problem in nature. For each iterative step l+1, a system of algebraic equations with nodal potential $\phi_m^{,l+1}$ as variables and all coefficients and other quantities evaluated from previous iterative step l is assembled from Eq. (11). The stiffness matrix is inverted to solve for nodal potentials at the $(l+1)^{\text{th}}$ iterative step. Then, nodal concentrations of the first chemical component at the $(l+1)^{\text{th}}$ iterative step is solved by inverting the stiffness matrix assembled from Eq. (12) with i =1. This is repeated until nodal concentrations of all chemical components are updated. Finally, Eq. (13) is solved to update velocity u. However, since the present problem is highly nonlinear, especially when concentrations reach their saturation values, this scheme with no relaxation may become unstable. Instead, the following over-relaxation scheme is used; for instance, for potential, $\phi_m^{,l+1} = \phi_m^{,l} + \alpha\Delta\phi_m$, where $\Delta\phi_m$ is the difference of above obtained new value of ϕ_m from $\phi_m^{,l}$, and α is the relaxation factor. Typically, a larger α leads to faster convergence, but greater chance of numerical instability. Trials are needed to identify reasonable value of α.

Chapter 3

PROBLEM FORMULATION

The electrical double layer structure is simulated by considering a 1-D planar problem. The double layer is analyzed for two temperature cases, 333 K and 373 K with applied potential varying from 0 to 1.2 V for each case. For each potential, the corresponding flux of Aluminium cations is applied which is calculated with the help of Aluminium polarization curve.

The ion/molecule mobility is introduced through the Stokes radius property which is calculated from the diffusivity of the particles at each temperature.

The simulation domain length is decided on the basis of Debye-Huckel length.

3.1. Flux due to polarization

In electrochemistry, polarization is a collective term for certain mechanical side-effects (of an electrochemical process) by which isolating barriers develop at the interface between electrode and electrolyte. These side-effects influence the reaction mechanisms, as well as the chemical kinetics of corrosion and metal deposition.

The term 'polarization' derives from the early 19th-century discovery that electrolysis causes the elements in an electrolyte to be attracted towards one or the other pole— i.e. the gasses were polarized towards the electrodes. Thus, initially 'polarization' was essentially a description of electrolysis itself, and in the context of electrochemical cells used to describe the effects on the electrolyte (which was then called "polarization liquid"). [11]

The flux of Aluminum Al^{3+} ions leaving the metal surface after oxidation and flowing into the electrolyte solution is incorporated through the polarization graph. The polarization graph is plotted as log current density v/s overpotential [12] [13] [7]. The current density is calculated for each voltage and temperature as,

$$ia = io \exp\left(\frac{\beta\, n\, F\, \eta}{R\, T}\right)$$ [7] [12]

where,

ia = anodic current density,

io = exchange current density,

ß = anodic charge transfer coefficient (0.123)

F = Faraday constant = 96500 C/mol

η = overpotential, V,

R = gas constant, 8.314 J mol^{-1} K^{-1}

T = Temperature

The slope of anodic Tafel plot is given as,

$$ba = 2.303 \frac{R\, T}{\beta\, n\, F},$$ [12]

The relationship between overpotential and current density is given by,

$$\eta = \text{ba}.\log(\text{i}/\text{io})$$ [12]

The slope ba is found to be 0.2, V with increasing voltage

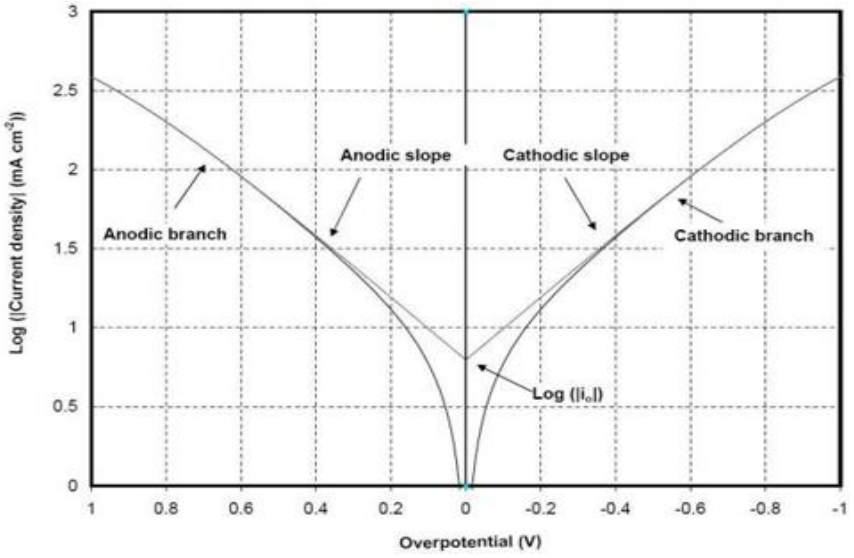

Figure 3.1: Polarization curve [12]

The exchange current density for Aluminum is generally 1e-6 A/m^2.

Metal	$\log_{10} i_0$ (A/cm^2)
Pb, Hg	-13
Zn	-11
Sn, Al, Be	-10
Ni, Ag, Cu, Cd	-7
Fe, Au, Mo	-6
W, Co, Ta	-5
Pd, Rh	-4
Pt	-2

Figure 3.2: Exchange current density [12]

3.2. Physical properties

To relate the ion mobility and diffusion rate of the ions involved in the electrolyte, Diffusion co-efficient of the involved ions/molecules are calculated at respective temperatures. Using the diffusion coefficient values, the **Stokes radii** of the corresponding ions/molecules are calculated as,

$$rH = \frac{kb\ T}{6\pi\ \mu\ D}$$

rH = stokes radius

k_b = Boltzmann constant,

T = temperature,

μ = dynamic viscosity of water

D = diffusion constant.

COMPONENT	DIFFUSIVITY (nm2/ns)	STOKES RADIUS (nm)	PHYSICAL RADIUS (nm)
Cl^-	9.03	0.107	0.181
$CH3OH2^+$	1.5	0.145	0.157
HCO^-	1.35	0.717	0.234
H^+	9.311	0.023	0.15
OH^-	5.273	0.041	0.137

Table 3.1: Stokes radius calculation from diffusivity

It is observed that ions/molecules having high diffusion coefficient, have low stokes radii and thus have high mobility. [14]

3.3. Physical Constant

Simulation domain is set up by integrating the numerical factors affecting the ion/molecule mobility, diffusion and chemical interactions within the electrical double layer. The simulation domain distance is expressed as the Debye length [15] [8]. It is a length parameter in the double layer over which the chemical interactions and diffusion of ions/molecules is supposed to be actively dominant. This is also called the double layer thickness. The thickness of the double layer is usually given as being approximately $1.5k^{-1}$,

$$k^{-1} = \sqrt{\frac{\varepsilon_r \varepsilon_0 k_B T}{2 N_A e^2 I}}, \text{[8]}$$

k^{-1} = Debye Length	T = Temperature
ε_r = Dielectric Constant	N_A = Avogadro's Number
ε_0 = Permittivity of Free space	e = Elementary Charge
k_b = Boltzmann Constant	I = Concentration

3.4. Numerical issues

The Debye length gives an approximation for the simulation domain length. Sometimes this length is inappropriate to carry out simulations. The Debye screening length decreases with increasing concentration of electrolyte. It may so happen that for large concentration values, the Debye length becomes smaller than an individual ionic radius of a certain ion itself. Therefore, the simulation domain length is calculated using trial and error method.

Simulations are carried out for 0.5nm, 0.85nm and 1nm.

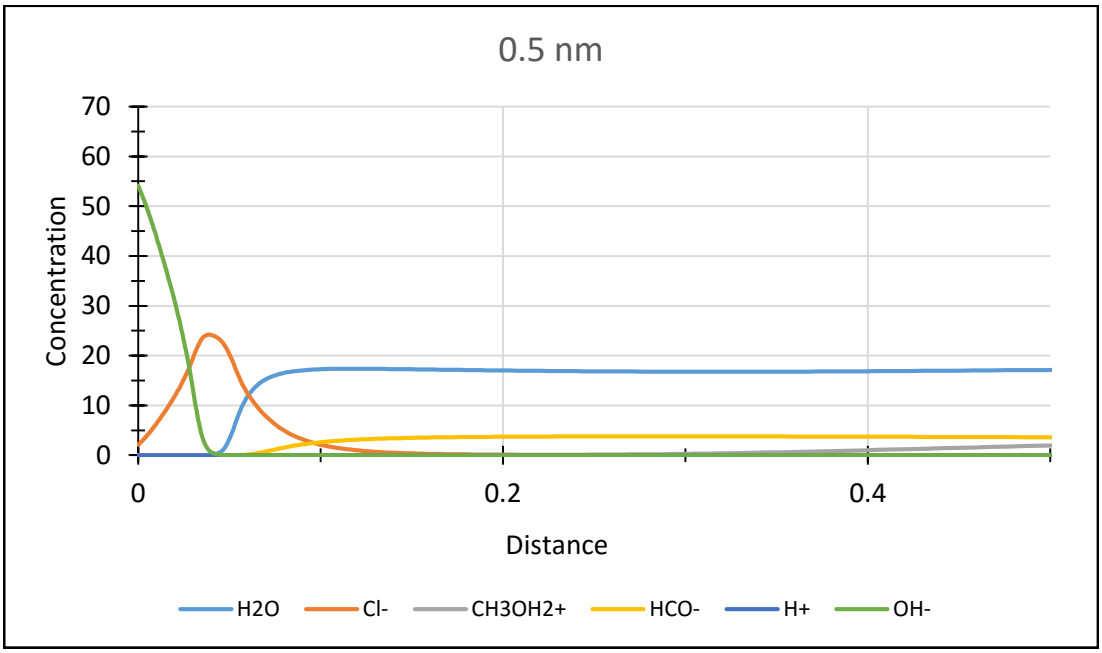

Figure 3.3: truncation distance 0.5 nm

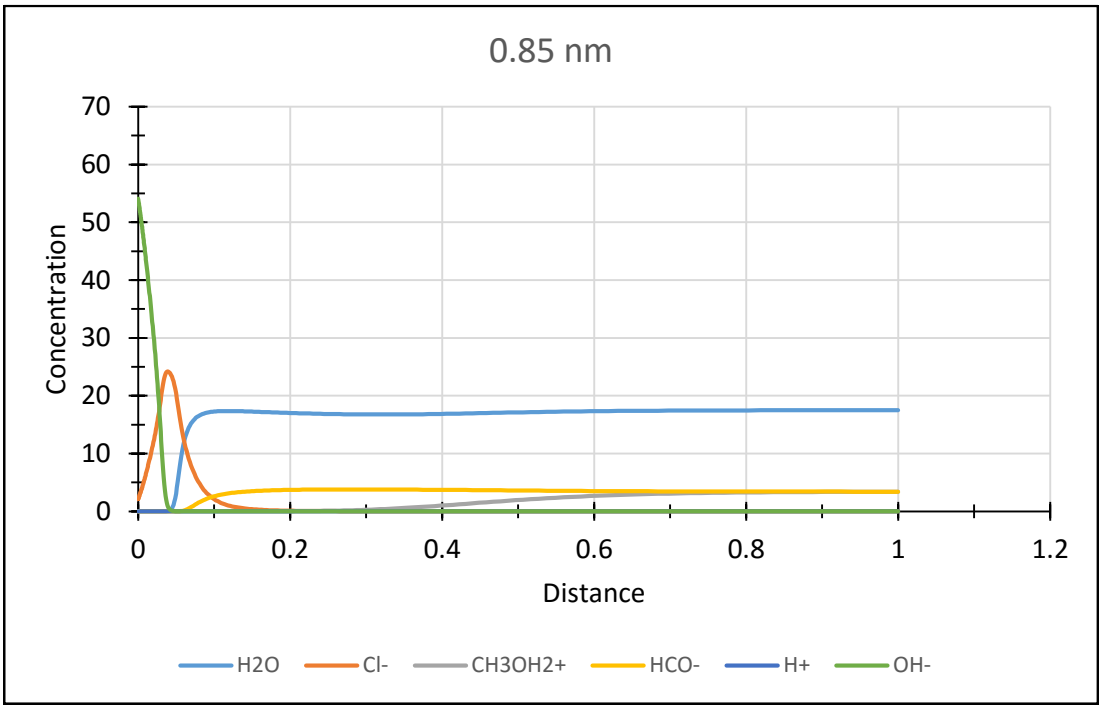

Figure 3.4: Truncation distance 0.85nm

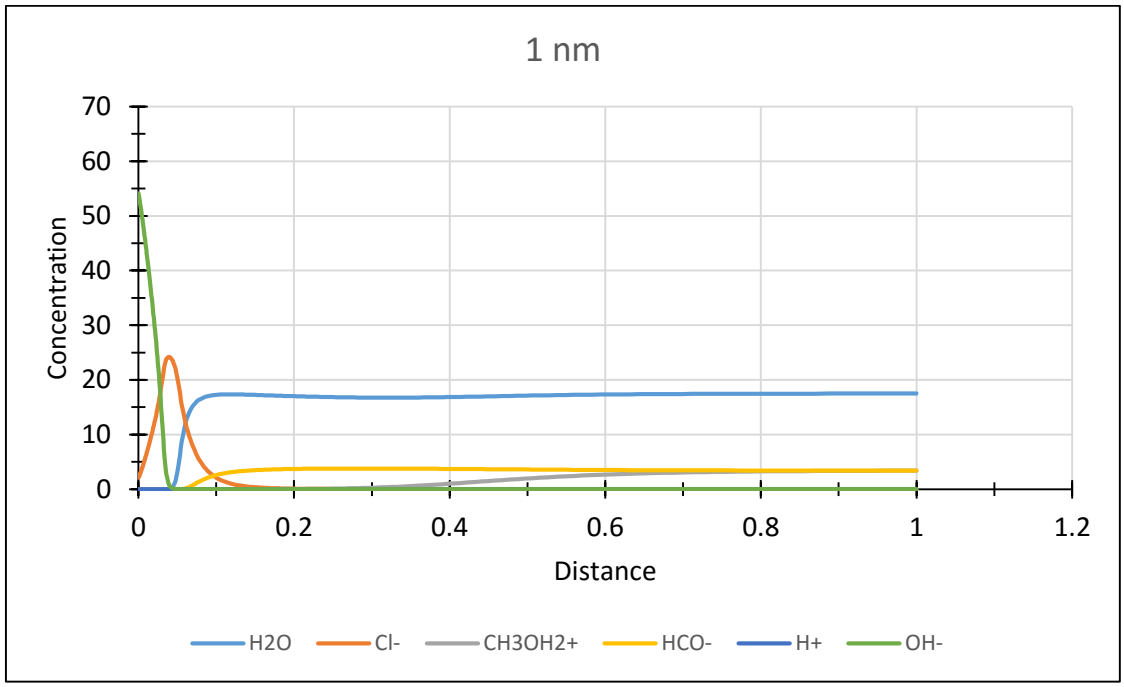

Figure 3.5: Truncation distance 1nm

Chapter 4

NUMERICAL RESULTS AND OBSERVATIONS

In order to gain a perspective of the dominant ions responsible for corrosion, the double layer simulation is performed by considering the concentrations of water and ethylene glycol in the ratio 50:50 by weight %. Parametric study of changes in chemical composition is carried out by taking flux of Al ions in correspondence with voltage and temperature as the parameters. The study is conducted in voltage range of 0-1.8V at two different temperatures, 60° C (333 K) and 100° C (373 K). The thermostat in the radiator normally opens the coolant valve when the engine temperature reaches 60° C.

4.1. 0.2 V,333 K temperature

Considering the case for 333 K temperature and 0.2 V, the flux of Al ions is 1.45d-11 e/nm^2/ns which is determined from the Tafel graph (overpotential v/s current density).

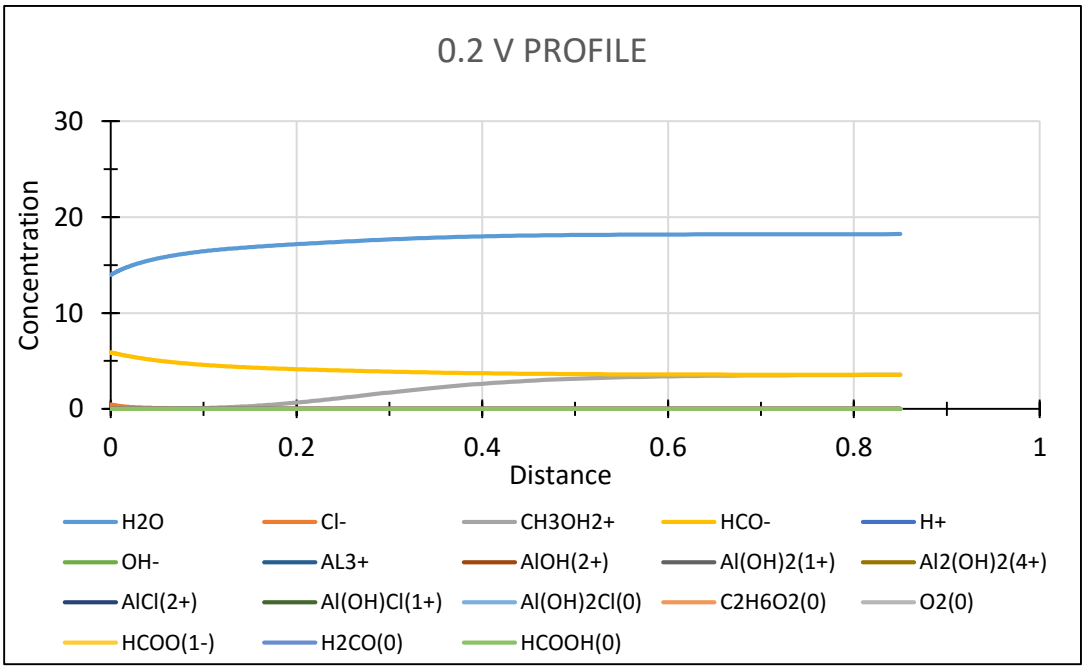

Figure 4.1.1: Concentration profile for 0.2 V at 333 K temperature

It is observed that HCO^- ions diffuse towards the metal surface and act as the dominating corroding species. The water concentration at the metal surface is high.

Significant observations are laid by considering the packing factor and pressure of the bulk concentration.

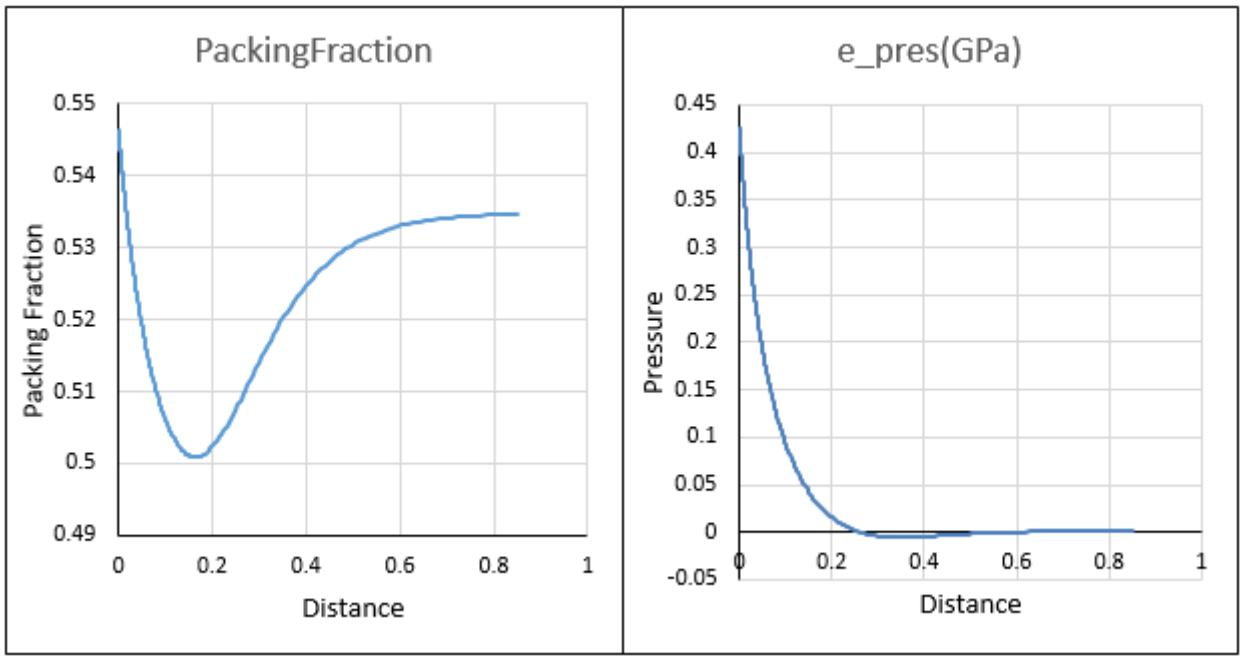

Figure 4.1.2: Packing Fraction and Pressure profiles for 0.2 V at 333 K temperature

Packing fraction is fraction of volume in the bulk electrolyte that is occupied by its constituent elements. It is nothing but the density or concentration of ions at a particular location along the simulation domain. The pressure is the driving force of the ions which helps in diffusion through the electrolyte towards the metal surface.

It is observed that the maximum packing fraction is obtained at the metal surface (0.5456), and gradually the packing fraction decreases along the positive x-axis up till 0.16nm distance from the surface and then increases exponentially. Correspondingly, the pressure is high(0.42GPa) at

the metal surface and there is a sudden change in pressure between the region of 0.14-0.27nm distance from the surface.

From the velocity profile, it is seen that density is inversely proportional to velocity.

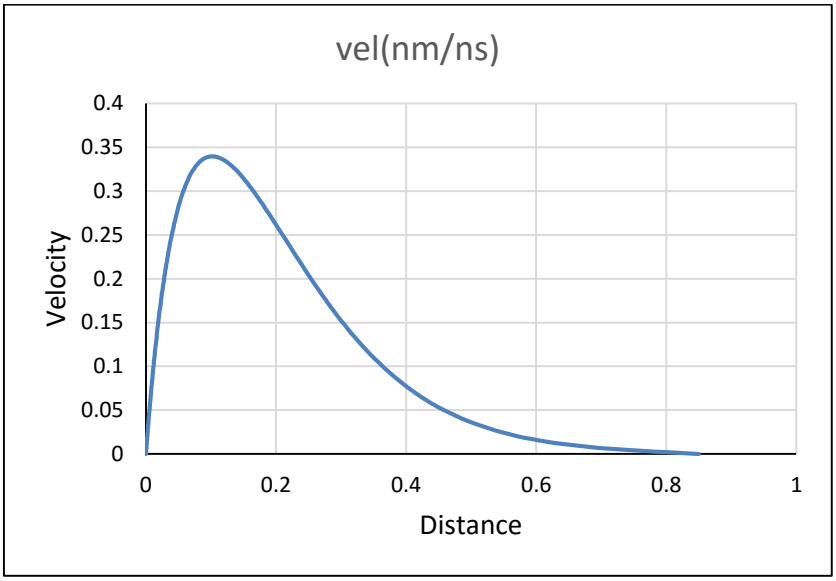

Figure 4.1.3: Velocity profile for 0.2 V at 333 K temperature

It is observed that low velocity of ions is attained at the metal surface where the packing fraction or the density is high. Highest velocity is obtained is 0.33 at a distance of 0.11nm from the surface where the density is the lowest.

4.2. 0.3 V, 333 K temperature

After increasing the voltage to 0.3V, at 333K temperature and Al flux of 2.08d-11 e/nm^2/ns,

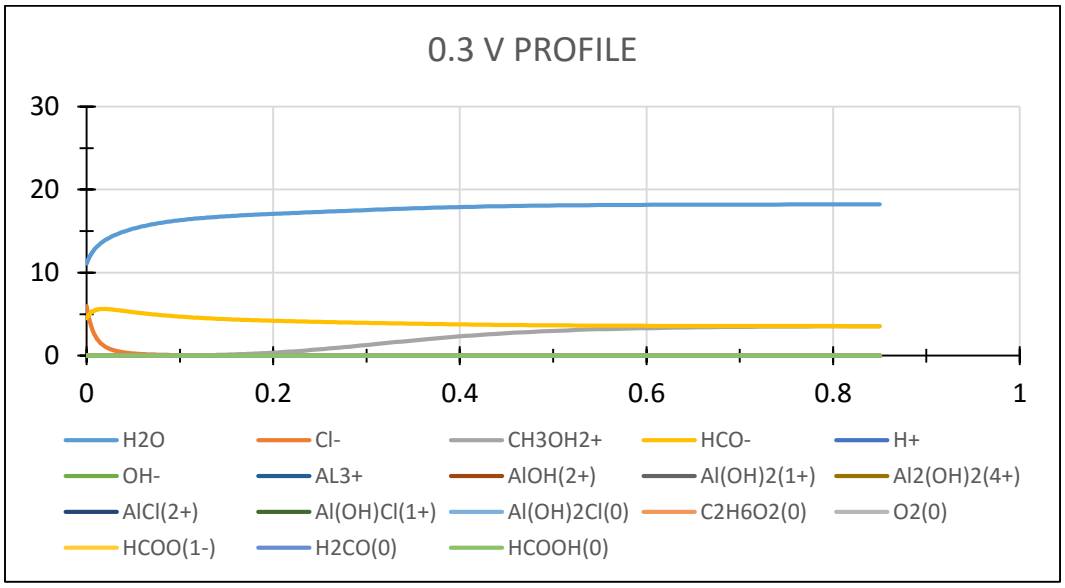

Figure 4.2.1: Concentration profile for 0.3 V at 333 K temperature

it is observed that HCO^- ion concentration begins to fall with a gradual increase in Cl^- ion concentration. Also, the water concentration falls to 11.13 at the metal surface.

The packing fraction profile shows the increase in density or concentration at the metal surface, with increase in voltage and hence increase in pressure of the ions.

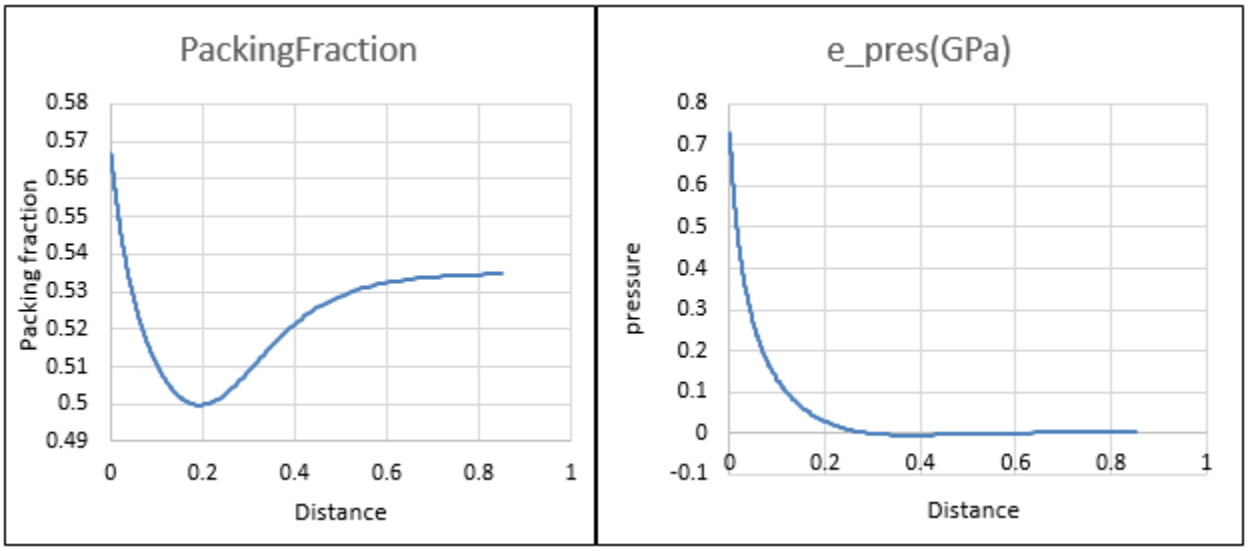

Figure 4.2.2: Packing fraction and Pressure profiles for 0.3 V at 333 K temperature

The maximum packing fraction attained at the metal surface is 0.564. The dip in the packing fraction profile is shifted to the distance of 0.19nm from the surface in comparison to the earlier case. The maximum pressure obtained at the surface is 0.72GPa which increases in correspondence with the packing fraction. The sudden pressure change range shifts to the region between 0.12-0.29nm distance from the surface.

The velocity profile is similar to earlier case. The maximum velocity of diffusing ions attained is

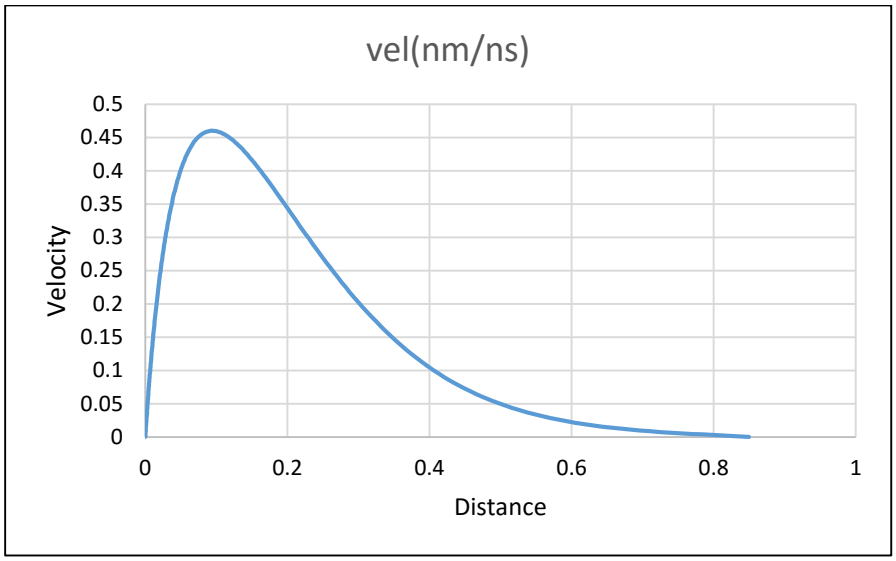

Figure 4.2.3: Velocity profile for 0.3 V at 333 K temperature

0.46, at a distance of 0.11nm from the surface.

4.3. 0.4 V, 333 K temperature

Applying 0.4V, at 333K temperature and Al flux of 3d-11 e/nm^2/ns, it is observed that,

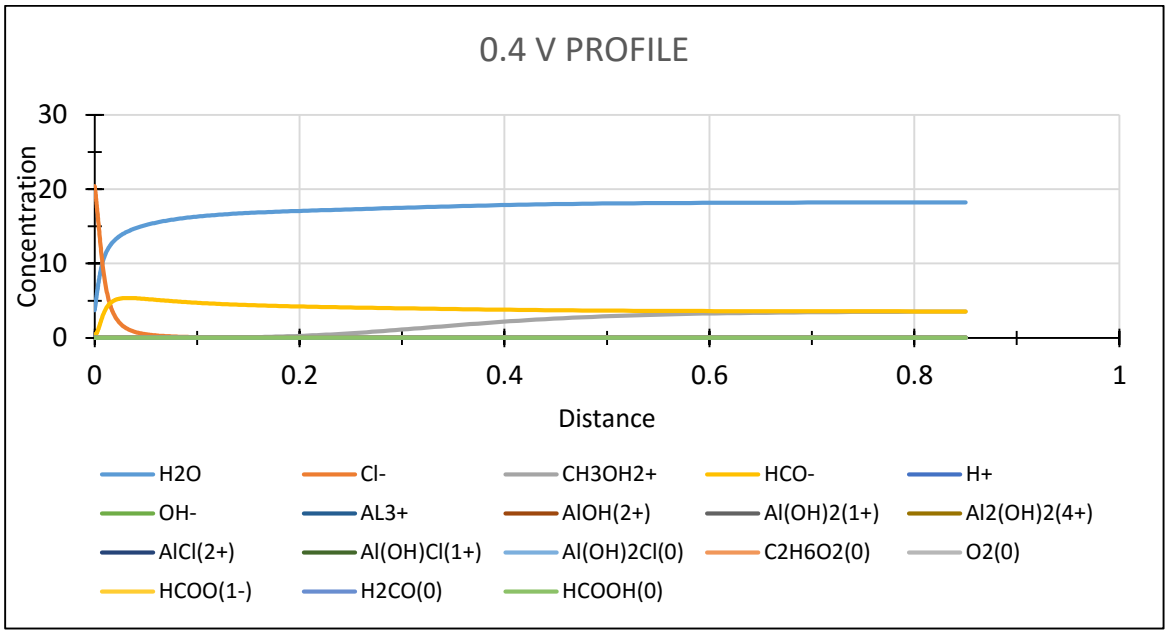

Figure 4.3.1: Concentration profile for 0.4 V at 333 K temperature

HCO^- ion concentration falls to zero and it no longer takes part in corrosion. Meanwhile, the Cl^- ion concentration increases to 20.28 and water concentration falls drastically to 3.8. This increased Cl^- ion concentration is the reason for the first pit formed on the Aluminum surface. There is a noticeable change in the packing fraction profile and pressure profile as well.

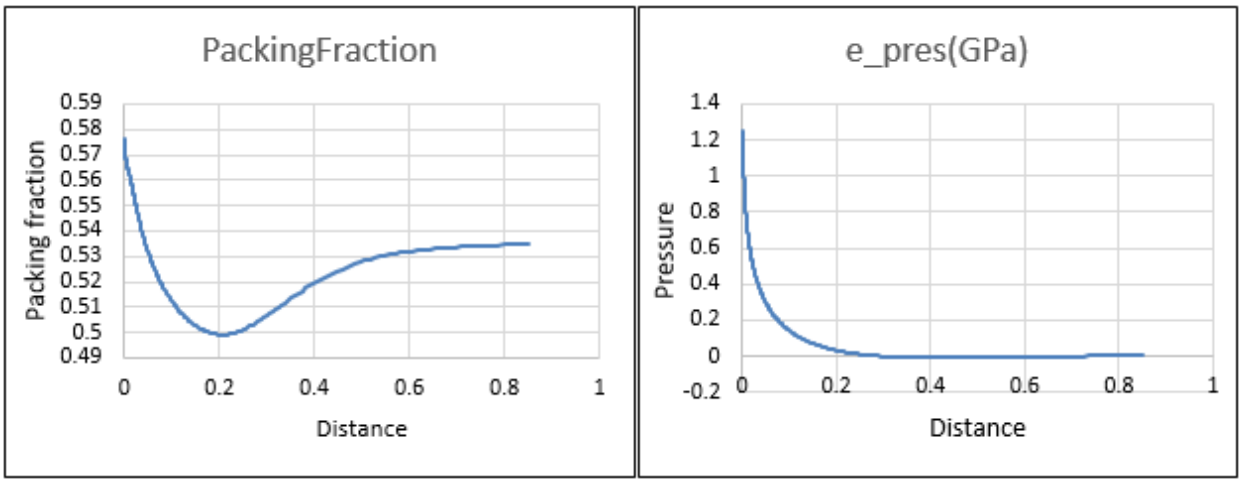

Figure 4.3.2: Packing fraction and Pressure profiles for 0.4 V at 333 K temperature

The maximum packing fraction obtained is 0.573 which shows the increase of density of ions with increase in voltage. The dip in the profile is shifted to the distance of 0.203nm from the surface. There is a corresponding increase in the diffusion pressure. The maximum pressure obtained at the metal surface is 1.27GPa. The sudden pressure change range is observed between 0.17-0.27nm distance from the surface.

The maximum velocity attained by diffusing ions in this case is 0.54nm/ns at a distance of 0.1nm from the metal surface.

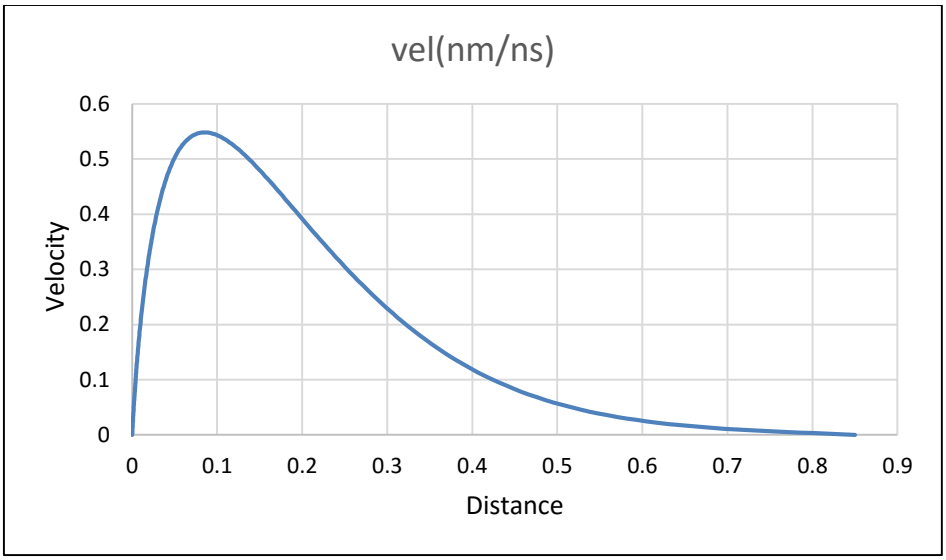

Figure 4.3.3: Velocity profile for 0.4 V at 333 K temperature

4.4. 0.5 V, 333 K temperature

Incrementing the voltage to 0.5V, at 333K temperature at Al flux of 2.08d-11 e/nm^2/ns, the following is observed.

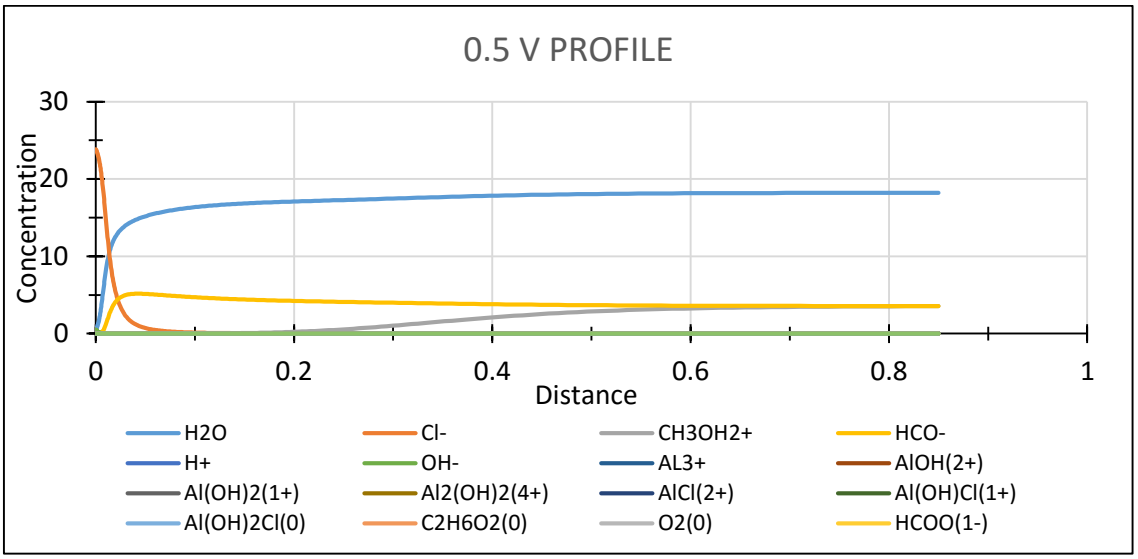

Figure 4.4.1: Concentration profile for 0.5 V at 333 K temperature

The Cl^- ion concentration reaches its peak value of 23.83. In this case, the pitting of Aluminum surface is maximum as chlorine is the only dominating corrosion species. The concentration of water falls to zero at the metal surface as it is displaced by Cl^- ions.

The packing fraction profile shows a drastic change than other cases.

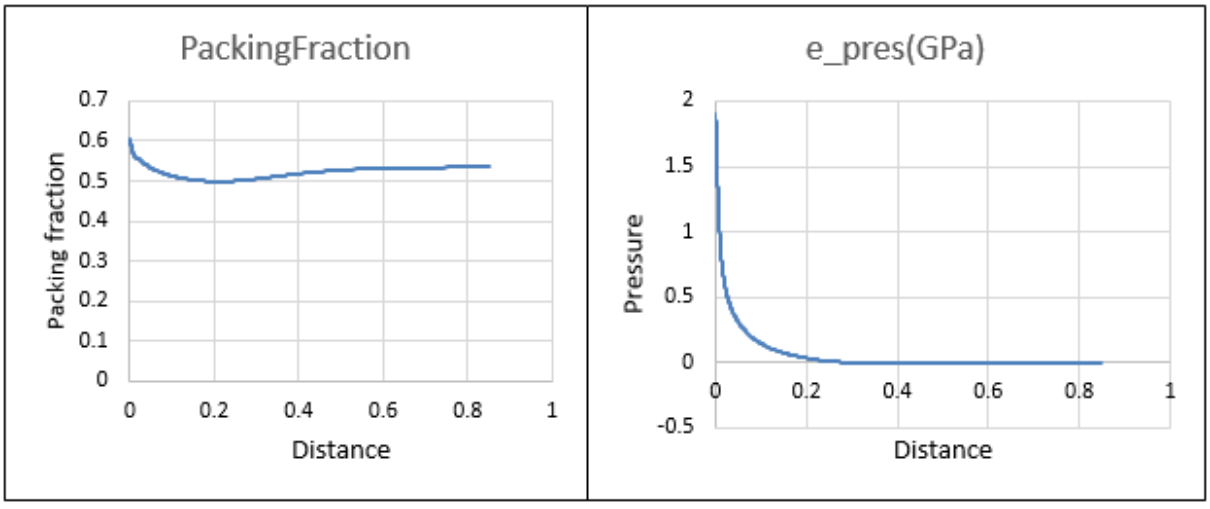

Figure 4.4.2: Packing fraction and Pressure profiles for 0.5 V at 333 K temperature

I this case there is a sudden change in packing fraction profile from metal surface towards the electrolyte bulk. The sudden dip profile is changed to gradual decrease and then followed by gradual increase in the packing fraction as we move towards the electrolyte side. The maximum packing fraction attained is 0.6 at the metal surface. Correspondingly, the maximum pressure obtained at the metal surface is 1.88GPa. The sudden change in pressure is observed between the distance from 0.03nm to 0.24nm.

The maximum velocity of 0.63nm/ns is attained at a distance of 0.078nm from the metal surface.

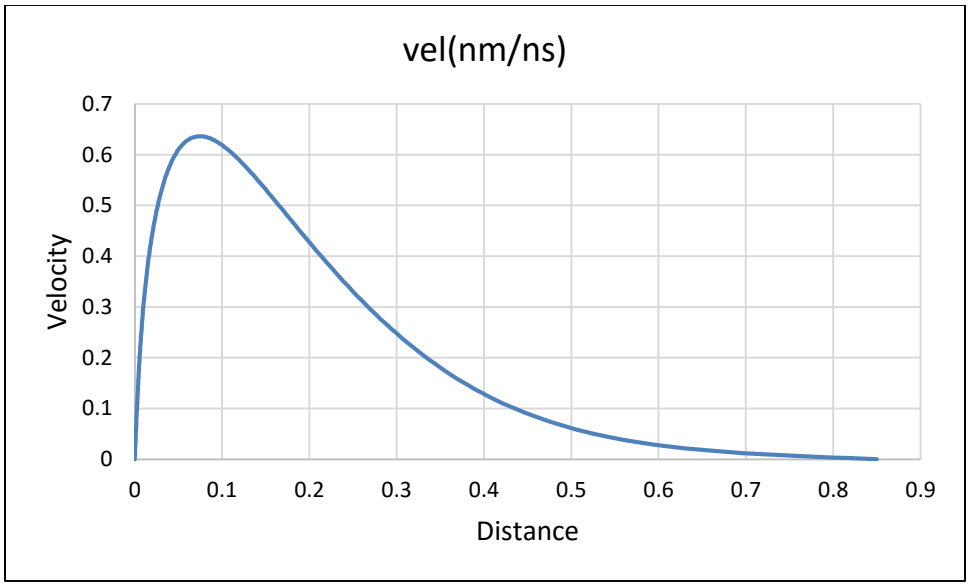

Figure 4.4.3: Velocity profile for 0.5 V at 333 K temperature

4.5. 0.8 V, 333 K temperature

Further incrementing the voltage to 0.8V, at 333K temperature and Al flux of 1d-10 e/nm^2/ns, a significant change is observed in the ion concentrations.

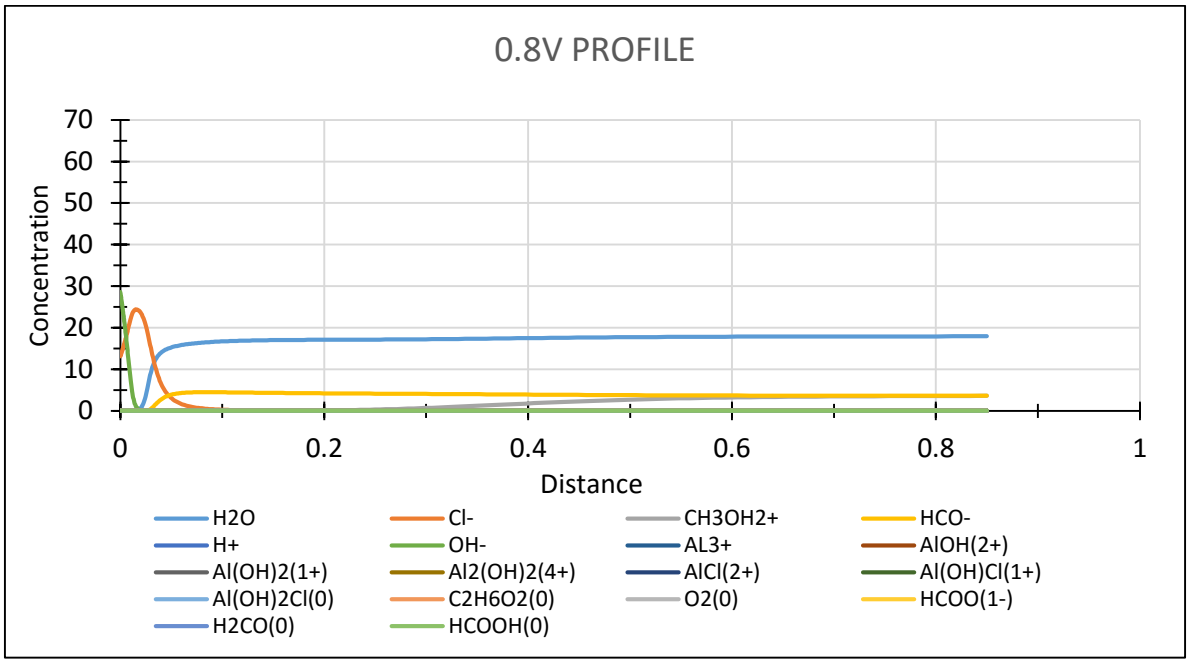

Figure 4.5.1: Concentration profile for 0.8 V at 333 K temperature

In this case, the Cl^- ion concentration decreases with increase in OH^- ion concentration. These two ions diffusing towards the metal surface leads to the displacement of water molecules away from the metal surface into the bulk of the electrolyte. Thus, the water concentration at the metal surface is zero. This is where pitting rate of Aluminum gradually starts decreasing as a result of formation of Aluminum hydroxide layer over the pit surface.

The packing fraction profile is similar to the earlier case with a maximum value of 0.63 at the

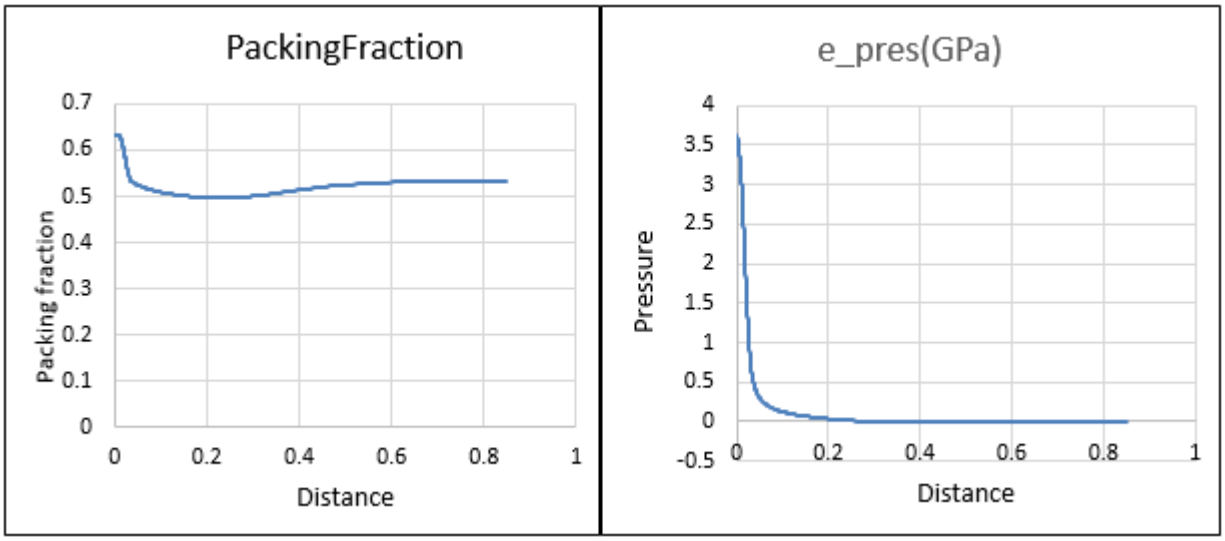

Figure 4.5.2: Packing fraction and Pressure profiles for 0.8 V at 333 K temperature

metal surface. The maximum pressure at the metal surface is 3.6GPa. The sudden pressure change region is obtained between the distance 0.04-0.22nm from the metal surface.

The velocity profile is similar to earlier cases.

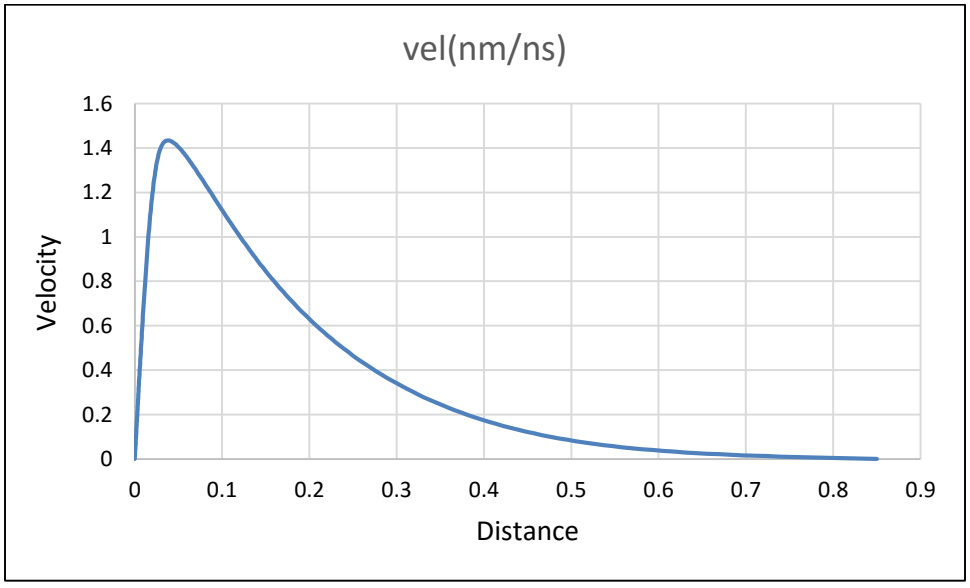

Figure 4.5.3: Velocity profile for 0.8 V at 333 K temperature

The maximum velocity attained is 1.43nm/ns at a distance of 0.04nm from the metal surface.

4.6. 1 V, 333 K temperature

After applying 1V, at 333K temperature with Al flux of 2d-10 e/nm^2/ns, it is observed that,

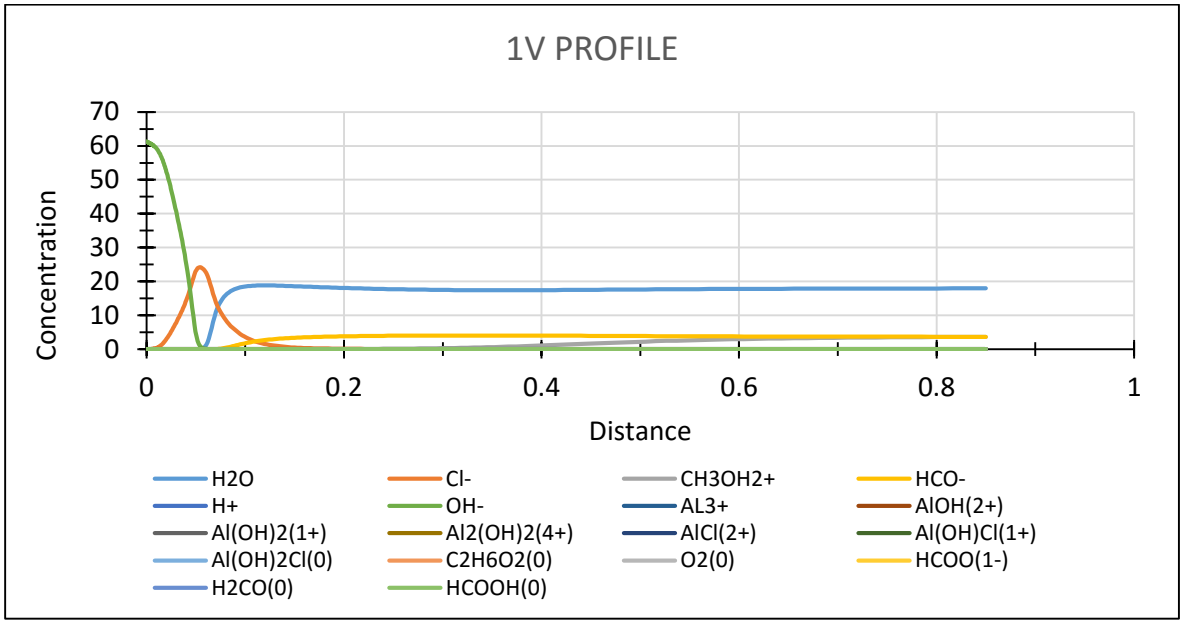

Figure 4.6.1: Concentration profile for 1 V at 333 K temperature

Cl^- ion concentration drops to zero. At this voltage, pitting stops completely as the pit is covered with a layer of Aluminum hydroxide to avoid further ion exchange. This is evident from the observation of the increased OH^- ion concentration diffusing towards the metal surface. The water molecules are displaced further away from the metal surface.

Packing fraction profile displays a change in nature than the earlier two cases.

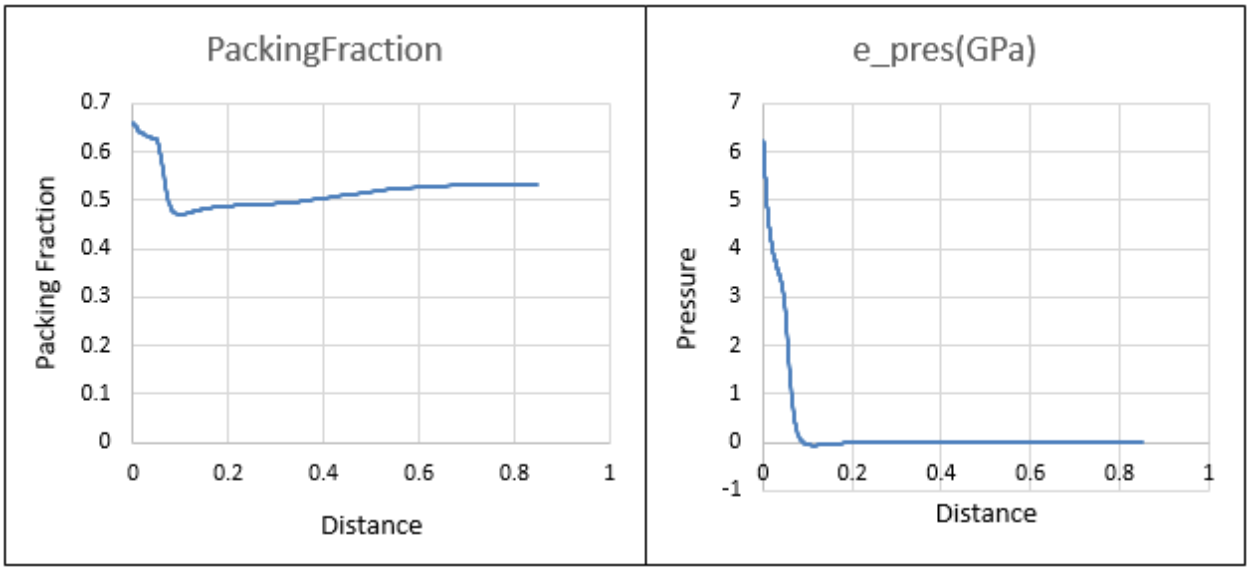

Figure 4.6.2: Packing fraction and Pressure profiles for 1 V at 333 K temperature

Maximum packing fraction at the surface is 0.65. There is a sudden decrease in the profile up to 0.04nm distance from the surface and then gradual decrease till 0.1nm distance. The maximum pressure is 6.12 GPa. The region of sudden pressure change is narrow as compared to earlier cases.

The maximum velocity is 3.72nm/ns at a distance of 0.07nm from the surface.

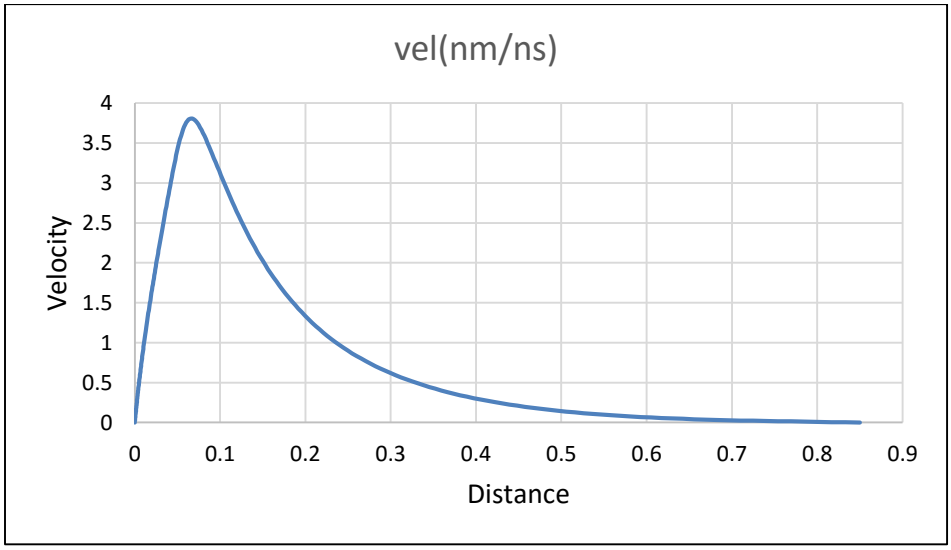

Figure 4.6.3: Velocity profile for 1 V at 333 K temperature

4.7. 1.2 V, 333 K temperature

Now, applying 1.2V, at 333 K temperature and Al flux of 6.45d-10 e/nm2/ns.

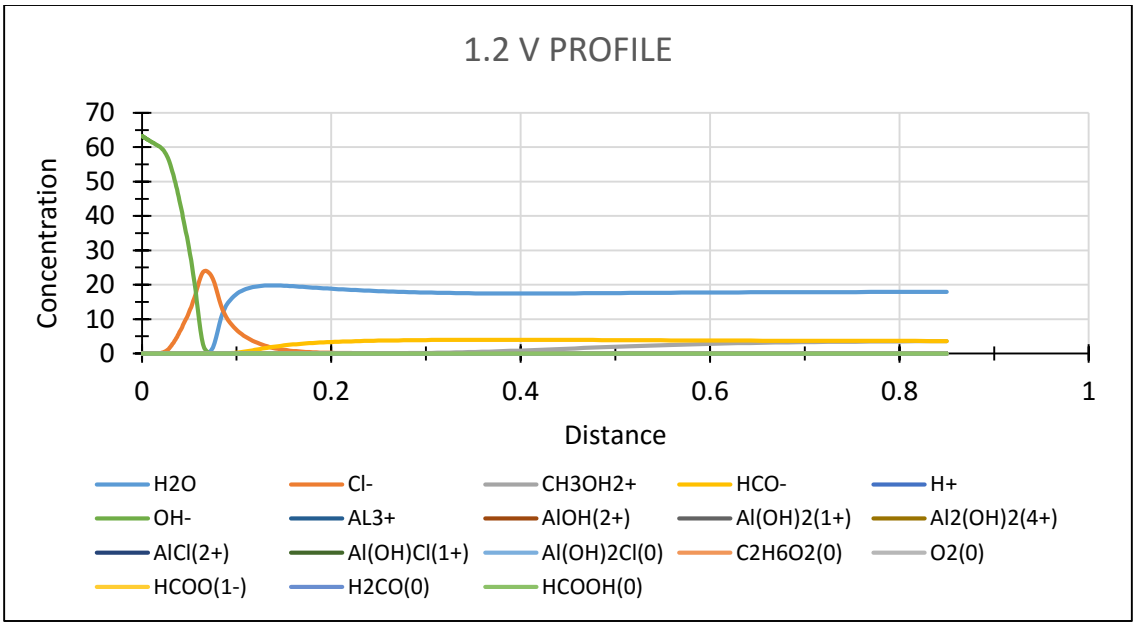

Figure 4.7.1: Concentration profile for 1.2 V at 333 K temperature

It is observed that OH^- ion concentration increases more than the earlier case. Cl^- ions and water are displaced further away from the metal surface. It implies that with further increase in voltage, concentration of hydroxyl ions diffusing towards the surface increases and hence impedes corrosion process.

The change in packing fraction profile is more gradual as compared to the earlier case with a maximum value of 0.68.

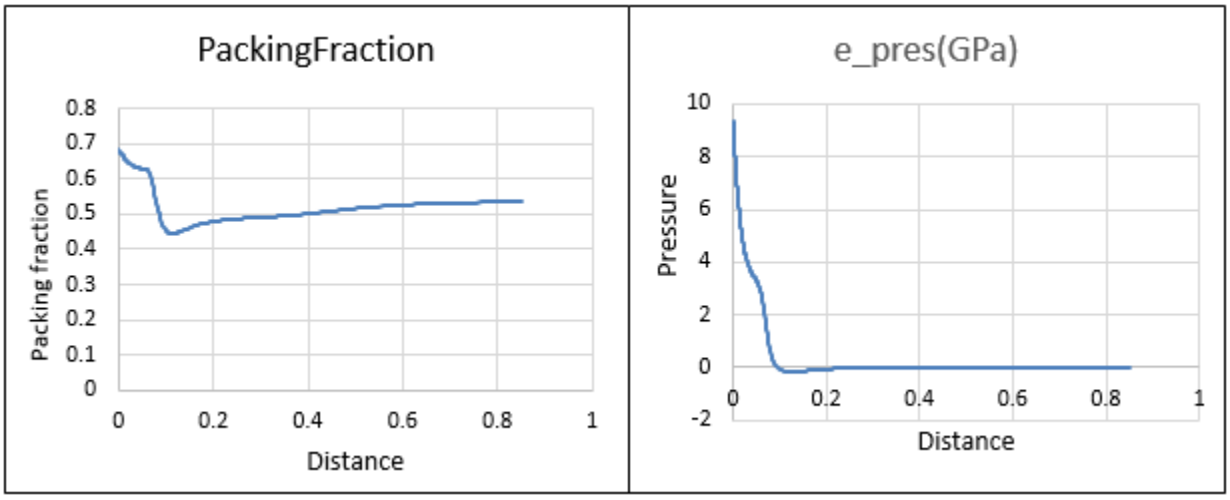

Figure 4.7.2: Packing fraction and Pressure profiles for 1.2 V at 333 K temperature

The maximum pressure is 9.31 GPa at the metal surface. There is a sudden change of pressure at 0.1nm from the surface. The cavitation must be highest in this case, compared to all other cases. Thus, the general trend in the observations at 333 K temperature with voltage increment is that corrosion process is active at low voltages and it tends to decrease gradually with increase in voltage. Simultaneously, the packing fraction and pressure values at the metal surface increase with voltage. From the pressure profiles it can be observed that as voltages increases the change in pressure is more drastic.

4.8. 0.3 V, 373 K temperature

Another case is studied with voltage increment at 100° C, 373 K temperature at same pH= 6.47.

Applying 0.3V, it is observed that HCO^- ions and Cl^- ions diffuse towards the metal surface but have very low concentrations.

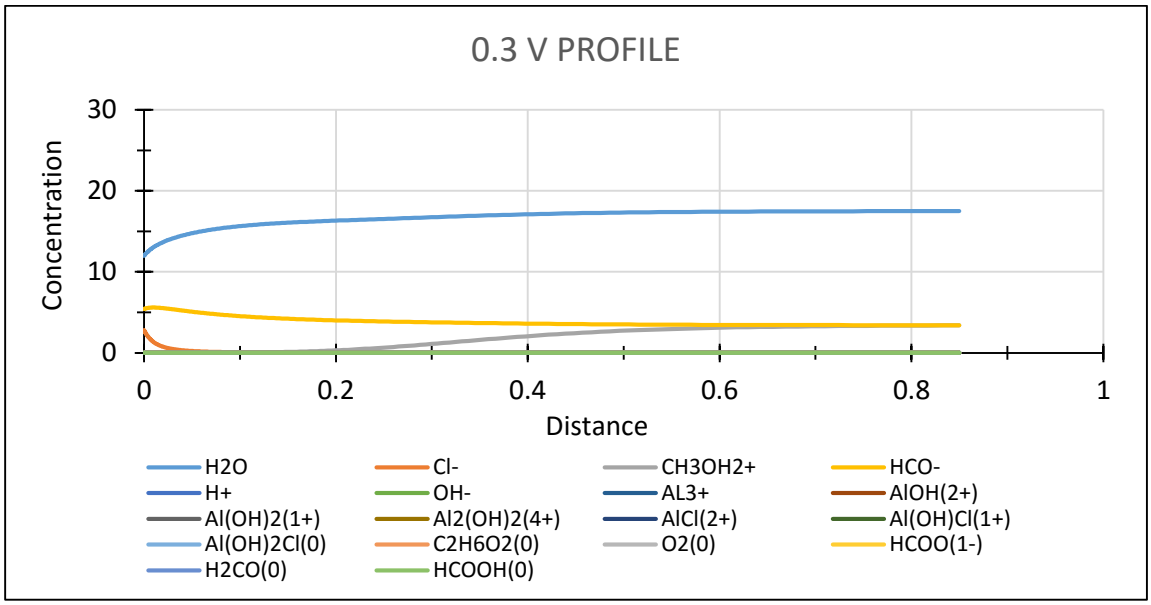

Figure 4.8.1: Concentration profile for 0.3 V at 373 K temperature

The water concentration is also high at the metal surface (about 12).

The packing fraction, i.e. is the density of ions in electrolyte is high close to the metal surface and decreases gradually to form a dip at a distance of 0.2nm from the surface.

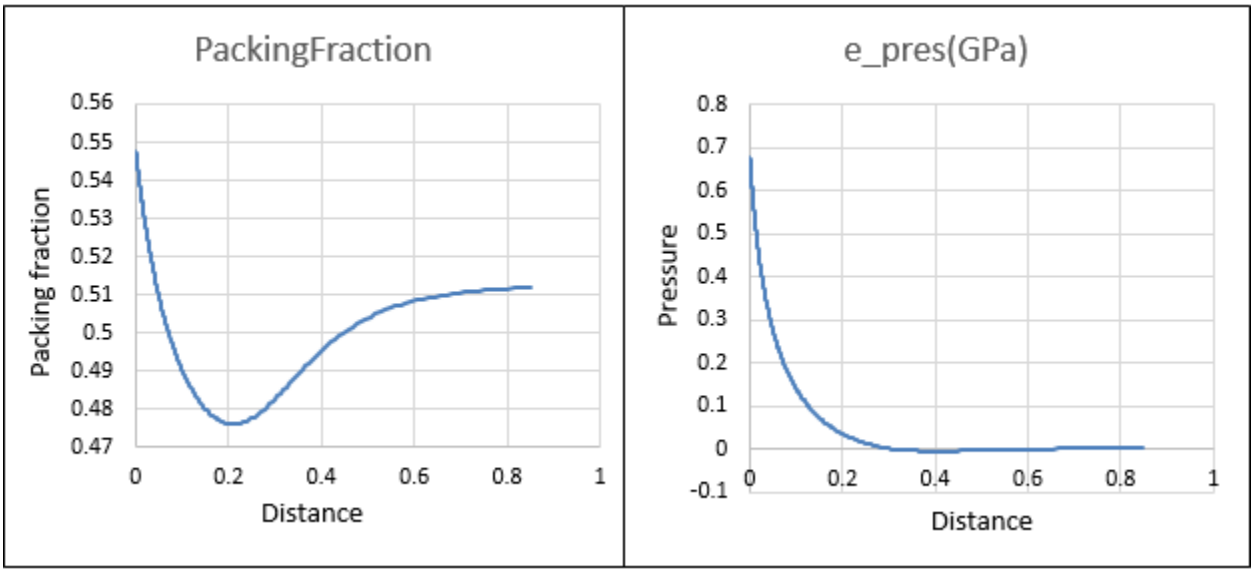

Figure 4.8.2: Packing fraction and Pressure profiles for 0.3 V at 373 K temperature

It then increases exponentially away from the surface. The maximum packing fraction attained at the surface is 0.546. Simultaneously, the diffuse pressure of ions is also high at the surface and then decreases gradually away from the surface. The maximum pressure is 0.656 GPa.

The velocity of diffusing ions is maximum at the point where there is minimum density or minimum packing fraction.

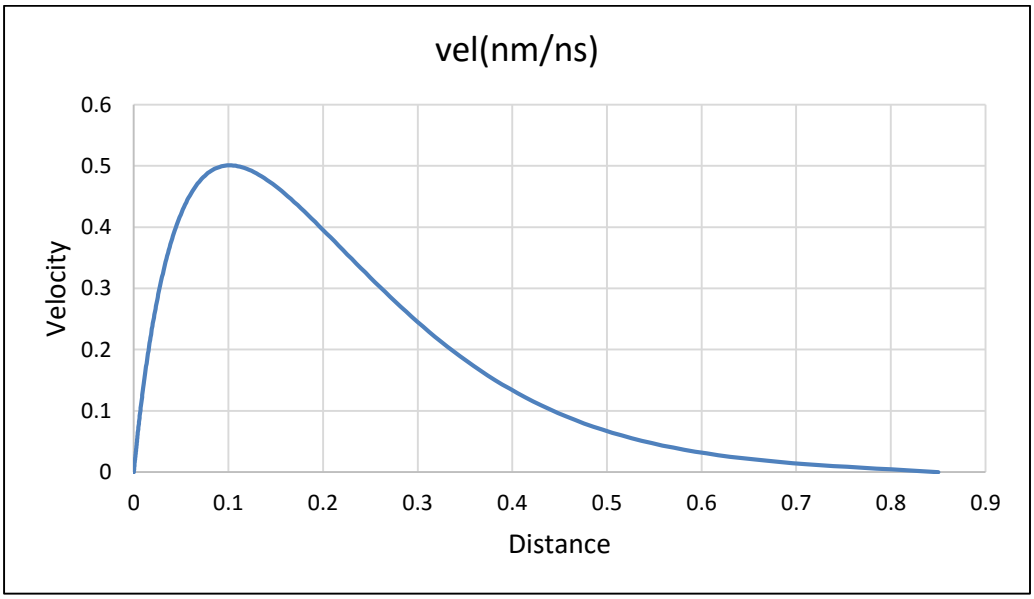

Figure 4.8.3: Velocity profile for 0.3 V at 373 K temperature

Maximum velocity is 0.5nm/ns, attained at 0.107 nm from the surface.

4.9. 0.4 V, 373 K temperature

Incrementing the voltage to 0.4V, it is observed that HCO^- ion and water concentration decreases, but water is still at the metal surface. Cl^- ion concentration increases and becomes dominant corroding species and diffuses towards the surface.

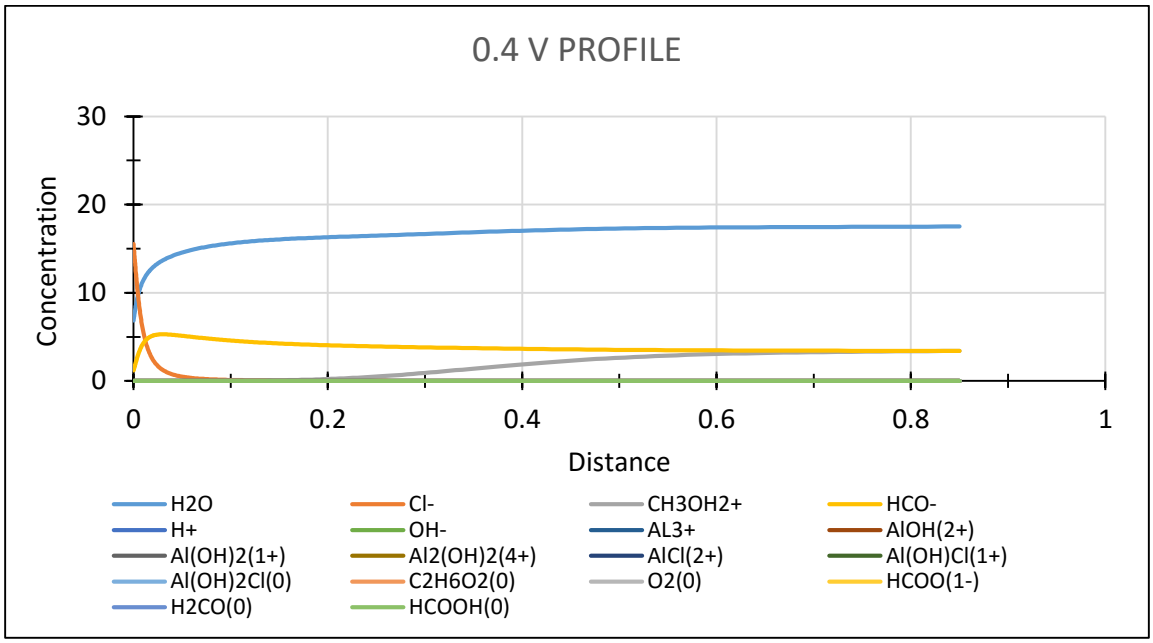

Figure 4.9.1: Concentration profile for 0.4 V at 373 K temperature

Packing fraction profile shows gradual changes as compared to the earlier case.

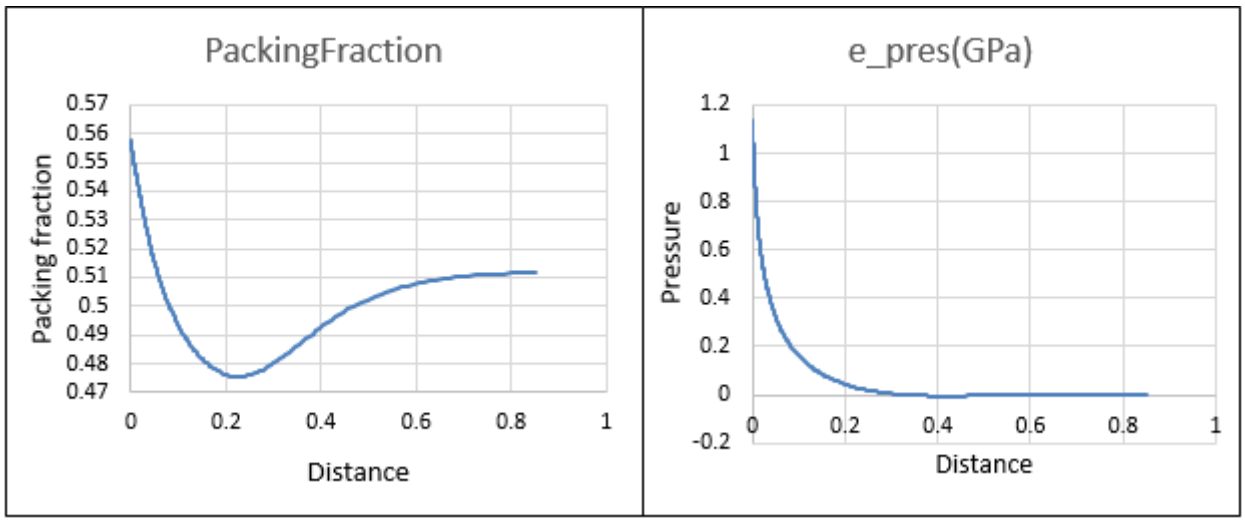

Figure 4.9.2: Packing fraction and Pressure profiles for 0.4 V at 373 K temperature

The maximum packing fraction is 0.555 at the metal surface. The sudden dip in the pressure profile is seen at 0.23nm from the surface. The maximum pressure at the surface is 1.11GPa. The pressure of diffuse ions increases as they near the surface.

The maximum velocity at 0.09nm distance is 0.604 nm/ns where the packing fraction is minimum.

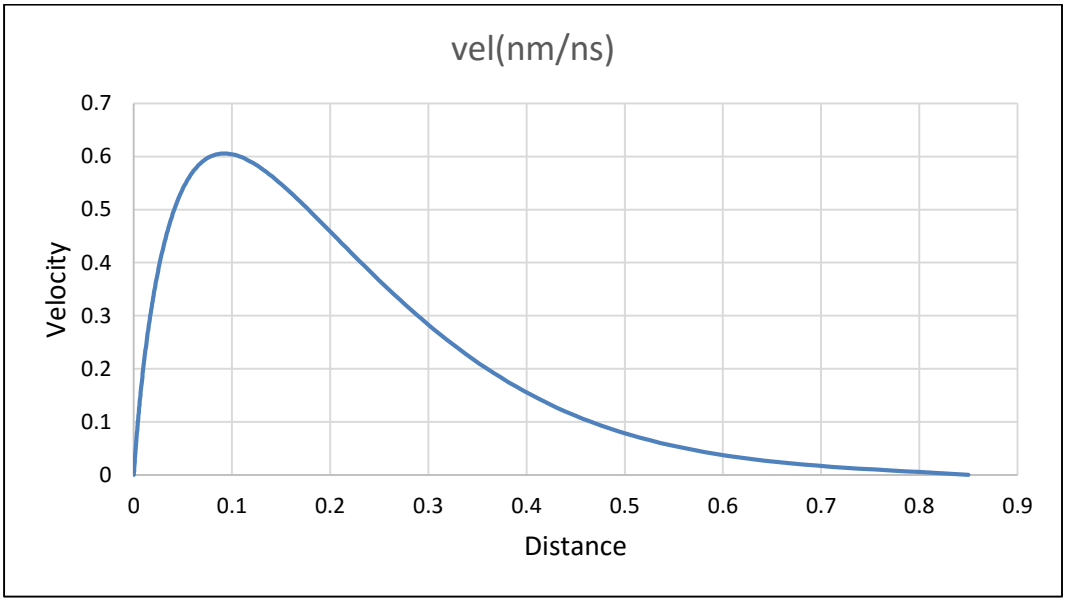

Figure 4.9.3: Velocity profile for 0.4 V at 373 K temperature

4.10. 0.8 V, 373 K temperature

At 0.8V, there is a significant change in the concentration profile.

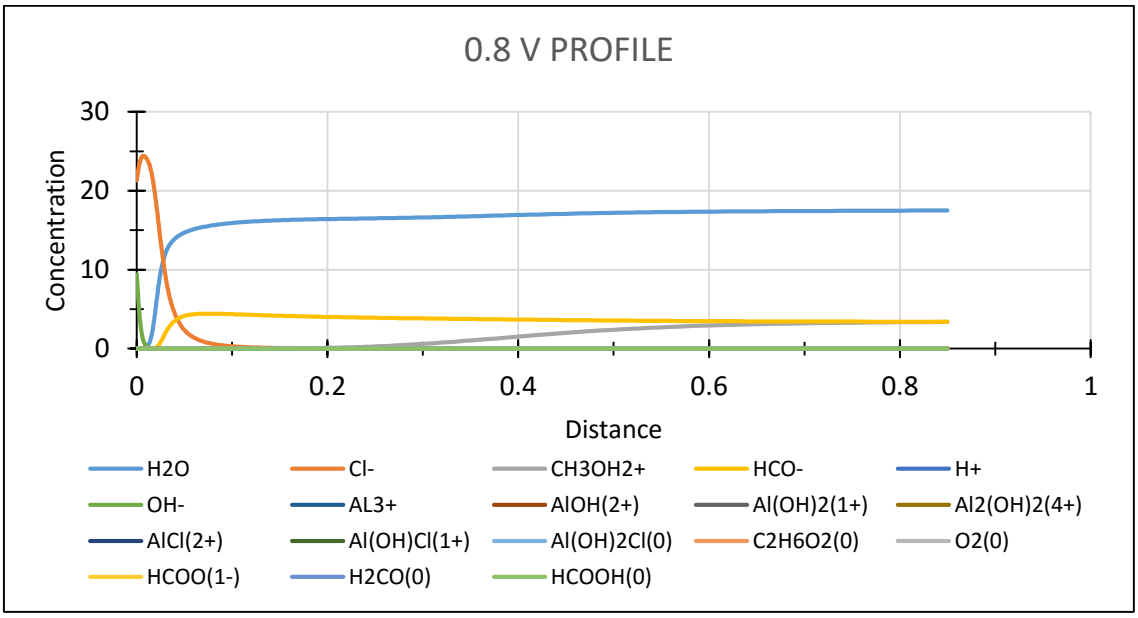

Figure 4.10.1: Concentration profile for 0.8 V at 373 K temperature

In this case, Cl^- ion concentration is high which causes pitting at the Aluminum surface. Simultaneously, at 373K and 0.8 V, water starts to split, thus raising the OH^- ion concentration. The diffusion of chloride and hydroxyl ions towards the metal surface, results in displacement of water away from the metal surface.

The packing fraction profile shows a significant change as well. The sudden dip in profile is changed to gradually decreasing and then increasing profile.

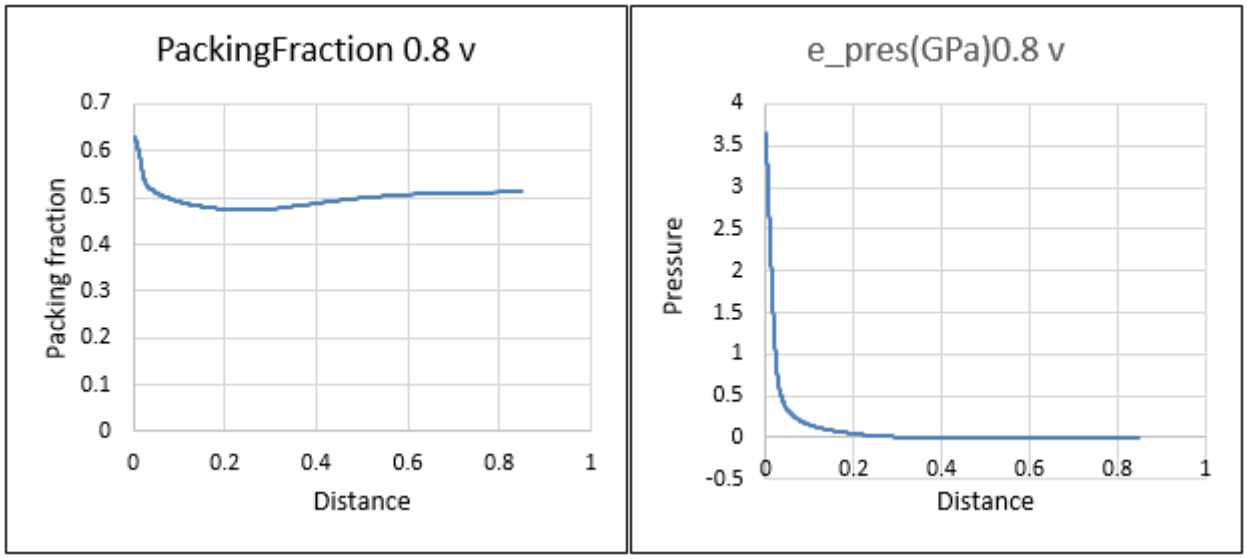

Figure 4.10.2: Packing fraction and Pressure profiles for 0.8 V at 373 K temperature

The maximum packing fraction at the metal surface is 0.63. Correspondingly, the pressure profile shows the distribution of pressure close to the surface is high as compared to earlier case. The maximum pressure attained is 3.6 GPa.

The maximum velocity (1.22nm/ns) is attained at 0.55nm distance where there is minimum packing density.

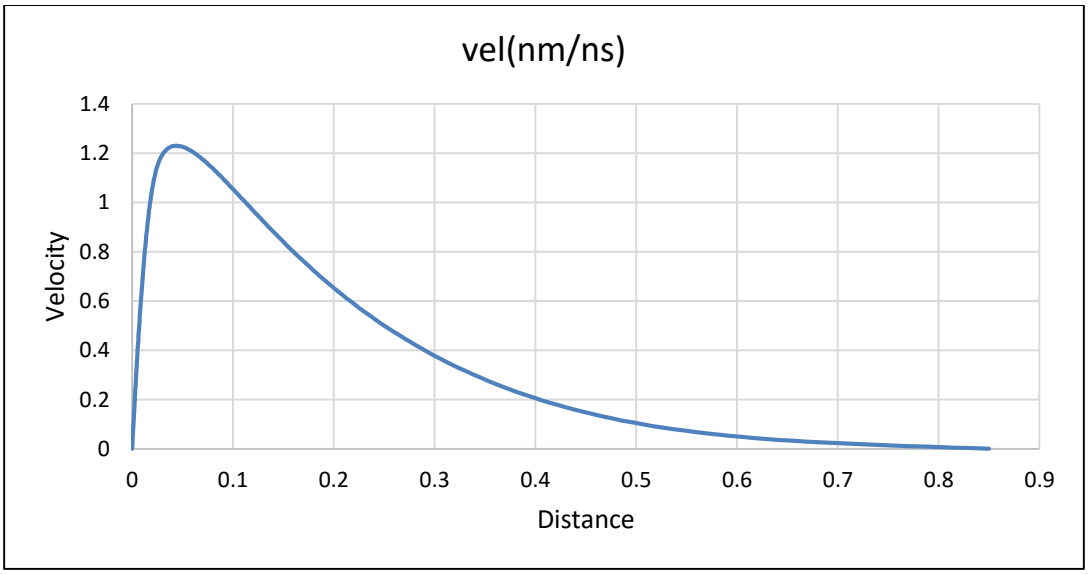

Figure 4.10.3: Velocity profile for 0.8 V at 373 K temperature

4.11. 1 V, 373 K temperature

Incrementing the voltage to 1V,

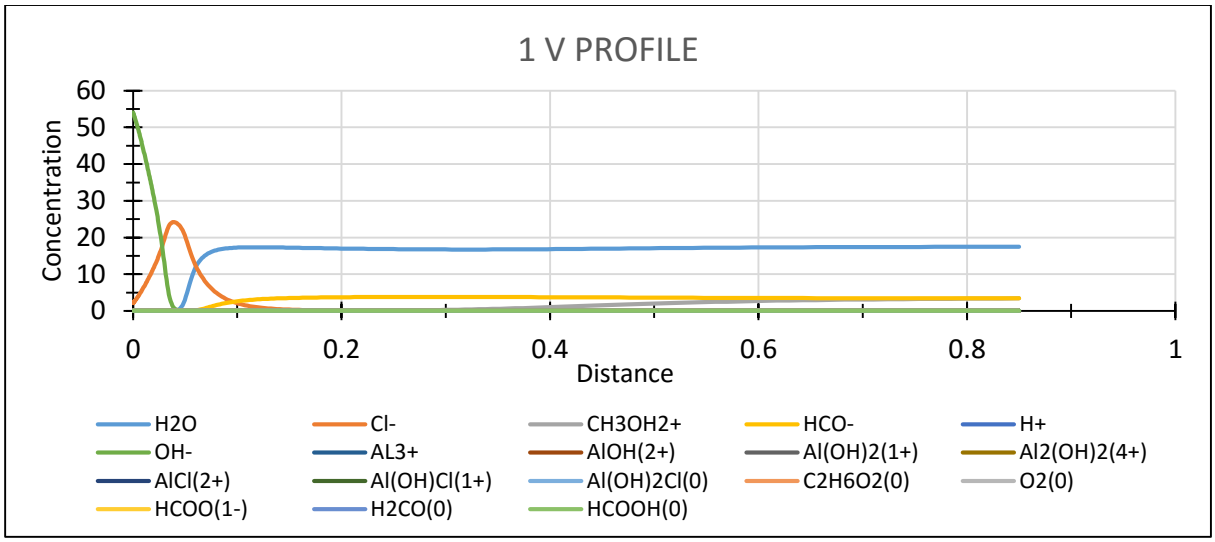

Figure 4.11.1: Concentration profile for 1 V at 373 K temperature

it is observed that Cl^- ion concentration drops drastically with increase in OH^-ion concentration. Here, the dominant OH^- ions diffuse towards the metal surface to form Aluminum hydroxide which precipitates along the pit boundary and avoids further ion exchange. The water is displaced further away from the Aluminum surface.

Packing fraction gradient is high till 0.04nm distance from the surface and then the profile decreases gradually till 0.09nm distance. The maximum packing fraction obtained is 0.634 at the metal surface.

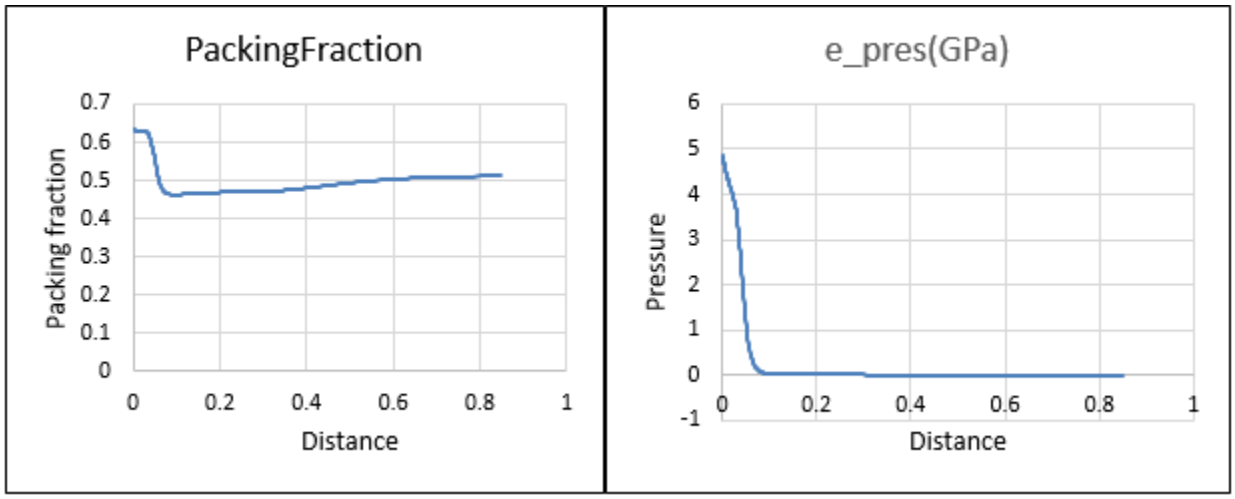

Figure 4.11.2: Packing fraction and Pressure profiles for 1 V at 373 K temperature

The maximum pressure at the wall is 5.48 GPa and there is a sudden change in pressure at 0.11nm from the surface.

The maximum velocity of 3.26nm/ns is achieved at a distance of 0.06nm from the surface.

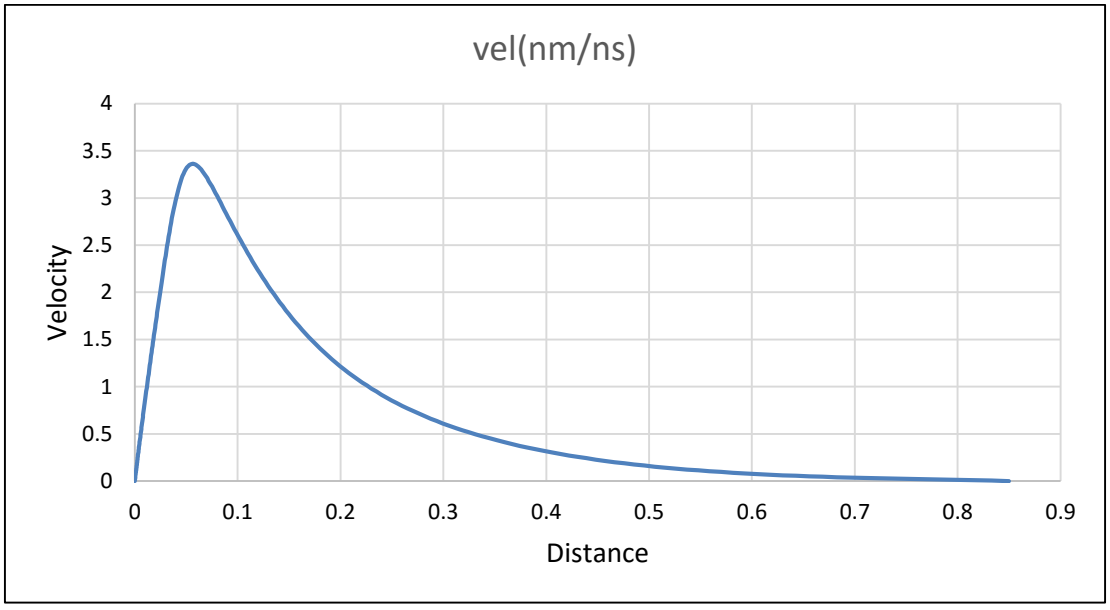

Figure 4.11.3: Velocity profile for 1 V at 373 K temperature

4.12. 1.2 V, 373 K temperature

At 1.2 V, Cl^- ions are displaced away from the metal surface due to increased concentration of OH^- ions at the metals surface.

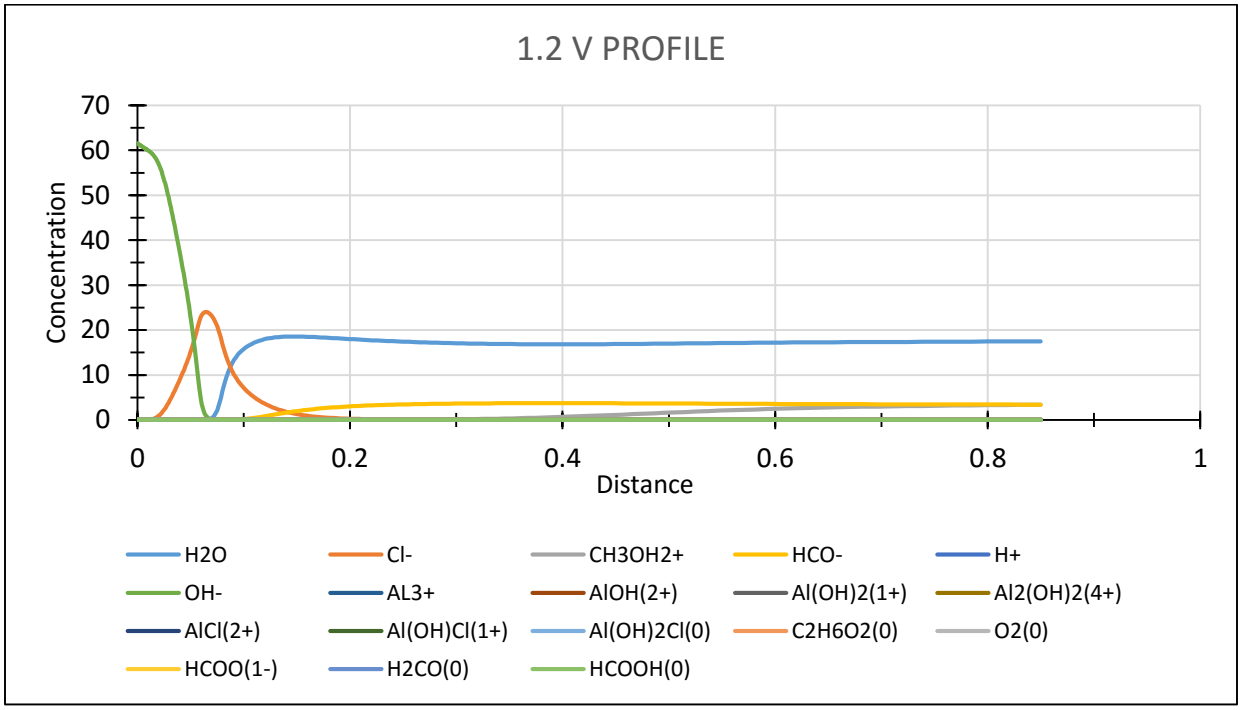

Figure 4.12.1: Concentration profile for 1.2 V at 373 K temperature

Water molecules are also displaced away from the metal surface. In this case, corrosive action stops completely unless acted upon by some other factors, as there is no ion exchange taking place between Aluminum surface and chloride ions in the electrolyte.

The packing fraction shows a gradual change in the profile as compared to the earlier case.

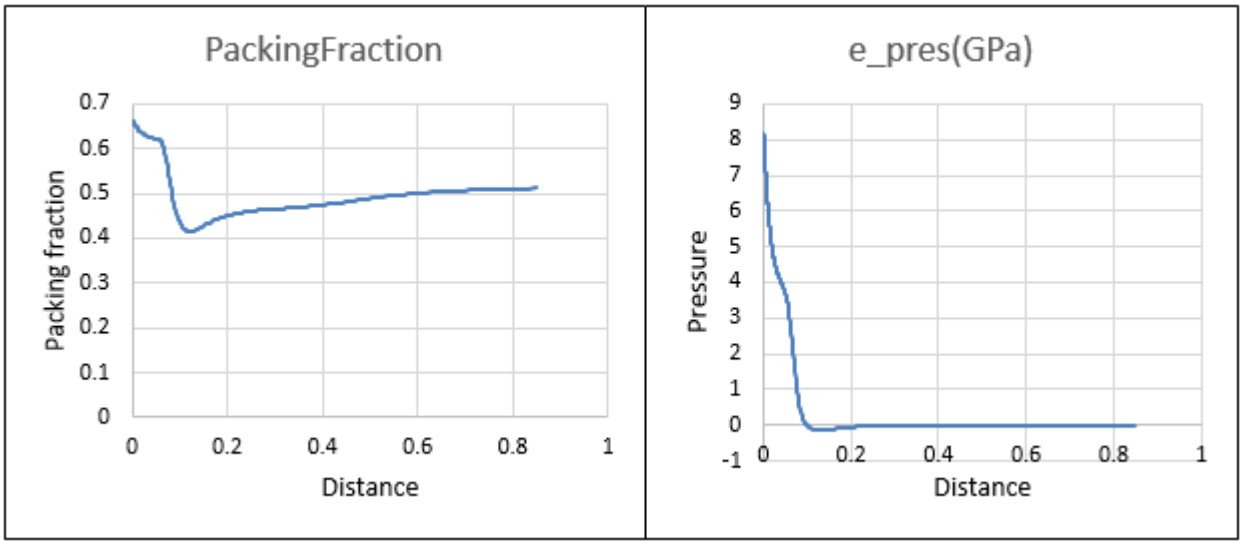

Figure 4.12.2: Packing fraction and Pressure profiles for 1.2 V at 373 K temperature

Maximum packing density attained is 0.64 at the metal surface. Correspondingly, the maximum pressure at the surface obtained is 8.1 GPa. Further increase in voltage will lead to increased OH^- ion concentration at the metal surface.

Parametric study at two different temperatures leads to the observation that at higher temperature (373 K), the OH^- ions diffuse to the surface at a later voltage (1V), compared to lower temperature (333 K), where it diffuses at lesser voltage (0.8 V). The packing fraction and pressure achieved at 373 K for a certain voltage is less than that achieved for 333 K. The velocity of the ions in the electrolyte is high at 373K because of weak intermolecular forces.

Study of pressure profile reveals that as the voltage is incremented, the slope increases. The dip in the packing fraction profile becomes more acute with increase in voltage.

Chapter 5

RESULTS DISCUSSION

At higher temperatures, ethylene glycol undergoes thermal degradation to form carboxylic acids like formic acid, glycolic acid and oxalic acid. The carboxylic acids are considered to be a highly polar organic functional group. This polarity results from the presence of a strongly polarized carbonyl (C=O) group and hydroxyl (O-H) group. In the case of carboxylic acids, the O-H group is even more strongly polarized than the O-H group of alcohols due to the presence of the adjacent carbonyl moiety. These structural features not only enhance dipole strength, but also are responsible for the acidity of these compounds [18].

Considering the case of 333 K temperature at two different voltages, it is observed that,

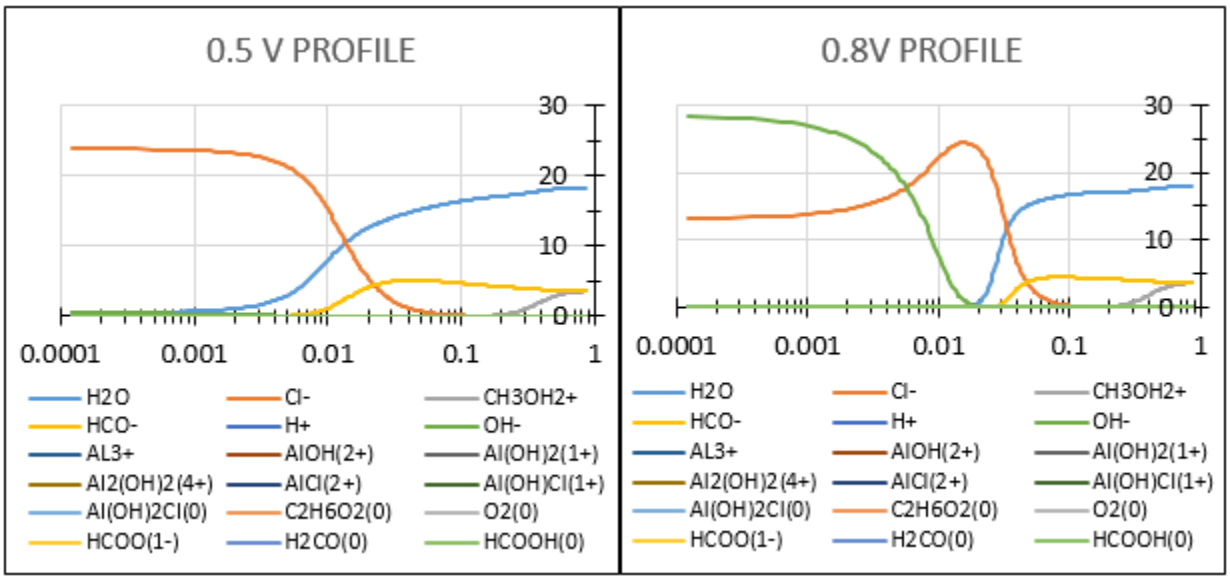

Figure 5.1: Comparison of concentration profile between 0.5 V and 0.8 V at 333 K temperature

at 0.5 V, Chloride ions are dominant which cause pitting in aluminum surface. As the voltage is increased to 0.8 V, Cl^- ions reach saturation and OH^- ion concentration rises. Moreover, carboxylic acids formed in the system dissociates to produce OH^- ions. This phenomenon is

explained by **Second Wien Effect** or **Dissociation Field Effect**. The **Wien effect** is the experimentally-observed increase in ionic mobility or conductivity of electrolytes at high electric potential. The dipoles present in carboxylic acids allow hydrogen bonding (H-bonding) interactions, which eats up the chloride ions and hence its concentration decreases. In addition to this, the stokes radius of OH^- ions is less than Cl^- ions and relative permittivity of the former is greater than the latter [16] [17]. At this voltage, OH^- ions react with Al^{3+} ions at the surface to form Aluminum hydroxide ($Al_2(OH)_3$) which precipitates along the pit surface and avoids any further ion exchange, unless this layer is broken by some other factors.

Similar phenomena are seen at 373 K temperature, but the influx of OH^- ions is observed at a greater voltage of 1V.

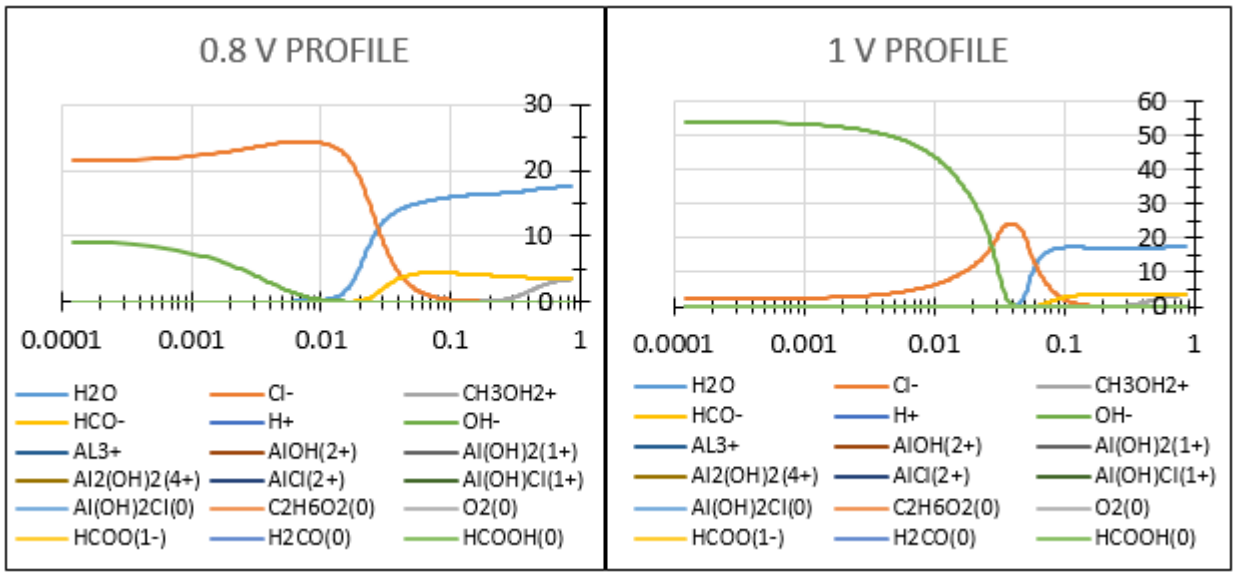

Figure 5.2: Comparison of concentration profile between 0.8V and 1 V at 373 K temperature

At high temperature of 373 K, chemical polarity of water decreases as its relative permittivity decreases with increase in temperature. Carboxylic acids are protic solvents (relative permittivity > 15). Protic solvents solvate anions strongly via Hydrogen bonding. The decreased chemical

polarity of carboxylic acids represses its ability to solvate Cl^- ions and produce OH^- ions in the electrolyte [18]. Thus, it takes greater voltage at 373 K temperature than 333 K for OH^- ions to diffuse towards the metal surface and form aluminum hydroxide that blocks the pit. Further ion exchange is prohibited until acted upon by other factors. Therefore, more corrosion is caused at higher temperature.

Now, considering the comparison of packing fraction and pressure profiles for 333 K temperature at 0.2V and 1.2 V respectively it is observed that, at 0.2 V, there is gradual change in pressure profile.

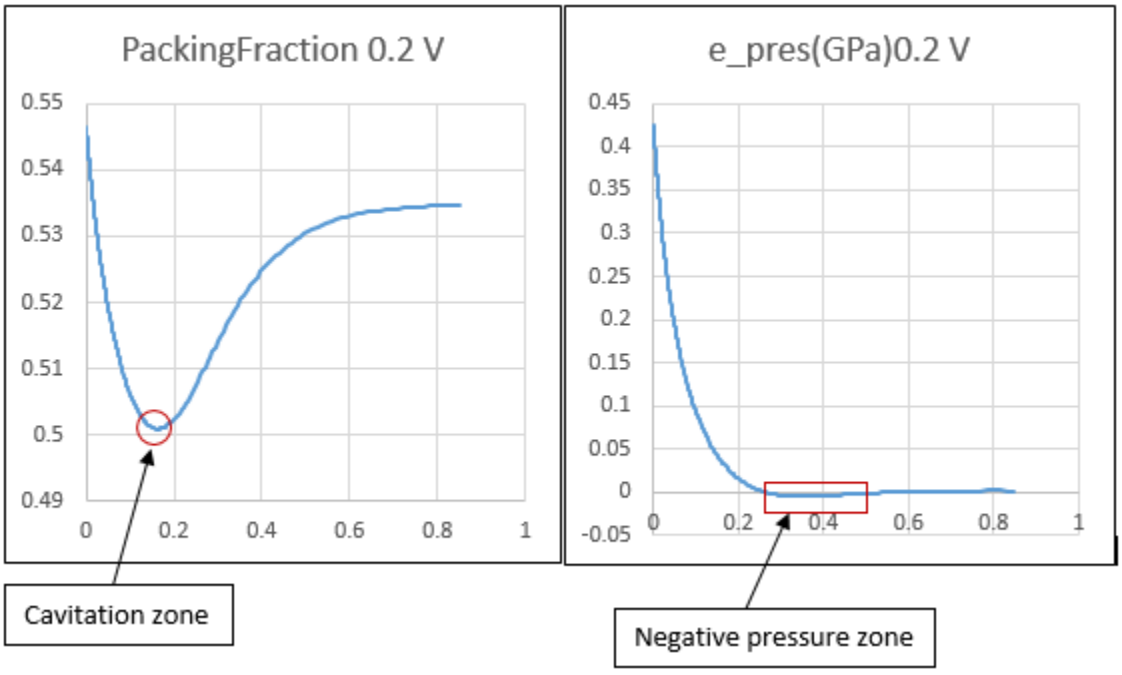

Figure 5.3: Cavitation phenomenon for 0.2 V at 333 K temperature

Change in packing fraction profile is gradual as well. There is a range of negative pressure obtained in region from 0.265nm to 0.58 nm distance. This zone is the vaporization zone [16]. Correspondingly, density of vapor is low and hence the packing fraction is small in this zone. Moving towards the metal surface, it is seen that there is a sudden pressure rise from negative to

positive pressure of 8.39e-5 GPa at 0.26 nm distance. This sudden rise in pressure leads to **cavitation. Cavitation** is the formation of vapor cavities or void spaces in a liquid that are the consequence of forces acting upon the liquid. It usually occurs when a liquid is subjected to rapid changes of pressure that cause the formation of cavities where the pressure is relatively low [19]. When subjected to higher pressure, the voids implode. The process that initiates cavitation is a sudden pressure drop and coolant temperature increase, which causes the coolant to change from a liquid to a vapor causing bubbles. As the bubbles contact the radiator tank, they burst. Liquid rushing in to occupy the space once occupied by the bubbles causes a high-pressure stream of liquid to contact the radiator tank, which causes erosion.

At a greater voltage of 1.2 V, due to increased mobility of ions it is observed that there is increase in packing fraction and pressure as well.

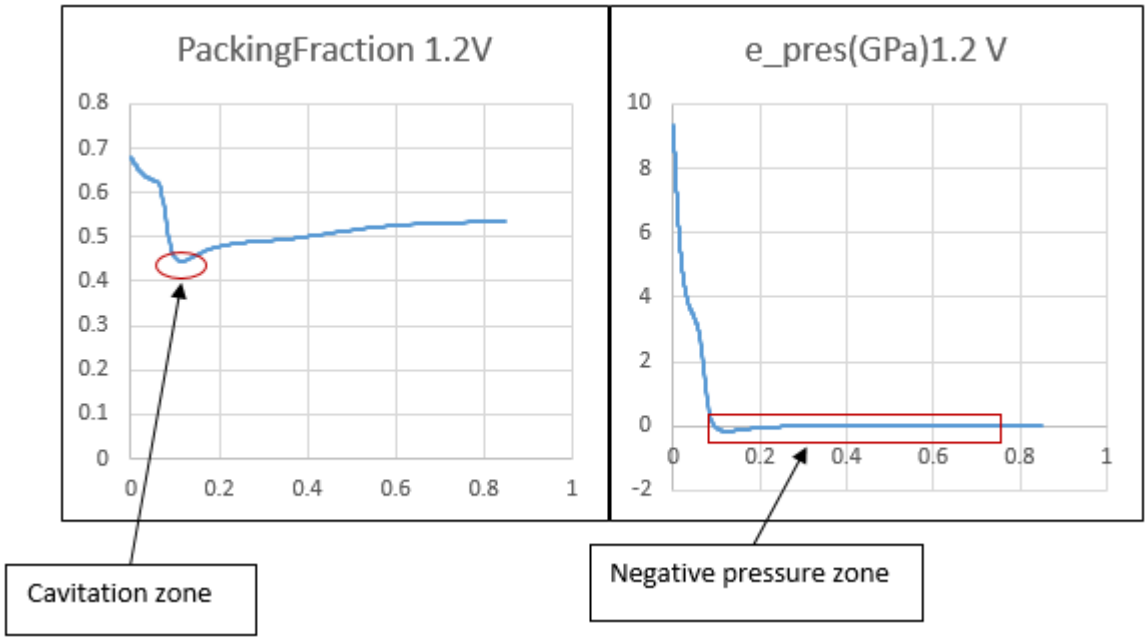

Figure 5.4: Cavitation phenomenon for 1.2 V at 333 K temperature

Pressure and Packing fraction changes suddenly as compared to the earlier case. There is a greater vaporization region which can be observed from the range of negative pressure values.

Moving towards the metal surface, it is seen that there is a sudden pressure rise from negative pressure value to positive pressure of 0.000217 GPa at 0.09 nm distance. This change in pressure is greater than the pressure change at 0.2 V. Therefore, in this case, cavitation rate is much higher as compared to the earlier case. **It should be noted that though OH^- ions accumulate at the surface to form Aluminum hydroxide, the cavitation phenomenon actively accelerates the pitting and erosion of aluminum surface.**

Same is the case at 373 K, where at high voltage the pressure is higher than lower voltage case. Considering the case for 1.2 V.

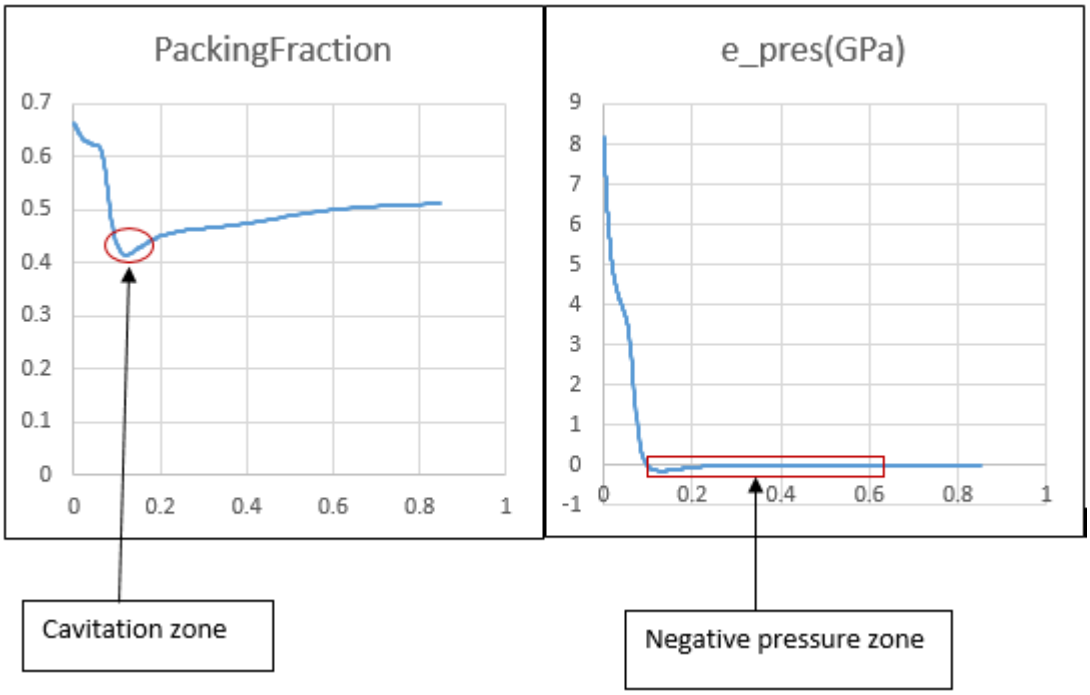

Figure 5.5: Cavitation phenomenon for 1.2 V at 373 K temperature

There is a large pressure change from -0.005 GPa to 0.024 GPa. This means greater cavitation occurring in the aluminum tubes. Therefore, it is suspected that coolant at higher temperature is more corrosive than at lower temperature.

Chapter 6

CONCLUSION

The parametric study through electrical double layer simulation leads to the following conclusions.

It is clear that chloride ions only dominate the corrosion process at lower voltage. At higher voltage, formation of aluminum hydroxide blocks further pitting of the metal surface. Although, chloride ions are inactive at higher voltages, high pressure changes of electrolyte ions lead to cavitation of the metal surface.

At higher temperature, the polarity of electrolyte decreases and its efficiency to solvate chloride ions through Hydrogen bonding decreases as well. Therefore, chloride ions are the dominant corrosion causing species until the voltage reaches 1V. Thus at higher temperature, it takes greater value of voltage to raise the production and diffusion of hydroxyl ions which forms aluminum hydroxide precipitating over the pit. At higher temperature, the pressure change is sudden than the low temperature case. This leads to increased cavitation process and pitting mechanism resumes at the metal surface.

Appendix A

Input profiles of the simulations for 0.2V and 1 V at 333 K and 373 K temperature each including the corresponding Flux of Al^{3+} cations.

A-1: Improfile for 0.2 V at 333 K temperature.

```
***********1D Problem*****************
1              !=1 if planar; =2 if cylindrical; =3 if spherical
333            !Temperature(K)
***********Domain and Grid******************
0, 0.85, 250, 1.02      !XStt,XEnd(nm),Total # of divisions,Mesh-grading power
***********Involved Chemical Components*********
18      !Total#Of Involved Chemical Components
1, 2, 3, 4, 5, 6, 7,8,9,10,11,12,13,14,17,18,19,20      !Above#X(ID_Glb Of Involved Chemical Component)
***********Involved Chemical Reactions*********
19      !Total#Of Involved Chemical Reactions
1,2,3,4,5,6,7,8,9,10,11,12,13,14,15,16,18,19,20 !Above#X(ID_Glb Of Involved Chemical Reaction)
*************Simulation Time & Steps*********************
1, 1           !NtotTimeSteps,NtotSnapShots
0              !ITimeStt(=0, first time run; >0, to restart based on ITimeStt-1 step)
*************Initial Uniform Concentrations*********************
17.9528,2.14d-3,3.629,3.629,2.03d-7,1.776d-8,0,0,0,0,0,0,0,0,0,0,!C(particle/nm^3)///MUST Follow the above order of involved chemical components
*************Boundary Condition************
!---repeat below !NthC,Ramp1Jump2,2(Flux0_End,SpringCoef_End,C_Eqilibrium_End)
0, 1, 0, 1.d3, 0.2, 0, 1.d3, 0         !electric (Displacement=Displacement0+Coef*(V-V0)) with displacement_unit:e/nm^2
1, 2, 0, 0, 0, 0, 1.d3, 17.9528        !chemical (flux=flux0+Coef*(C-C0)) with flux_unit:particle/nm^2/ns, and C_unit:particle/nm^3
2, 2, 0, 0, 0, 0, 1.d3, 2.14d-3        !chemical (flux=flux0+Coef*(C-C0)) with flux_unit:particle/nm^2/ns, and C_unit:particle/nm^3
3, 2, 0, 0, 0, 0, 1.d3, 3.629          !chemical (flux=flux0+Coef*(C-C0)) with flux_unit:particle/nm^2/ns, and C_unit:particle/nm^3
4, 2, 0, 0, 0, 0, 1.d3, 3.629          !chemical (flux=flux0+Coef*(C-C0)) with flux_unit:particle/nm^2/ns, and C_unit:particle/nm^3
5, 2, 0, 0, 0, 0, 1.d3, 2.03d-7        !chemical (flux=flux0+Coef*(C-C0)) with flux_unit:particle/nm^2/ns, and C_unit:particle/nm^3
6, 2, 0, 0, 0, 0, 1.d3, 1.776d-8       !chemical (flux=flux0+Coef*(C-C0)) with flux_unit:particle/nm^2/ns, and C_unit:particle/nm^3
7, 2, 1.45d-11, 0, 0, 0, 1.d3, 0       !chemical (flux=flux0+Coef*(C-C0)) with flux_unit:particle/nm^2/ns, and C_unit:particle/nm^3
8, 2, 0, 0, 0, 0, 1.d3, 0              !chemical (flux=flux0+Coef*(C-C0)) with flux_unit:particle/nm^2/ns, and C_unit:particle/nm^3
9, 2, 0, 0, 0, 0, 1.d3, 0              !chemical (flux=flux0+Coef*(C-C0)) with flux_unit:particle/nm^2/ns, and C_unit:particle/nm^3
10, 2, 0, 0, 0, 0, 1.d3, 0             !chemical (flux=flux0+Coef*(C-C0)) with flux_unit:particle/nm^2/ns, and C_unit:particle/nm^3
11, 2, 0, 0, 0, 0, 1.d3, 0             !chemical (flux=flux0+Coef*(C-C0)) with flux_unit:particle/nm^2/ns, and C_unit:particle/nm^3
12, 2, 0, 0, 0, 0, 1.d3, 0             !chemical (flux=flux0+Coef*(C-C0)) with flux_unit:particle/nm^2/ns, and C_unit:particle/nm^3
13, 2, 0, 0, 0, 0, 1.d3, 0             !chemical (flux=flux0+Coef*(C-C0)) with flux_unit:particle/nm^2/ns, and C_unit:particle/nm^3
14, 2, 0, 0, 0, 0, 1.d3, 0             !chemical (flux=flux0+Coef*(C-C0)) with flux_unit:particle/nm^2/ns, and C_unit:particle/nm^3
15, 2, 0, 0, 0, 0, 1.d3, 0             !chemical (flux=flux0+Coef*(C-C0)) with flux_unit:particle/nm^2/ns, and C_unit:particle/nm^3
16, 2, 0, 0, 0, 0, 1.d3, 0                !chemical (flux=flux0+Coef*(C-C0)) with flux_unit:particle/nm^2/ns, and C_unit:particle/nm^3
17, 2, 0, 0, 0, 0, 1.d3, 0                !chemical (flux=flux0+Coef*(C-C0)) with flux_unit:particle/nm^2/ns, and C_unit:particle/nm^3
18, 2, 0, 0, 0, 0, 1.d3, 0                !chemical (flux=flux0+Coef*(C-C0)) with flux_unit:particle/nm^2/ns, and C_unit:particle/nm^3
*************Numerical Parameters*********************
90000, 1.d-3, 1000, 0.002       !IteratMax,ErrAllow,IteratDisplay,ARelax
************************************************************
***********All Chemical Components*********************
21      !Total # of chemical components
--repeat (above #) below--!ID;Valance;Relative_Permittivity@Linear;StokesRadius;PhysicalRadius;EtaOverEpsil0((V/nm)^2-nS);AvdW0
 1,  0,   55.6,  0.09687,   0.1552,  0.113d1, 0.20294                  !H2O(0)(10)
 2, -1,    7,    0.107,     0.181,   0.113d1, 0.241                    !Cl(1-)
 3,  1,    10,   0.145,     0.157,   0.113d1, 0.68294                  !CH3OH2(1+)
 4, -1,    10,   0.717,     0.234,   0.113d1, 0.68294                  !HCO(1-)
 5,  1,    0,    0.023,     0.15,    0.113d1, 0.20294                  !H(+)
 6, -1,   50,    0.041,     0.137,   0.113d1, 0.20294                  !OH(-)
 7,  3,   4.5,  0.4026,    0.039,   0.113d1, 0                 !Al(3+)(13)
 8,  2,   2.2,   0.4026,    0.138,   0.113d1, 0                 !AlOH(2+)
 9,  1,   2.2,   0.4026,   0.1733,   0.113d1, 0                 !Al(OH)2(1+)
10,  4,   2.2,   0.4026,   0.1739,   0.113d1, 0                 !Al2(OH)2(4+)
11,  2,   5.1,   0.4026,   0.1816,   0.113d1, 0                 !AlCl(2+)
12,  1,    3,    0.4026,   0.2046,   0.113d1, 0                 !Al(OH)Cl(1+)
13,  0,    3,    0.4026,   0.2233,   0.113d1, 0                 !Al(OH)2Cl(0)
14,  0,    1,    0.278,    0.175,    0.113d1, 0.68294           !C2H6O2(0)
15, -2,    10,    0.221,     0.17,    0.113d1, 0.439             !C2O4(2-)
16,  0,   0.5,   0.113,     0.178,   0.113d1, 0.134             !CO2(0)
17,  0,  0.89,  0.109,     0.135,   0.113d1, 0.0502            !O2(0)
18, -1,    5,    0.2,       0.162,   0.113d1, 0.650             !HCOO(1-)
19,  0,    10,   0.75,    0.334,    0.113d1, 0.68294           !H2CO(0)
20,  0,    10,   0.7,    0.35,    0.113d1, 0.68294             !HCOOH(0)
21,  0,    5,    0.041,    0.039,    0.113d1, 0                !Al(OHCH2CH2O)3
***********All Chemical Reactions*********************
20      !Total # of Chemical Reactions
--repeat (above #) below--ID,KConst(MUST be consistent to generate rate by particle/nm^3/ns),4(NCLnr,KLnr),8(NC_Involved,Vnce#)
 1, 6.44d-6,  0, 0, 0, 0, 0, 0, 0, 0,                  7, -1, 1, -1, 8, 1, 5, 1,  0, 0, 0, 0, 0, 0, 0, 0       !Al(3+)+H2O>AlOH(2+)+H(+)
 2, 7.31, 0,  0, 0, 0, 0, 0, 0, 0,                     8, -1, 5, -1, 7, 1, 1, 1, 0, 0, 0, 0, 0, 0, 0, 0       !AlOH(2+)+H(+)>Al(3+)+H2O
 3, 6.44d-6,  0, 0, 0, 0, 0, 0, 0, 0,                  8, -1, 1, -1, 9, 1, 5, 1, 0, 0, 0, 0, 0, 0, 0, 0       !AlOH(2+)+H2O>Al(OH)2(+)+H(+)
 4, 7.31, 0,  0, 0, 0, 0, 0, 0, 0,                     9, -1, 5, -1, 8, 1, 1, 1, 0, 0, 0, 0, 0, 0, 0, 0       !Al(OH)2(+)+H(+)>Al(OH)(2+)+H2O
 5, 5.8d-10,  0, 0, 0, 0, 0, 0, 0, 0,                  7, -2, 1, -2, 10, 1, 5, 2, 0, 0, 0, 0, 0, 0, 0, 0      !2Al(3+)+2H2O>Al2(OH)2(4+)+2H(+)
 6, 2.76d-1,  0, 0, 0, 0, 0, 0, 0, 0,                  10, -1, 5, -2, 7, 2, 1, 2, 0, 0, 0, 0, 0, 0, 0, 0      !Al2(OH)2(4+)+2H(+)>2Al(3+)+2H2O
 7, 3.75d-7,  0, 0, 0, 0, 0, 0, 0, 0,                  7, -1, 2, -1, 11, 1, 0, 0, 0, 0, 0, 0, 0, 0, 0, 0      !Al(3+)+Cl(-)>AlCl(2+)
 8, 7.5d-8,   7, 3.75d-7, 6, -3.75d-7, 0, 0, 0, 0,      11, -1, 7, 1, 2, 1, 0, 0, 0, 0, 0, 0, 0, 0, 0, 0       !AlCl(2+)>Al(3+)+Cl(-)
 9, 3.16d-5,  0, 0, 0, 0, 0, 0, 0, 0,                  8, -1, 2, -1, 12, 1, 0, 0, 0, 0, 0, 0, 0, 0, 0, 0      !AlOH(2+)+Cl(-)>Al(OH)Cl(+)
10, 5.7d-6,   8, -3.16d-5, 0, 0, 0, 0, 0, 0,           12, -1, 8, 1, 2, 1, 0, 0, 0, 0, 0, 0, 0, 0, 0, 0       !Al(OH)Cl(+)>AlOH(2+)+Cl(-)
11, 1.4d-17,  0, 0, 0, 0, 0, 0, 0, 0,                  11, -1, 1, -2, 13, 1, 5, 2,  0, 0, 0, 0, 0, 0, 0, 0    !AlCl(2+)+2H2O>Al(OH)2Cl+2H(+)
12, 2.36d-16, 0, 0, 0, 0, 0, 0, 0, 0,                  12, -1, 1, -1, 13, 1, 5, 1,  0, 0, 0, 0, 0, 0, 0, 0    !Al(OH)Cl(+)+H2O>Al(OH)2Cl+H(+)
13, 5.13d-14, 0, 0, 0, 0, 0, 0, 0, 0,                  1, -1, 5, 1, 6, 1, 0, 0, 0, 0, 0, 0, 0, 0, 0, 0        !H2O>H(+)+OH(-)
14, 2.16d2,   0, 0, 0, 0, 0, 0, 0, 0,                  5, -1, 6, -1, 1, 1, 0, 0, 0, 0, 0, 0, 0, 0, 0, 0       !H(+)+OH(-)>H2O
15, 1.63d-37,  0, 0, 0, 0, 0, 0, 0, 0,                 14,-1, 17,-2, 15, 1, 5, 2, 1, 2, 0, 0, 0, 0, 0, 0      !C2H6O2+2O2>C2O4(2-)+2H(+)+2H2O
16, 1.d-5, 0, 0, 0, 0, 0, 0, 0, 0,                     14, -1, 3, 1, 4, 1,  0, 0, 0, 0, 0, 0, 0, 0, 0, 0      !C2H6O2>CH3OH2(+)+CHO(-)
17, 1.77d-4,  0, 0, 0, 0, 0, 0, 0, 0,                  15, -2, 5,-4, 17, -2, 16, 4, 1, 2, 0, 0, 0, 0, 0, 0    !2C2O4(2-)+4H(+)+O2>4CO2+2H2O
18, 7.89d-18, 0, 0, 0, 0, 0, 0, 0, 0,                  17, -1, 1, -2, 6, 4, 0, 0, 0, 0, 0, 0, 0, 0, 0, 0      !O2+2H2O+4e(-)>4OH(-)
19, 4d-11, 0, 0, 0, 0, 0, 0, 0, 0,                     19, -1, 4, 1, 5, 1, 0, 0, 0, 0, 0, 0, 0, 0, 0, 0       !H(+)+CHO(-)>H2CO
20, 1.5d-11, 0, 0, 0, 0, 0, 0, 0, 0,                   20, -1, 18, 1, 5, 1, 0, 0, 0, 0, 0, 0, 0, 0, 0, 0      !H(+)+HCOO(-)>HCOOH
```

A-2: Improfile for 1 V at 333 K temperature

```
***********1D Problem******************
1              !=1 if planar; =2 if cylindrical; =3 if spherical
333            !Temperature(K)
***********Domain and Grid******************
0, 0.85, 250, 1.02      !XStt,XEnd(nm),Total # of divisions,Mesh-grading power
***********Involved Chemical Components********
18      !Total#Of Involved Chemical Components
1, 2, 3, 4, 5, 6, 7,8,9,10,11,12,13,14,17,18,19,20      !Above#X(ID_Glb Of Involved Chemical Component)
***********Involved Chemical Reactions*********
19      !Total#Of Involved Chemical Reactions
1,2,3,4,5,6,7,8,9,10,11,12,13,14,15,16,18,19,20 !Above#X(ID_Glb Of Involved Chemical Reaction)
*************Simulation Time & Steps*********************
1, 1            !NtotTimeSteps,NtotSnapShots
0               !ITimeStt(=0, first time run; >0, to restart based on ITimeStt-1 step)
*************Initial Uniform Concentrations*********************
17.9528,2.14d-3,3.629,3.629,2.03d-7,1.776d-8,0,0,0,0,0,0,0,0,0,0,0!C(particle/nm^3)///MUST Follow the above order of involved chemical components
*************Boundary Condition************
!---repeat below !NthC,Ramp1Jump2,2(Flux0_End,SpringCoef_End,C_Eqilibrium_End)
0, 1, 0, 1.d3, 1, 0, 1.d3, 0            !electric (Displacement=Displacement0+Coef*(V-V0)) with displacement_unit:e/nm^2
1, 2, 0, 0, 0, 0, 1.d3, 17.9528         !chemical (flux=flux0+Coef*(C-C0)) with flux_unit:particle/nm^2/ns, and C_unit:particle/nm^3
2, 2, 0, 0, 0, 0, 1.d3, 2.14d-3         !chemical (flux=flux0+Coef*(C-C0)) with flux_unit:particle/nm^2/ns, and C_unit:particle/nm^3
3, 2, 0, 0, 0, 0, 1.d3, 3.629           !chemical (flux=flux0+Coef*(C-C0)) with flux_unit:particle/nm^2/ns, and C_unit:particle/nm^3
4, 2, 0, 0, 0, 0, 1.d3, 3.629           !chemical (flux=flux0+Coef*(C-C0)) with flux_unit:particle/nm^2/ns, and C_unit:particle/nm^3
5, 2, 0, 0, 0, 0, 1.d3, 2.03d-7         !chemical (flux=flux0+Coef*(C-C0)) with flux_unit:particle/nm^2/ns, and C_unit:particle/nm^3
6, 2, 0, 0, 0, 0, 1.d3, 1.776d-8        !chemical (flux=flux0+Coef*(C-C0)) with flux_unit:particle/nm^2/ns, and C_unit:particle/nm^3
7, 2, 5.85d-10, 0, 0, 0, 1.d3, 0        !chemical (flux=flux0+Coef*(C-C0)) with flux_unit:particle/nm^2/ns, and C_unit:particle/nm^3
8, 2, 0, 0, 0, 0, 1.d3, 0               !chemical (flux=flux0+Coef*(C-C0)) with flux_unit:particle/nm^2/ns, and C_unit:particle/nm^3
9, 2, 0, 0, 0, 0, 1.d3, 0               !chemical (flux=flux0+Coef*(C-C0)) with flux_unit:particle/nm^2/ns, and C_unit:particle/nm^3
10, 2, 0, 0, 0, 0, 1.d3, 0              !chemical (flux=flux0+Coef*(C-C0)) with flux_unit:particle/nm^2/ns, and C_unit:particle/nm^3
11, 2, 0, 0, 0, 0, 1.d3, 0              !chemical (flux=flux0+Coef*(C-C0)) with flux_unit:particle/nm^2/ns, and C_unit:particle/nm^3
12, 2, 0, 0, 0, 0, 1.d3, 0              !chemical (flux=flux0+Coef*(C-C0)) with flux_unit:particle/nm^2/ns, and C_unit:particle/nm^3
13, 2, 0, 0, 0, 0, 1.d3, 0              !chemical (flux=flux0+Coef*(C-C0)) with flux_unit:particle/nm^2/ns, and C_unit:particle/nm^3
14, 2, 0, 0, 0, 0, 1.d3, 0              !chemical (flux=flux0+Coef*(C-C0)) with flux_unit:particle/nm^2/ns, and C_unit:particle/nm^3
15, 2, 0, 0, 0, 0, 1.d3, 0              !chemical (flux=flux0+Coef*(C-C0)) with flux_unit:particle/nm^2/ns, and C_unit:particle/nm^3
16, 2, 0, 0, 0, 0, 1.d3, 0               !chemical (flux=flux0+Coef*(C-C0)) with flux_unit:particle/nm^2/ns, and C_unit:particle/nm^3
17, 2, 0, 0, 0, 0, 1.d3, 0               !chemical (flux=flux0+Coef*(C-C0)) with flux_unit:particle/nm^2/ns, and C_unit:particle/nm^3
18, 2, 0, 0, 0, 0, 1.d3, 0               !chemical (flux=flux0+Coef*(C-C0)) with flux_unit:particle/nm^2/ns, and C_unit:particle/nm^3
*************Numerical Parameters*********************
90000, 1.d-3, 1000, 0.002       !IteratMax,ErrAllow,IteratDisplay,ARelax
*****************************************************************
***********All Chemical Components*********************
21      !Total # of chemical components
--repeat (above #) below--!ID;Valance;Relative_Permittivity@Linear;StokesRadius;PhysicalRadius;EtaOverEpsil0((V/nm)^2-nS);AvdW0
 1,  0,   55.6,  0.09687,   0.1552,  0.113d1, 0.20294                   !H2O(0)(10)
 2, -1,    7,    0.107,     0.181,   0.113d1, 0.241                     !Cl(1-)
 3,  1,    10,   0.145,    0.157,    0.113d1, 0.68294                   !CH3OH2(1+)
 4, -1,    10,   0.717,    0.234,    0.113d1, 0.68294                   !HCO(1-)
 5,  1,    0,    0.023,     0.15,    0.113d1, 0.20294                   !H(+)
 6, -1,   50,    0.041,     0.137,   0.113d1, 0.20294                   !OH(-)
 7,  3,   4.5,  0.4026,    0.039,   0.113d1, 0                 !Al(3+)(13)
 8,  2,   2.2,   0.4026,    0.138,   0.113d1, 0                 !AlOH(2+)
 9,  1,   2.2,   0.4026,   0.1733,   0.113d1, 0                 !Al(OH)2(1+)
10,  4,   2.2,   0.4026,   0.1739,   0.113d1, 0                 !Al2(OH)2(4+)
11,  2,   5.1,   0.4026,   0.1816,   0.113d1, 0                 !AlCl(2+)
12,  1,    3,    0.4026,   0.2046,   0.113d1, 0                 !Al(OH)Cl(1+)
13,  0,    3,    0.4026,   0.2233,   0.113d1, 0                 !Al(OH)2Cl(0)
14,  0,    1,    0.278,    0.175,    0.113d1, 0.68294           !C2H6O2(0)
15, -2,    10,    0.221,     0.17,    0.113d1, 0.439            !C2O4(2-)
16,  0,   0.5,   0.113,     0.178,   0.113d1, 0.134             !CO2(0)
17,  0,  0.89,  0.109,     0.135,   0.113d1, 0.0502            !O2(0)
18, -1,    5,    0.2,       0.162,   0.113d1, 0.650             !HCOO(1-)
19,  0,    10,   0.75,    0.334,    0.113d1, 0.68294           !H2CO(0)
20,  0,    10,   0.7,    0.35,    0.113d1, 0.68294             !HCOOH(0)
21,  0,    5,    0.041,    0.039,    0.113d1, 0                !Al(OHCH2CH2O)3
***********All Chemical Reactions*********************
20      !Total # of Chemical Reactions
--repeat (above #) below--ID,KConst(MUST be consistent to generate rate by particle/nm^3/ns),4(NCLnr,KLnr),8(NC_Involved,Vnce#)
 1, 6.44d-6,  0, 0, 0, 0, 0, 0, 0, 0,                 7, -1, 1, -1, 8, 1, 5, 1,  0, 0, 0, 0, 0, 0, 0, 0       !Al(3+)+H2O>AlOH(2+)+H(+)
 2, 7.31, 0,  0, 0, 0, 0, 0, 0, 0, 0,                 8, -1, 5, -1, 7, 1, 1, 1, 0, 0, 0, 0, 0, 0, 0, 0        !AlOH(2+)+H(+)>Al(3+)+H2O
 3, 6.44d-6,  0, 0, 0, 0, 0, 0, 0, 0,                 8, -1, 1, -1, 9, 1, 5, 1, 0, 0, 0, 0, 0, 0, 0, 0        !AlOH(2+)+H2O>Al(OH)2(+)+H(+)
 4, 7.31, 0,  0, 0, 0, 0, 0, 0, 0, 0,                 9, -1, 5, -1, 8, 1, 1, 1, 0, 0, 0, 0, 0, 0, 0, 0        !Al(OH)2(+)+H(+)>Al(OH)(2+)+H2O
 5, 5.8d-10,  0, 0, 0, 0, 0, 0, 0, 0,                 7, -2, 1, -2, 10, 1, 5, 2, 0, 0, 0, 0, 0, 0, 0, 0       !2Al(3+)+2H2O>Al2(OH)2(4+)+2H(+)
 6, 2.76d-1,  0, 0, 0, 0, 0, 0, 0, 0,                 10, -1, 5, -2, 7, 2, 1, 2, 0, 0, 0, 0, 0, 0, 0, 0       !Al2(OH)2(4+)+2H(+)>2Al(3+)+2H2O
 7, 3.75d-7,  0, 0, 0, 0, 0, 0, 0, 0,                 7, -1, 2, -1, 11, 1, 0, 0, 0, 0, 0, 0, 0, 0, 0, 0       !Al(3+)+Cl(-)>AlCl(2+)
 8, 7.5d-8,   7, 3.75d-7, 6, -3.75d-7, 0, 0, 0, 0,    11, -1, 7, 1, 2, 1, 0, 0, 0, 0, 0, 0, 0, 0, 0, 0        !AlCl(2+)>Al(3+)+Cl(-)
 9, 3.16d-5,  0, 0, 0, 0, 0, 0, 0, 0,                 8, -1, 2, -1, 12, 1, 0, 0, 0, 0, 0, 0, 0, 0, 0, 0       !AlOH(2+)+Cl(-)>Al(OH)Cl(+)
10, 5.7d-6,   8, -3.16d-5, 0, 0, 0, 0, 0, 0,          12, -1, 8, 1, 2, 1, 0, 0, 0, 0, 0, 0, 0, 0, 0, 0        !Al(OH)Cl(+)>AlOH(2+)+Cl(-)
11, 1.4d-17,  0, 0, 0, 0, 0, 0, 0, 0,                 11, -1, 1, -2, 13, 1, 5, 2,  0, 0, 0, 0, 0, 0, 0, 0     !AlCl(2+)+2H2O>Al(OH)2Cl+2H(+)
12, 2.36d-16, 0, 0, 0, 0, 0, 0, 0, 0,                 12, -1, 1, -1, 13, 1, 5, 1,  0, 0, 0, 0, 0, 0, 0, 0     !Al(OH)Cl(+)+H2O>Al(OH)2Cl+H(+)
13, 5.13d-14, 0, 0, 0, 0, 0, 0, 0, 0,                 1, -1, 5, 1, 6, 1, 0, 0, 0, 0, 0, 0, 0, 0, 0, 0         !H2O>H(+)+OH(-)
14, 2.16d2,   0, 0, 0, 0, 0, 0, 0, 0,                 5, -1, 6, -1, 1, 1, 0, 0, 0, 0, 0, 0, 0, 0, 0, 0        !H(+)+OH(-)>H2O
15, 1.63d-37,  0, 0, 0, 0, 0, 0, 0, 0,                14,-1, 17,-2, 15, 1, 5, 2, 1, 2, 0, 0, 0, 0, 0, 0       !C2H6O2+2O2>C2O4(2-)+2H(+)+2H2O
16, 1.d-5, 0, 0, 0, 0, 0, 0, 0, 0,                    14, -1, 3, 1, 4, 1,  0, 0, 0, 0, 0, 0, 0, 0, 0, 0       !C2H6O2>CH3OH2(+)+CHO(-)
17, 1.77d-4,  0, 0, 0, 0, 0, 0, 0, 0,                 15, -2, 5,-4, 17, -2, 16, 4, 1, 2, 0, 0, 0, 0, 0, 0     !2C2O4(2-)+4H(+)+O2>4CO2+2H2O
18, 7.89d-18, 0, 0, 0, 0, 0, 0, 0, 0,                 17, -1, 1, -2, 6, 4, 0, 0, 0, 0, 0, 0, 0, 0, 0, 0       !O2+2H2O+4e(-)>4OH(-)
19, 4d-11, 0, 0, 0, 0, 0, 0, 0, 0,                    19, -1, 4, 1, 5, 1, 0, 0, 0, 0, 0, 0, 0, 0, 0, 0        !H(+)+CHO(-)>H2CO
20, 1.5d-11, 0, 0, 0, 0, 0, 0, 0, 0,                  20, -1, 18, 1, 5, 1, 0, 0, 0, 0, 0, 0, 0, 0, 0, 0       !H(+)+HCOO(-)>HCOOH
```

A-3: Improfile for 0.2 V at 373 K temperature

```
***********1D Problem*****************
1             !=1 if planar; =2 if cylindrical; =3 if spherical
373           !Temperature(K)
***********Domain and Grid*****************
0, 0.85, 250, 1.02      !XStt,XEnd(nm),Total # of divisions,Mesh-grading power
***********Involved Chemical Components*********
18      !Total#Of Involved Chemical Components
1, 2, 3, 4, 5, 6, 7,8,9,10,11,12,13,14,17,18,19,20      !Above#X(ID_Glb Of Involved Chemical Component)
***********Involved Chemical Reactions*********
19      !Total#Of Involved Chemical Reactions
1,2,3,4,5,6,7,8,9,10,11,12,13,14,15,16,18,19,20 !Above#X(ID_Glb Of Involved Chemical Reaction)
*************Simulation Time & Steps********************
1, 1            !NtotTimeSteps,NtotSnapShots
0               !ITimeStt(=0, first time run; >0, to restart based on ITimeStt-1 step)
*************Initial Uniform Concentrations*********************
17.5129,2.9998d-3,3.3999,3.3999,2.03d-7,1.776d-8,0,0,0,0,0,0,0,0,0,0,0!C(particle/nm^3)///MUST Follow the order of involved chemical components
*************Boundary Condition************
!---repeat below !NthC,Ramp1Jump2,2(Flux0_End,SpringCoef_End,C_Eqilibrium_End)
0, 1, 0, 1.d3, 0.2, 0, 1.d3, 0          !electric (Displacement=Displacement0+Coef*(V-V0)) with displacement_unit:e/nm^2
1, 2, 0, 0, 0, 0, 1.d3, 17.5129         !chemical (flux=flux0+Coef*(C-C0)) with flux_unit:particle/nm^2/ns, and C_unit:particle/nm^3
2, 2, 0, 0, 0, 0, 1.d3, 2.9998d-3       !chemical (flux=flux0+Coef*(C-C0)) with flux_unit:particle/nm^2/ns, and C_unit:particle/nm^3
3, 2, 0, 0, 0, 0, 1.d3, 3.3999          !chemical (flux=flux0+Coef*(C-C0)) with flux_unit:particle/nm^2/ns, and C_unit:particle/nm^3
4, 2, 0, 0, 0, 0, 1.d3, 3.3999          !chemical (flux=flux0+Coef*(C-C0)) with flux_unit:particle/nm^2/ns, and C_unit:particle/nm^3
5, 2, 0, 0, 0, 0, 1.d3, 2.03d-7         !chemical (flux=flux0+Coef*(C-C0)) with flux_unit:particle/nm^2/ns, and C_unit:particle/nm^3
6, 2, 0, 0, 0, 0, 1.d3, 1.776d-8        !chemical (flux=flux0+Coef*(C-C0)) with flux_unit:particle/nm^2/ns, and C_unit:particle/nm^3
7, 2, 1.45d-11, 0, 0, 0, 1.d3, 0        !chemical (flux=flux0+Coef*(C-C0)) with flux_unit:particle/nm^2/ns, and C_unit:particle/nm^3
8, 2, 0, 0, 0, 0, 1.d3, 0               !chemical (flux=flux0+Coef*(C-C0)) with flux_unit:particle/nm^2/ns, and C_unit:particle/nm^3
9, 2, 0, 0, 0, 0, 1.d3, 0               !chemical (flux=flux0+Coef*(C-C0)) with flux_unit:particle/nm^2/ns, and C_unit:particle/nm^3
10, 2, 0, 0, 0, 0, 1.d3, 0              !chemical (flux=flux0+Coef*(C-C0)) with flux_unit:particle/nm^2/ns, and C_unit:particle/nm^3
11, 2, 0, 0, 0, 0, 1.d3, 0              !chemical (flux=flux0+Coef*(C-C0)) with flux_unit:particle/nm^2/ns, and C_unit:particle/nm^3
12, 2, 0, 0, 0, 0, 1.d3, 0              !chemical (flux=flux0+Coef*(C-C0)) with flux_unit:particle/nm^2/ns, and C_unit:particle/nm^3
13, 2, 0, 0, 0, 0, 1.d3, 0              !chemical (flux=flux0+Coef*(C-C0)) with flux_unit:particle/nm^2/ns, and C_unit:particle/nm^3
14, 2, 0, 0, 0, 0, 1.d3, 0              !chemical (flux=flux0+Coef*(C-C0)) with flux_unit:particle/nm^2/ns, and C_unit:particle/nm^3
15, 2, 0, 0, 0, 0, 1.d3, 0              !chemical (flux=flux0+Coef*(C-C0)) with flux_unit:particle/nm^2/ns, and C_unit:particle/nm^3
16, 2, 0, 0, 0, 0, 1.d3, 0              !chemical (flux=flux0+Coef*(C-C0)) with flux_unit:particle/nm^2/ns, and C_unit:particle/nm^3
17, 2, 0, 0, 0, 0, 1.d3, 0              !chemical (flux=flux0+Coef*(C-C0)) with flux_unit:particle/nm^2/ns, and C_unit:particle/nm^3
18, 2, 0, 0, 0, 0, 1.d3, 0              !chemical (flux=flux0+Coef*(C-C0)) with flux_unit:particle/nm^2/ns, and C_unit:particle/nm^3
*************Numerical Parameters*********************
90000, 1.d-3, 1000, 0.002       !IteratMax,ErrAllow,IteratDisplay,ARelax
*****************************************************************
***********All Chemical Components*********************
21      !Total # of chemical components
--repeat (above #) below--!ID;Valance;Relative_Permittivity@Linear;StokesRadius;PhysicalRadius;EtaOverEpsil0((V/nm)^2-nS);AvdW0
 1,  0,   55.6,  0.09687,   0.1552,  0.113d1, 0.20294                   !H2O(0)(10)
 2, -1,    7,    0.107,     0.181,   0.113d1, 0.241                     !Cl(1-)
 3,  1,   10,    0.145,     0.157,   0.113d1, 0.68294                   !CH3OH2(1+)
 4, -1,   10,    0.717,     0.234,   0.113d1, 0.68294                   !HCO(1-)
 5,  1,    0,    0.023,     0.15,    0.113d1, 0.20294                   !H(+)
 6, -1,   50,    0.041,     0.137,   0.113d1, 0.20294                   !OH(-)
 7,  3,   4.5,  0.4026,    0.039,   0.113d1, 0                 !Al(3+)(13)
 8,  2,   2.2,   0.4026,    0.138,   0.113d1, 0                 !AlOH(2+)
 9,  1,   2.2,   0.4026,   0.1733,   0.113d1, 0                 !Al(OH)2(1+)
10,  4,   2.2,   0.4026,   0.1739,   0.113d1, 0                 !Al2(OH)2(4+)
11,  2,   5.1,   0.4026,   0.1816,   0.113d1, 0                 !AlCl(2+)
12,  1,    3,    0.4026,   0.2046,   0.113d1, 0                 !Al(OH)Cl(1+)
13,  0,    3,    0.4026,   0.2233,   0.113d1, 0                 !Al(OH)2Cl(0)
14,  0,    1,    0.278,    0.175,    0.113d1, 0.68294           !C2H6O2(0)
15, -2,   10,     0.221,     0.17,    0.113d1, 0.439             !C2O4(2-)
16,  0,   0.5,   0.113,     0.178,   0.113d1, 0.134             !CO2(0)
17,  0,  0.89,  0.109,     0.135,   0.113d1, 0.0502            !O2(0)
18, -1,    5,    0.2,       0.162,   0.113d1, 0.650             !HCOO(1-)
19,  0,   10,    0.75,     0.334,    0.113d1, 0.68294           !H2CO(0)
20,  0,   10,    0.7,     0.35,    0.113d1, 0.68294             !HCOOH(0)
21,  0,    5,    0.041,    0.039,    0.113d1, 0                 !Al(OHCH2CH2O)3
***********All Chemical Reactions*********************
20      !Total # of Chemical Reactions
--repeat (above #) below--ID,KConst(MUST be consistent to generate rate by particle/nm^3/ns),4(NCLnr,KLnr),8(NC_Involved,Vnce#)
 1, 6.44d-6,  0, 0, 0, 0, 0, 0, 0, 0,                  7, -1, 1, -1, 8, 1, 5, 1,  0, 0, 0, 0, 0, 0, 0, 0       !Al(3+)+H2O>AlOH(2+)+H(+)
 2, 7.31, 0,  0, 0, 0, 0, 0, 0, 0, 0,                  8, -1, 5, -1, 7, 1, 1, 1, 0, 0, 0, 0, 0, 0, 0, 0       !AlOH(2+)+H(+)>Al(3+)+H2O
 3, 6.44d-6,  0, 0, 0, 0, 0, 0, 0, 0,                  8, -1, 1, -1, 9, 1, 5, 1, 0, 0, 0, 0, 0, 0, 0, 0       !AlOH(2+)+H2O>Al(OH)2(+)+H(+)
 4, 7.31, 0,  0, 0, 0, 0, 0, 0, 0, 0,                  9, -1, 5, -1, 8, 1, 1, 1, 0, 0, 0, 0, 0, 0, 0, 0       !Al(OH)2(+)+H(+)>Al(OH)(2+)+H2O
 5, 5.8d-10,  0, 0, 0, 0, 0, 0, 0, 0,                  7, -2, 1, -2, 10, 1, 5, 2, 0, 0, 0, 0, 0, 0, 0, 0      !2Al(3+)+2H2O>Al2(OH)2(4+)+2H(+)
 6, 2.76d-1,  0, 0, 0, 0, 0, 0, 0, 0,                  10, -1, 5, -2, 7, 2, 1, 2, 0, 0, 0, 0, 0, 0, 0, 0      !Al2(OH)2(4+)+2H(+)>2Al(3+)+2H2O
 7, 3.75d-7,  0, 0, 0, 0, 0, 0, 0, 0,                  7, -1, 2, -1, 11, 1, 0, 0, 0, 0, 0, 0, 0, 0, 0, 0      !Al(3+)+Cl(-)>AlCl(2+)
 8, 7.5d-8,   7, 3.75d-7, 6, -3.75d-7, 0, 0, 0, 0,      11, -1, 7, 1, 2, 1, 0, 0, 0, 0, 0, 0, 0, 0, 0, 0       !AlCl(2+)>Al(3+)+Cl(-)
 9, 3.16d-5,  0, 0, 0, 0, 0, 0, 0, 0,                  8, -1, 2, -1, 12, 1, 0, 0, 0, 0, 0, 0, 0, 0, 0, 0      !AlOH(2+)+Cl(-)>Al(OH)Cl(+)
10, 5.7d-6,   8, -3.16d-5, 0, 0, 0, 0, 0, 0,           12, -1, 8, 1, 2, 1, 0, 0, 0, 0, 0, 0, 0, 0, 0, 0       !Al(OH)Cl(+)>AlOH(2+)+Cl(-)
11, 1.4d-17,  0, 0, 0, 0, 0, 0, 0, 0,                  11, -1, 1, -2, 13, 1, 5, 2,  0, 0, 0, 0, 0, 0, 0, 0    !AlCl(2+)+2H2O>Al(OH)2Cl+2H(+)
12, 2.36d-16, 0, 0, 0, 0, 0, 0, 0, 0,                  12, -1, 1, -1, 13, 1, 5, 1,  0, 0, 0, 0, 0, 0, 0, 0    !Al(OH)Cl(+)+H2O>Al(OH)2Cl+H(+)
13, 5.13d-14, 0, 0, 0, 0, 0, 0, 0, 0,                  1, -1, 5, 1, 6, 1, 0, 0, 0, 0, 0, 0, 0, 0, 0, 0        !H2O>H(+)+OH(-)
14, 2.16d2,   0, 0, 0, 0, 0, 0, 0, 0,                  5, -1, 6, -1, 1, 1, 0, 0, 0, 0, 0, 0, 0, 0, 0, 0       !H(+)+OH(-)>H2O
15, 1.63d-37,  0, 0, 0, 0, 0, 0, 0, 0,                 14,-1, 17,-2, 15, 1, 5, 2, 1, 2, 0, 0, 0, 0, 0, 0      !C2H6O2+2O2>C2O4(2-)+2H(+)+2H2O
16, 1.d-5, 0, 0, 0, 0, 0, 0, 0, 0,                     14, -1, 3, 1, 4, 1,  0, 0, 0, 0, 0, 0, 0, 0, 0, 0      !C2H6O2>CH3OH2(+)+CHO(-)
17, 1.77d-4,  0, 0, 0, 0, 0, 0, 0, 0,                  15, -2, 5,-4, 17, -2, 16, 4, 1, 2, 0, 0, 0, 0, 0, 0    !2C2O4(2-)+4H(+)+O2>4CO2+2H2O
18, 7.89d-18, 0, 0, 0, 0, 0, 0, 0, 0,                  17, -1, 1, -2, 6, 4, 0, 0, 0, 0, 0, 0, 0, 0, 0, 0      !O2+2H2O+4e(-)>4OH(-)
19, 4d-11, 0, 0, 0, 0, 0, 0, 0, 0,                     19, -1, 4, 1, 5, 1, 0, 0, 0, 0, 0, 0, 0, 0, 0, 0       !H(+)+CHO(-)>H2CO
20, 1.5d-11, 0, 0, 0, 0, 0, 0, 0, 0,                   20, -1, 18, 1, 5, 1, 0, 0, 0, 0, 0, 0, 0, 0, 0, 0      !H(+)+HCOO(-)>HCOOH
```

A-4: Improfile for 1 V at 373 K temperature

```
************1D Problem******************
1              !=1 if planar; =2 if cylindrical; =3 if spherical
373            !Temperature(K)
************Domain and Grid******************
0, 0.85, 250, 1.02      !XStt,XEnd(nm),Total # of divisions,Mesh-grading power
************Involved Chemical Components*********
18      !Total#Of Involved Chemical Components
1, 2, 3, 4, 5, 6, 7,8,9,10,11,12,13,14,17,18,19,20      !Above#X(ID_Glb Of Involved Chemical Component)
************Involved Chemical Reactions*********
19      !Total#Of Involved Chemical Reactions
1,2,3,4,5,6,7,8,9,10,11,12,13,14,15,16,18,19,20 !Above#X(ID_Glb Of Involved Chemical Reaction)
**************Simulation Time & Steps*********************
1, 1            !NtotTimeSteps,NtotSnapShots
0               !ITimeStt(=0, first time run; >0, to restart based on ITimeStt-1 step)
**************Initial Uniform Concentrations*********************
17.5129,2.9998d-3,3.3999,3.3999,2.03d-7,1.776d-8,0,0,0,0,0,0,0,0,0,0,0,0 !C(particle/nm^3)MUST Follow order of involved chemical components
**************Boundary Condition************
!---repeat below !NthC,Ramp1Jump2,2(Flux0_End,SpringCoef_End,C_Eqilibrium_End)
0, 1, 0, 1.d3, 1, 0, 1.d3, 0            !electric (Displacement=Displacement0+Coef*(V-V0)) with displacement_unit:e/nm^2
1, 2, 0, 0, 0, 0, 1.d3, 17.5129         !chemical (flux=flux0+Coef*(C-C0)) with flux_unit:particle/nm^2/ns, and C_unit:particle/nm^3
2, 2, 0, 0, 0, 0, 1.d3, 2.9998d-3       !chemical (flux=flux0+Coef*(C-C0)) with flux_unit:particle/nm^2/ns, and C_unit:particle/nm^3
3, 2, 0, 0, 0, 0, 1.d3, 3.3999          !chemical (flux=flux0+Coef*(C-C0)) with flux_unit:particle/nm^2/ns, and C_unit:particle/nm^3
4, 2, 0, 0, 0, 0, 1.d3, 3.3999          !chemical (flux=flux0+Coef*(C-C0)) with flux_unit:particle/nm^2/ns, and C_unit:particle/nm^3
5, 2, 0, 0, 0, 0, 1.d3, 2.03d-7         !chemical (flux=flux0+Coef*(C-C0)) with flux_unit:particle/nm^2/ns, and C_unit:particle/nm^3
6, 2, 0, 0, 0, 0, 1.d3, 1.776d-8        !chemical (flux=flux0+Coef*(C-C0)) with flux_unit:particle/nm^2/ns, and C_unit:particle/nm^3
7, 2, 5.85d-10, 0, 0, 0, 1.d3, 0        !chemical (flux=flux0+Coef*(C-C0)) with flux_unit:particle/nm^2/ns, and C_unit:particle/nm^3
8, 2, 0, 0, 0, 0, 1.d3, 0               !chemical (flux=flux0+Coef*(C-C0)) with flux_unit:particle/nm^2/ns, and C_unit:particle/nm^3
9, 2, 0, 0, 0, 0, 1.d3, 0               !chemical (flux=flux0+Coef*(C-C0)) with flux_unit:particle/nm^2/ns, and C_unit:particle/nm^3
10, 2, 0, 0, 0, 0, 1.d3, 0              !chemical (flux=flux0+Coef*(C-C0)) with flux_unit:particle/nm^2/ns, and C_unit:particle/nm^3
11, 2, 0, 0, 0, 0, 1.d3, 0              !chemical (flux=flux0+Coef*(C-C0)) with flux_unit:particle/nm^2/ns, and C_unit:particle/nm^3
12, 2, 0, 0, 0, 0, 1.d3, 0              !chemical (flux=flux0+Coef*(C-C0)) with flux_unit:particle/nm^2/ns, and C_unit:particle/nm^3
13, 2, 0, 0, 0, 0, 1.d3, 0              !chemical (flux=flux0+Coef*(C-C0)) with flux_unit:particle/nm^2/ns, and C_unit:particle/nm^3
14, 2, 0, 0, 0, 0, 1.d3, 0              !chemical (flux=flux0+Coef*(C-C0)) with flux_unit:particle/nm^2/ns, and C_unit:particle/nm^3
15, 2, 0, 0, 0, 0, 1.d3, 0              !chemical (flux=flux0+Coef*(C-C0)) with flux_unit:particle/nm^2/ns, and C_unit:particle/nm^3
16, 2, 0, 0, 0, 0, 1.d3, 0              !chemical (flux=flux0+Coef*(C-C0)) with flux_unit:particle/nm^2/ns, and C_unit:particle/nm^3
17, 2, 0, 0, 0, 0, 1.d3, 0              !chemical (flux=flux0+Coef*(C-C0)) with flux_unit:particle/nm^2/ns, and C_unit:particle/nm^3
18, 2, 0, 0, 0, 0, 1.d3, 0              !chemical (flux=flux0+Coef*(C-C0)) with flux_unit:particle/nm^2/ns, and C_unit:particle/nm^3
**************Numerical Parameters*********************
90000, 1.d-3, 1000, 0.002       !IteratMax,ErrAllow,IteratDisplay,ARelax
*********************************************************************
************All Chemical Components*********************
21      !Total # of chemical components
--repeat (above #) below--!ID;Valance;Relative_Permittivity@Linear;StokesRadius;PhysicalRadius;EtaOverEpsil0((V/nm)^2-nS);AvdW0
 1,  0,   55.6,  0.09687,   0.1552,  0.113d1, 0.20294                   !H2O(0)(10)
 2, -1,    7,    0.107,     0.181,   0.113d1, 0.241                     !Cl(1-)
 3,  1,   10,    0.145,     0.157,   0.113d1, 0.68294                   !CH3OH2(1+)
 4, -1,   10,    0.717,     0.234,   0.113d1, 0.68294                   !HCO(1-)
 5,  1,    0,    0.023,     0.15,    0.113d1, 0.20294                   !H(+)
 6, -1,   50,    0.041,     0.137,   0.113d1, 0.20294                   !OH(-)
 7,  3,   4.5,  0.4026,    0.039,   0.113d1, 0                 !Al(3+)(13)
 8,  2,   2.2,   0.4026,    0.138,   0.113d1, 0                 !AlOH(2+)
 9,  1,   2.2,   0.4026,   0.1733,   0.113d1, 0                 !Al(OH)2(1+)
10,  4,   2.2,   0.4026,   0.1739,   0.113d1, 0                 !Al2(OH)2(4+)
11,  2,   5.1,   0.4026,   0.1816,   0.113d1, 0                 !AlCl(2+)
12,  1,    3,    0.4026,   0.2046,   0.113d1, 0                 !Al(OH)Cl(1+)
13,  0,    3,    0.4026,   0.2233,   0.113d1, 0                 !Al(OH)2Cl(0)
14,  0,    1,    0.278,    0.175,    0.113d1, 0.68294           !C2H6O2(0)
15, -2,   10,     0.221,     0.17,    0.113d1, 0.439             !C2O4(2-)
16,  0,   0.5,    0.113,     0.178,   0.113d1, 0.134             !CO2(0)
17,  0,  0.89,  0.109,     0.135,   0.113d1, 0.0502            !O2(0)
18, -1,    5,    0.2,       0.162,   0.113d1, 0.650             !HCOO(1-)
19,  0,   10,    0.75,    0.334,    0.113d1, 0.68294           !H2CO(0)
20,  0,   10,    0.7,    0.35,    0.113d1, 0.68294             !HCOOH(0)
21,  0,    5,    0.041,    0.039,    0.113d1, 0                !Al(OHCH2CH2O)3
************All Chemical Reactions*********************
20      !Total # of Chemical Reactions
--repeat (above #) below--ID,KConst(MUST be consistent to generate rate by particle/nm^3/ns),4(NCLnr,KLnr),8(NC_Involved,Vnce#)
 1, 6.44d-6,  0, 0, 0, 0, 0, 0, 0, 0,                  7, -1, 1, -1, 8, 1, 5, 1,  0, 0, 0, 0, 0, 0, 0, 0       !Al(3+)+H2O>AlOH(2+)+H(+)
 2, 7.31, 0,  0, 0, 0, 0, 0, 0, 0,                     8, -1, 5, -1, 7, 1, 1, 1, 0, 0, 0, 0, 0, 0, 0, 0       !AlOH(2+)+H(+)>Al(3+)+H2O
 3, 6.44d-6,  0, 0, 0, 0, 0, 0, 0, 0,                  8, -1, 1, -1, 9, 1, 5, 1, 0, 0, 0, 0, 0, 0, 0, 0       !AlOH(2+)+H2O>Al(OH)2(+)+H(+)
 4, 7.31, 0,  0, 0, 0, 0, 0, 0, 0,                     9, -1, 5, -1, 8, 1, 1, 1, 0, 0, 0, 0, 0, 0, 0, 0       !Al(OH)2(+)+H(+)>Al(OH)(2+)+H2O
 5, 5.8d-10,  0, 0, 0, 0, 0, 0, 0, 0,                  7, -2, 1, -2, 10, 1, 5, 2, 0, 0, 0, 0, 0, 0, 0, 0      !2Al(3+)+2H2O>Al2(OH)2(4+)+2H(+)
 6, 2.76d-1,  0, 0, 0, 0, 0, 0, 0, 0,                  10, -1, 5, -2, 7, 2, 1, 2, 0, 0, 0, 0, 0, 0, 0, 0      !Al2(OH)2(4+)+2H(+)>2Al(3+)+2H2O
 7, 3.75d-7,  0, 0, 0, 0, 0, 0, 0, 0,                  7, -1, 2, -1, 11, 1, 0, 0, 0, 0, 0, 0, 0, 0, 0, 0      !Al(3+)+Cl(-)>AlCl(2+)
 8, 7.5d-8,   7, 3.75d-7, 6, -3.75d-7, 0, 0, 0, 0,      11, -1, 7, 1, 2, 1, 0, 0, 0, 0, 0, 0, 0, 0, 0, 0       !AlCl(2+)>Al(3+)+Cl(-)
 9, 3.16d-5,  0, 0, 0, 0, 0, 0, 0, 0,                  8, -1, 2, -1, 12, 1, 0, 0, 0, 0, 0, 0, 0, 0, 0, 0      !AlOH(2+)+Cl(-)>Al(OH)Cl(+)
10, 5.7d-6,   8, -3.16d-5, 0, 0, 0, 0, 0, 0,           12, -1, 8, 1, 2, 1, 0, 0, 0, 0, 0, 0, 0, 0, 0, 0       !Al(OH)Cl(+)>AlOH(2+)+Cl(-)
11, 1.4d-17,  0, 0, 0, 0, 0, 0, 0, 0,                  11, -1, 1, -2, 13, 1, 5, 2,  0, 0, 0, 0, 0, 0, 0, 0    !AlCl(2+)+2H2O>Al(OH)2Cl+2H(+)
12, 2.36d-16, 0, 0, 0, 0, 0, 0, 0, 0,                  12, -1, 1, -1, 13, 1, 5, 1,  0, 0, 0, 0, 0, 0, 0, 0    !Al(OH)Cl(+)+H2O>Al(OH)2Cl+H(+)
13, 5.13d-14, 0, 0, 0, 0, 0, 0, 0, 0,                  1, -1, 5, 1, 6, 1, 0, 0, 0, 0, 0, 0, 0, 0, 0, 0        !H2O>H(+)+OH(-)
14, 2.16d2,   0, 0, 0, 0, 0, 0, 0, 0,                  5, -1, 6, -1, 1, 1, 0, 0, 0, 0, 0, 0, 0, 0, 0, 0       !H(+)+OH(-)>H2O
15, 1.63d-37,  0, 0, 0, 0, 0, 0, 0, 0,                 14,-1, 17,-2, 15, 1, 5, 2, 1, 2, 0, 0, 0, 0, 0, 0      !C2H6O2+2O2>C2O4(2-)+2H(+)+2H2O
16, 1.d-5, 0, 0, 0, 0, 0, 0, 0, 0,                     14, -1, 3, 1, 4, 1,  0, 0, 0, 0, 0, 0, 0, 0, 0, 0      !C2H6O2>CH3OH2(+)+CHO(-)
17, 1.77d-4,  0, 0, 0, 0, 0, 0, 0, 0,                  15, -2, 5,-4, 17, -2, 16, 4, 1, 2, 0, 0, 0, 0, 0, 0    !2C2O4(2-)+4H(+)+O2>4CO2+2H2O
18, 7.89d-18, 0, 0, 0, 0, 0, 0, 0, 0,                  17, -1, 1, -2, 6, 4, 0, 0, 0, 0, 0, 0, 0, 0, 0, 0      !O2+2H2O+4e(-)>4OH(-)
19, 4d-11, 0, 0, 0, 0, 0, 0, 0, 0,                     19, -1, 4, 1, 5, 1, 0, 0, 0, 0, 0, 0, 0, 0, 0, 0       !H(+)+CHO(-)>H2CO
20, 1.5d-11, 0, 0, 0, 0, 0, 0, 0, 0,                   20, -1, 18, 1, 5, 1, 0, 0, 0, 0, 0, 0, 0, 0, 0, 0      !H(+)+HCOO(-)>HCOOH
```

Appendix B

Input profile for Double layer structure without considering the flux of Al^{3+} cations

B-1:Double layer structure for 373 K temperature at 1 V

```
************1D Problem******************
1               !=1 if planar; =2 if cylindrical; =3 if spherical
373             !Temperature(K)
************Domain and Grid******************
0, 0.85, 250, 1.02      !XStt,XEnd(nm),Total # of divisions,Mesh-grading power
************Involved Chemical Components*********
6       !Total#Of Involved Chemical Components
1, 2, 3, 4, 5, 6        !Above#X(ID_Glb Of Involved Chemical Component)
************Involved Chemical Reactions*********
3       !Total#Of Involved Chemical Reactions
13,14,16        !Above#X(ID_Glb Of Involved Chemical Reaction)
*************Simulation Time & Steps*********************
3, 3            !NtotTimeSteps,NtotSnapShots
0               !ITimeStt(=0, first time run; >0, to restart based on ITimeStt-1 step)
*************Initial Uniform Concentrations*********************
17.5129, 2.9998d-3, 3.3999, 3.3999, 2.03d-7, 1.776d-8     !C(particle/nm^3)///MUST Follow the above order of involved chemical components
*************Boundary Condition************
!---repeat below !NthC,Ramp1Jump2,2(Flux0_End,SpringCoef_End,C_Eqilibrium_End)
0, 1, 0, 1.d3, 1, 0, 1.d3, 0            !electric (Displacement=Displacement0+Coef*(V-V0)) with displacement_unit:e/nm^2
1, 2, 0, 0, 0, 0, 1.d3, 17.5129         !chemical (flux=flux0+Coef*(C-C0)) with flux_unit:particle/nm^2/ns, and C_unit:particle/nm^3
2, 2, 0, 0, 0, 0, 1.d3, 2.9998d-3       !chemical (flux=flux0+Coef*(C-C0)) with flux_unit:particle/nm^2/ns, and C_unit:particle/nm^3
3, 2, 0, 0, 0, 0, 1.d3, 3.3999          !chemical (flux=flux0+Coef*(C-C0)) with flux_unit:particle/nm^2/ns, and C_unit:particle/nm^3
4, 2, 0, 0, 0, 0, 1.d3, 3.3999          !chemical (flux=flux0+Coef*(C-C0)) with flux_unit:particle/nm^2/ns, and C_unit:particle/nm^3
5, 2, 0, 0, 0, 0, 1.d3, 2.03d-7         !chemical (flux=flux0+Coef*(C-C0)) with flux_unit:particle/nm^2/ns, and C_unit:particle/nm^3
6, 2, 0, 0, 0, 0, 1.d3, 1.776d-8        !chemical (flux=flux0+Coef*(C-C0)) with flux_unit:particle/nm^2/ns, and C_unit:particle/nm^3
*************Numerical Parameters*********************
90000, 1.d-3, 1000, 0.005       !IteratMax,ErrAllow,IteratDisplay,ARelax
************************************************************
************All Chemical Components*********************
21      !Total # of chemical components
--repeat (above #) below--!ID;Valance;Relative_Permittivity@Linear;StokesRadius;PhysicalRadius;EtaOverEpsil0((V/nm)^2-nS);AvdW0
 1,  0,   55.6,  0.09687,   0.1552,  0.113d1, 0.20294                  !H2O(0)(10)
 2, -1,    7,    0.107,     0.181,   0.113d1, 0.241                    !Cl(1-)
 3,  1,    10,   0.145,     0.157,    0.113d1, 0.68294                 !CH3OH2(1+)
 4, -1,    10,   0.717,    0.234,    0.113d1, 0.68294                  !HCO(1-)
 5,  1,    0,    0.023,     0.15,    0.113d1, 0.20294                  !H(+)
 6, -1,   50,    0.041,     0.137,   0.113d1, 0.20294                  !OH(-)
 7,  3,   4.5,  0.4026,    0.039,   0.113d1, 0                 !Al(3+)(13)
 8,  2,   2.2,   0.4026,    0.138,   0.113d1, 0                 !AlOH(2+)
 9,  1,   2.2,   0.4026,   0.1733,   0.113d1, 0                 !Al(OH)2(1+)
10,  4,   2.2,   0.4026,   0.1739,   0.113d1, 0                 !Al2(OH)2(4+)
11,  2,   5.1,   0.4026,   0.1816,   0.113d1, 0                 !AlCl(2+)
12,  1,    3,    0.4026,   0.2046,   0.113d1, 0                 !Al(OH)Cl(1+)
13,  0,    3,    0.4026,   0.2233,   0.113d1, 0                 !Al(OH)2Cl(0)
14,  0,    1,    0.278,    0.175,    0.113d1, 0.68294           !C2H6O2(0)
15, -2,    10,    0.221,     0.17,    0.113d1, 0.439            !C2O4(2-)
16,  0,   0.5,   0.113,     0.178,   0.113d1, 0.134             !CO2(0)
17,  0,  0.89,  0.109,     0.135,   0.113d1, 0.0502            !O2(0)
18, -1,    5,    0.2,       0.162,   0.113d1, 0.650             !HCOO(1-)
19,  0,    10,   0.75,    0.334,    0.113d1, 0.68294           !H2CO(0)
20,  0,    10,   0.7,    0.35,    0.113d1, 0.68294             !HCOOH(0)
21,  0,    5,    0.041,    0.039,    0.113d1, 0                !Al(OHCH2CH2O)3
************All Chemical Reactions*********************
20      !Total # of Chemical Reactions
--repeat (above #) below--ID,KConst(MUST be consistent to generate rate by particle/nm^3/ns),4(NCLnr,KLnr),8(NC_Involved,Vnce#)
 1, 6.44d-6,  0, 0, 0, 0, 0, 0, 0, 0,                  7, -1, 1, -1, 8, 1, 5, 1,  0, 0, 0, 0, 0, 0, 0, 0       !Al(3+)+H2O>AlOH(2+)+H(+)
 2, 7.31, 0,  0, 0, 0, 0, 0, 0, 0, 0,                  8, -1, 5, -1, 7, 1, 1, 1, 0, 0, 0, 0, 0, 0, 0, 0        !AlOH(2+)+H(+)>Al(3+)+H2O
 3, 6.44d-6,  0, 0, 0, 0, 0, 0, 0, 0,                  8, -1, 1, -1, 9, 1, 5, 1, 0, 0, 0, 0, 0, 0, 0, 0        !AlOH(2+)+H2O>Al(OH)2(+)+H(+)
 4, 7.31, 0,  0, 0, 0, 0, 0, 0, 0, 0,                  9, -1, 5, -1, 8, 1, 1, 1, 0, 0, 0, 0, 0, 0, 0, 0        !Al(OH)2(+)+H(+)>Al(OH)(2+)+H2O
 5, 5.8d-10,  0, 0, 0, 0, 0, 0, 0, 0,                  7, -2, 1, -2, 10, 1, 5, 2, 0, 0, 0, 0, 0, 0, 0, 0       !2Al(3+)+2H2O>Al2(OH)2(4+)+2H(+)
 6, 2.76d-1,  0, 0, 0, 0, 0, 0, 0, 0,                  10, -1, 5, -2, 7, 2, 1, 2, 0, 0, 0, 0, 0, 0, 0, 0       !Al2(OH)2(4+)+2H(+)>2Al(3+)+2H2O
 7, 3.75d-7,  0, 0, 0, 0, 0, 0, 0, 0,                  7, -1, 2, -1, 11, 1, 0, 0, 0, 0, 0, 0, 0, 0, 0, 0       !Al(3+)+Cl(-)>AlCl(2+)
 8, 7.5d-8,   7, 3.75d-7, 6, -3.75d-7, 0, 0, 0, 0,      11, -1, 7, 1, 2, 1, 0, 0, 0, 0, 0, 0, 0, 0, 0, 0        !AlCl(2+)>Al(3+)+Cl(-)
 9, 3.16d-5,  0, 0, 0, 0, 0, 0, 0, 0,                  8, -1, 2, -1, 12, 1, 0, 0, 0, 0, 0, 0, 0, 0, 0, 0       !AlOH(2+)+Cl(-)>Al(OH)Cl(+)
10, 5.7d-6,   8, -3.16d-5, 0, 0, 0, 0, 0, 0,           12, -1, 8, 1, 2, 1, 0, 0, 0, 0, 0, 0, 0, 0, 0, 0        !Al(OH)Cl(+)>AlOH(2+)+Cl(-)
11, 1.4d-17,  0, 0, 0, 0, 0, 0, 0, 0,                  11, -1, 1, -2, 13, 1, 5, 2,  0, 0, 0, 0, 0, 0, 0, 0     !AlCl(2+)+2H2O>Al(OH)2Cl+2H(+)
12, 2.36d-16, 0, 0, 0, 0, 0, 0, 0, 0,                 12, -1, 1, -1, 13, 1, 5, 1,  0, 0, 0, 0, 0, 0, 0, 0    !Al(OH)Cl(+)+H2O>Al(OH)2Cl+H(+)
13, 5.13d-14, 0, 0, 0, 0, 0, 0, 0, 0,                 1, -1, 5, 1, 6, 1, 0, 0, 0, 0, 0, 0, 0, 0, 0, 0          !H2O>H(+)+OH(-)
14, 2.16d2,   0, 0, 0, 0, 0, 0, 0, 0,                 5, -1, 6, -1, 1, 1, 0, 0, 0, 0, 0, 0, 0, 0, 0, 0         !H(+)+OH(-)>H2O
15, 1.63d-37,  0, 0, 0, 0, 0, 0, 0, 0,                14,-1, 17,-2, 15, 1, 5, 2, 1, 2, 0, 0, 0, 0, 0, 0       !C2H6O2+2O2>C2O4(2-)+2H(+)+2H2O
16, 1.d-5, 0, 0, 0, 0, 0, 0, 0, 0,                    14, -1, 3, 1, 4, 1,  0, 0, 0, 0, 0, 0, 0, 0, 0, 0       !C2H6O2>CH3OH2(+)+CHO(-)
17, 1.77d-4,  0, 0, 0, 0, 0, 0, 0, 0,                 15, -2, 5,-4, 17, -2, 16, 4, 1, 2, 0, 0, 0, 0, 0, 0     !2C2O4(2-)+4H(+)+O2>4CO2+2H2O
18, 7.89d-18, 0, 0, 0, 0, 0, 0, 0, 0,                 17, -1, 1, -2, 6, 4, 0, 0, 0, 0, 0, 0, 0, 0, 0, 0       !O2+2H2O+4e(-)>4OH(-)
19, 4d-11, 0, 0, 0, 0, 0, 0, 0, 0,                    19, -1, 4, 1, 5, 1, 0, 0, 0, 0, 0, 0, 0, 0, 0, 0        !H(+)+CHO(-)>H2CO
20, 1.5d-11, 0, 0, 0, 0, 0, 0, 0, 0,                  20, -1, 18, 1, 5, 1, 0, 0, 0, 0, 0, 0, 0, 0, 0, 0       !H(+)+HCOO(-)>HCOOH
```

References

1. Natishan, P. M., & O'grady, W. E. (2014). Chloride Ion Interactions with Oxide-Covered Aluminum Leading to Pitting Corrosion: A Review. *Journal of the Electrochemical Society, 161*(9). doi: 10.1149/2.1011409jes
2. Zhang, G., Xu, L., & Cheng, Y. (2009). Investigation of erosion–corrosion of 3003 aluminum alloy in ethylene glycol–water solution by impingement jet system. *Corrosion Science, 51*(2), 283-290. doi: 10.1016/j.corsci.2008.10.026
3. Cooling System Electrolysis Corrosion. (n.d.). Retrieved May 01, 2016, from http://www.aa1car.com/library/cooling_system_electrolysis_corrosion.htm
4. Rossiter, W. J., Brown, P. W., & Godette, M. (1983). The determination of acidic degradation products in aqueous ethylene glycol and propylene glycol solutions using ion chromatography. *Solar Energy Materials, 9*(3), 267-279. doi:10.1016/0165-1633(83)90049-7
5. S. M., H. T., & E. A. (n.d.). AluMATTER | Aluminium | Forms of Corrosion | Forms of Corrosion: Introduction. Retrieved May 01, 2016, from http://www.aluminium.matter.org.uk/content/html/eng/default.asp?catid=180
6. 3003 Aluminum Material Property Data Sheet - Product availability and request a quote. (n.d.). Retrieved May 01, 2016, from http://www.suppliersonline.com/propertypages/3003.asp
7. Zhang, G., Xu, L., & Cheng, Y. (2008). Mechanistic aspects of electrochemical corrosion of aluminum alloy in ethylene glycol–water solution. *Electrochimica Acta, 53*(28), 8245-8252. doi: 10.1016/j.electacta.2008.06.043

8. Stojek, Z. (2005). The Electrical Double Layer and Its Structure. *Electroanalytical Methods*, 3-8. doi:10.1007/978-3-662-04757-6_1
9. Kirby, B.J. (2010). Micro- and Nano scale Fluid Mechanics: Transport in Microfluidic Devices. Cambridge University Press. ISBN 978-0-521-11903-0.
10. Chapter 2. (n.d.). Retrieved May 01, 2016, from http://depts.washington.edu/solgel/pages/courses/MSE_502/Electrostatic_Stabilization.html
11. Curioni, M., & Scenini, F. (2015). The Mechanism of Hydrogen Evolution During Anodic Polarization of Aluminum. Electrochimica Acta, 180, 712-721. doi: 10.1016/j.electacta.2015.08.076
12. Activation Polarization. (n.d.). Retrieved May 01, 2016, from http://corrosion-doctors.org/Corrosion-Kinetics/Overpotential-activation.htm
13. Zhu, M., Ding, D., GAO, Y., Chen, G., Li, M., & Mao, D. (2010). Effect of Zn content on tensile and electrochemical properties of 3003 Al alloy. Transactions of Nonferrous Metals Society of China, 20(11), 2118-2123. doi:10.1016/s1003-6326(09)60427-1
14. Dutta, S., & Bhattacharyya, D. (2001). Journal of Biological Physics, 27(1), 59-71. doi:10.1023/a:1011826525684
15. Boughammoura, S., & Mhalla, J. (2016). Generalization of the model of Debye-Hückel according to a matrix approach. Application to the calculation of the potential of mean force in the case of electrolytes, polyelectrolytes and colloids. Journal of Molecular Liquids, 214, 196-206. doi: 10.1016/j.molliq.2015.12.089.
16. Grigor'Ev, A. I. (2001). The field-induced ion evaporation from electrolyte solutions. Technical Physics Letters Tech. Phys. Lett., 27(4), 305-307. doi:10.1134/1.1370208.

17. Eckstrom, H. C., & Schmelzer, C. (1939). The Wien Effect: Deviations of Electrolytic Solutions from Ohm's Law under High Field Strengths. Chemical Reviews Chem. Rev., 24(3), 367-414. doi:10.1021/cr60079a001
18. Deruiter, J., Davis, R. A., Wandrekar, V. G., & Mayfield, C. A. (1991). Relative structure-inhibition analyses of the N-benzoyl and N-(phenylsulfonyl) amino acid aldose reductase inhibitors. J. Med. Chem. Journal of Medicinal Chemistry, 34(7), 2120-2126. Doi: 10.1021/jm00111a030.
19. Browne, C., Tabor, R. F., Chan, D. Y., Dagastine, R. R., Ashokkumar, M., & Grieser, F. (2011). Bubble Coalescence during Acoustic Cavitation in Aqueous Electrolyte Solutions. Langmuir, 27(19), 12025-12032. doi:10.1021/la202804c
20. Melcher, J. R. Continuum electro mechanics. Vol. 2 (MIT press Cambridge, 1981).
21. Carnahan, N. F. & Starling, K. E. Equation of state for nonattracting rigid spheres. The Journal of chemical physics 51, 635-636 (1969).
22. Carnahan, N. F. & Starling, K. E. Intermolecular repulsions and the equation of state for fluids. AIChE Journal 18, 1184-1189 (1972).
23. Heinz, H., Vaia, R., Farmer, B. & Naik, R. Accurate simulation of surfaces and interfaces of face-centered cubic metals using 12− 6 and 9− 6 Lennard-Jones potentials. The Journal of Physical Chemistry C 112, 17281-17290 (2008).
24. Wei, Y. S. & Sadus, R. J. Equations of state for the calculation of fluid-phase equilibria. AIChE Journal 46, 169-196 (2000).

Biographical Information

Saurabh Deobhankar completed his undergraduate degree in Mechanical Engineering from University of Pune, India in 2014. He then sought admission in University of Texas Arlington for Master's program in Mechanical Engineering in Fall 2014 and graduated in May 2016. He completed the thesis requirement under the guidance of Dr. Bo Yang. His research interests include stress analysis, fracture mechanics, finite element modelling, electrical double layer analysis, and electrolyte film evaporation in high electric fields.